

1 **Efa6 protects axons and regulates their growth and branching by inhibiting**  
2 **microtubule polymerisation at the cortex**

3  
4 Yue Qu<sup>\*,1</sup>, Ines Hahn<sup>\*,#1</sup>, Meredith Lees<sup>1</sup>, Jill Parkin<sup>1</sup>, André Voelzmann<sup>1</sup>, Karel Dorey<sup>1</sup>, Alex  
5 Rathbone<sup>2</sup>, Claire Friel<sup>2</sup>, Viki Allan<sup>1</sup>, Pilar Okenve-Ramos<sup>3</sup>, Natalia Sanchez-Soriano<sup>3</sup>,  
6 Andreas Prokop<sup>1</sup>

7  
8 1) The University of Manchester, Manchester Academic Health Science Centre, Faculty of  
9 Biology, Medicine and Health, School of Biology, Manchester, UK

10 2) The University of Nottingham, School of Life Sciences, Faculty of Medicine & Health  
11 Sciences, Nottingham, UK

12 3) Department of Cellular and Molecular Physiology, Institute of Translational Medicine,  
13 University of Liverpool, Liverpool, United Kingdom

14  
15 Running title: The role of Efa6 in axon maintenance

16 Key words: *Drosophila*, neurodegeneration, axons, actin, cytoskeleton, microtubules

17  
18 \* authors contributed equally

19 # authors for correspondence:

20 The University of Manchester

21 Faculty of Life Sciences

22 Oxford Road

23 Manchester M13 9PT

24 Tel: +44-(0)161-27-51556

25 Fax: +44-(0)161-27-51505

26 Ines.Hahn@manchester.ac.uk

27  
28 **Summary statement (30 words max):**

29 The cortical collapse factor Efa6 inhibits microtubule polymerising outside axonal bundles.  
30 Thereby it limits axon growth and branching, but preserves microtubule bundle organisation  
31 crucial for axon maintenance.

32  
33 **Abstract**

34 Cortical collapse factors affect microtubule (MT) dynamics at the plasma membrane. They  
35 play important roles in neurons, as suggested by inhibition of axon growth and regeneration  
36 through the Arf activator Efa6 in *C. elegans*, and by neurodevelopmental disorders linked to  
37 the mammalian kinesin Kif21A. How cortical collapse factors influence axon growth is little  
38 understood. Here we studied them, focussing on the function of *Drosophila* Efa6 in  
39 experimentally and genetically amenable fly neurons. First, we show that *Drosophila* Efa6 can  
40 inhibit MTs directly without interacting molecules via an N-terminal 18 amino acid motif (MT  
41 elimination domain/MTED) that binds tubulin and inhibits microtubule growth *in vitro* and cells.  
42 If N-terminal MTED-containing fragments are in the cytoplasm they abolish entire microtubule  
43 networks of mouse fibroblasts and whole axons of fly neurons. Full-length Efa6 is membrane-

44 attached, hence primarily blocks MTs in the periphery of fibroblasts, and explorative MTs that  
45 have left axonal bundles in neurons. Accordingly, loss of Efa6 causes an increase of  
46 explorative MTs: in growth cones, they enhance axon growth, in axon shafts, explorative MTs  
47 cause excessive branching, as well as atrophy through perturbations of MT bundles. Efa6  
48 over-expression causes the opposite phenotypes. Taken together, our work conceptually links  
49 molecular and sub-cellular functions of cortical collapse factors to axon growth regulation and  
50 reveals new roles in axon branching and in the prevention of axonal atrophy. Furthermore, the  
51 MTED delivers a promising tool that can be used to inhibit MTs in a compartmentalised  
52 fashion when fusing it to specifically localising protein domains.

53

## 54 Introduction

55 Axons are the cable-like neuronal extensions that wire the nervous system. They are only 0.1-  
56 15µm in diameter (Hoffman, 1995), but can be up to a meter long in humans (Debanne et al.,  
57 2011; Prokop, 2013a). It is a fascinating challenge to understand how axons can extend over  
58 these enormous distances and branch in orderly manners, but also how these delicate  
59 structures can be maintained for a lifetime, i.e. many decades in humans. It is not surprising  
60 that we gradually lose about half of our axons towards old age (Calkins, 2013; Marnier et al.,  
61 2003), and that axon decay is a prominent neurodegenerative phenomenon (Adalbert and  
62 Coleman, 2012; Fang and Bonini, 2012; Medana and Esiri, 2003; Wang et al., 2012).

63 Essential for axon biology are the parallel bundles of microtubules (MTs) running all  
64 along the axon shaft; these bundles provide (1) structural support, (2) highways for life-  
65 sustaining cargo transport, and (3) a source of MTs that can leave these bundles to drive  
66 morphogenetic changes. Through being organised in this way, MTs essentially drive  
67 processes of axon growth, branching and maintenance (Conde and Caceres, 2009; Dent et al.,  
68 2011; Hahn et al., 2019; Prokop, 2013a; Voelzmann et al., 2016a). The dynamics of MTs are  
69 orchestrated through MT-binding and -regulating proteins, for most of which we know the  
70 molecular mechanisms of function. However, such knowledge alone is usually not sufficient to  
71 explain their cellular roles.

72 For example, cortical collapse factors are cell surface-associated proteins specifically  
73 inhibit MTs that approach the cell periphery. Previous reports suggested important roles for  
74 cortical collapse factors in regulating axon growth: the ARF activator Efa6 in *C. elegans*  
75 negatively impacts on developmental and regenerative axon growth (Chen et al., 2015; Chen  
76 et al., 2011; O'Rourke et al., 2010); the mammalian type 4 kinesin KIF21A also affects axon  
77 growth and links to the neurodevelopmental eye movement disorder "congenital fibrosis of  
78 extraocular muscles" (OMIM reference [#135700](#); Heidary et al., 2008; Tiab et al., 2004; van  
79 der Vaart et al., 2013). However, we can currently only hypothesise how the molecular  
80 function of these two collapse factors links to axon growth, most likely by acting in growth  
81 cones (GCs).

82 GCs are the amoeboid tip structures where axons extend to wire the nervous system  
83 during development or regeneration. The axonal MT bundles terminate in the centre of GCs;  
84 from here, single MTs splay into the actin-rich periphery of GCs. These explorative MTs can  
85 trigger extension of the entire MT bundle into their direction, thus elongating the axon (Dent et  
86 al., 2011; Lowery and van Vactor, 2009; Prokop et al., 2013); their (partial) inhibition through  
87 cortical collapse factors could provide a potential mechanism through which cortical collapse  
88 factors negatively impact on axon growth.

89 In line with this argumentation, and depending on where cortical collapse factors are  
90 present and functionally active, further functional predictions could be made: for example,  
91 collateral branching of axons along their shafts has been described to depend on explorative  
92 MTs that leave the parallel axonal bundles and polymerise towards the periphery (Kalil and  
93 Dent, 2014; Lewis et al., 2013; Tymanskyj et al., 2017; Yu et al., 2008). Cortical collapse  
94 factors might therefore be negative regulators of axon branching.

95 Other roles might concern axon maintenance: the model of 'local axon homeostasis'  
96 states that the force-enriched environment in axons biases MTs to buckle or project out of the  
97 bundle to seed pathological areas of MT disorganisation (Hahn et al., 2019; Prokop, 2016;  
98 Voelzmann et al., 2016a). By inhibiting off-track MTs in the axon shaft, cortical collapse  
99 factors might prevent such processes, acting in parallel to other bundle-maintaining factors.  
100 For example, spectraplakins serve as spacers that keep polymerising MTs away from the  
101 cortex by linking the tips of extending MTs to the axonal surface and guiding them into parallel  
102 bundles (Alves-Silva et al., 2012). Their deficiency in any organism causes severe MT  
103 disorganisation, potentially explaining human dystonin-linked HSN6 ('type 6 hereditary  
104 sensory and autonomic neuropathy"; #614653; Voelzmann et al., 2017). If our hypothesis is  
105 correct, loss of cortical collapse factors in axon shafts would also cause MT disorganisation,  
106 but through a very different mechanistic route.

107 Here we make use of *Drosophila* neurons as a well-established, powerful model for  
108 studying roles of MT regulators (Hahn et al., 2019; Prokop et al., 2013; Sánchez-Soriano et  
109 al., 2007). Using *in vitro* and cellular assays, we show that *Drosophila* Efa6 is a cortical  
110 collapse factor acting through its N-terminal MT-eliminating domain (MTED). We find that the  
111 MTED binds tubulin and blocks MT polymerisation *in vitro* which shows that the effect of the  
112 peptide is due to a direct interaction between the peptide and tubulin and does not require any  
113 other molecules. By localising to neuronal membranes, it only abolishes explorative MTs. This  
114 subcellular role translates into negative regulation of axon growth and branching and the  
115 prevention of pathological MT disorganisation, both in cultured neurons and *in vivo*. We  
116 propose Efa6 to function as a quality control or axonal maintenance factor that keeps  
117 explorative MTs in check, thus playing a complementary role to spectraplakins that prevent  
118 MTs from leaving axonal bundles.

119

## 120 **Methods**

121

### 122 Fly stocks

123 Loss-of-function mutant stocks used in this study were the two deficiencies uncovering the  
124 *Efa6* locus *Df(3R)Exel6273* (94B2-94B11 or 3R:22,530,780..22,530,780) and *Df(3R)ED6091i*  
125 (94B5-94C4 or 3R:22,587,681..22,587,681), *shot*<sup>3</sup> (the strongest available allele of *short stop*)  
126 (Kolodziej et al., 1995; Sánchez-Soriano et al., 2009), and the null mutant alleles *Efa6*<sup>KO#1</sup>,  
127 *Efa6*<sup>GX6[w-]</sup>, *Efa6*<sup>GX6[w+]</sup> and *Arf51F*<sup>GX16[w-]</sup> (all genomically engineered precise deletions) (Huang  
128 et al., 2009). Gal4 driver lines used were the pan-neuronal lines *sca-Gal4* (strongest in  
129 embryos) (Sánchez-Soriano et al., 2010) and *elav-Gal4* (1<sup>st</sup> and 3<sup>rd</sup> chromosomal, both  
130 expressing at all stages) (Luo et al., 1994), as well as the *ato-Gal4* line expressing in a subset  
131 of neurons in the adult brain (Hassan et al., 2000; Voelzmann et al., 2016b). Lines for targeted  
132 gene expression were *UAS-Efa6*<sup>RNAi</sup> (VDRC #42321), *UAS-Gal80<sup>ts</sup>* (Zeidler et al., 2004), *UAS-*  
133 *Eb1-GFP* (Alves-Silva et al., 2012), *UAS- $\alpha$ -tubulin84B* (Grieder et al., 2000) and *UAS-*  
134 *tdTomato* (Zschätzsch et al., 2014). Efa6 expression was detected via the genomically

135 engineered *Efa6-GFP* allele, where a GFP was inserted after the last amino acid in exon 14  
136 (Huang et al., 2009).

#### 137 *Drosophila* primary cell culture

138 *Drosophila* primary neuron cultures were performed as published previously (Prokop et al.,  
139 2012; Qu et al., 2017). In brief, stage 11 embryos were treated for 1 min with bleach to  
140 remove the chorion, sterilized for ~30 s in 70% ethanol, washed in sterile Schneider's/FCS,  
141 and eventually homogenized with micro-pestles in 1.5 centrifuge tubes containing 21 embryos  
142 per 100  $\mu$ l dispersion medium (Prokop et al., 2012) and left to incubated for 5 min at 37°C.  
143 Cells are washed with Schneider's medium (Gibco), spun down for 4 mins at 650 g,  
144 supernatant was removed and cells re-suspended in 90  $\mu$ l of Schneider's medium containing  
145 20% fetal calf serum (Gibco). 30  $\mu$ l drops were placed on cover slips. Cells were allowed to  
146 adhere for 90-120 min either directly on glass or on cover slips coated with a 5  $\mu$ g/ml solution  
147 of concanavalin A, and then grown as a hanging drop culture for hours or days at 26°C as  
148 indicated.

149 To abolish maternal rescue of mutants, i.e. masking of the mutant phenotype caused by  
150 deposition of normal gene product from the healthy gene copy of the heterozygous mothers in  
151 the oocyte (Prokop, 2013b), we used a pre-culture strategy (Prokop et al., 2012; Sánchez-  
152 Soriano et al., 2010) where cells were kept for 5 days in a tube before they were plated on a  
153 coverslip.

154 For the transfection of *Drosophila* primary neurons, a quantity of 70-75 embryos per 100  $\mu$ l  
155 dispersion medium was used. After the washing step and centrifugation, cells were re-  
156 suspended in 100  $\mu$ l transfection medium [final media containing 0.1-0.5  $\mu$ g DNA and 2  $\mu$ l  
157 Lipofecatmine 2000 (L2000)]. To generate this media, dilutions of 0.1-0.5  $\mu$ g DNA in 50  $\mu$ l  
158 Schneider's medium and 2  $\mu$ l L2000 in 50  $\mu$ l Schneider's medium were prepared, then mixed  
159 together and incubated at room temperature for 5-30 mins, before being added to the cells in  
160 centrifuge tubes where they were kept for 24 hrs at 26°C. Cells were then treated again with  
161 dispersion medium, re-suspended in culture medium and plated out as described above.

162 For temporally controlled knock-down experiments we used flies carrying the driver construct  
163 *elav-Gal4*, the knock-down construct *UAS-Efa6-RNAi*, and the temperature-sensitive Gal4  
164 inhibitor *UAS-Gal80<sup>ts</sup>*, all in parallel. At the restrictive temperature of 19°C, Gal80<sup>ts</sup> blocks  
165 Gal4-induced expression of *Efa6-RNAi*, and this repressive action is removed at the  
166 permissive temperature of 27°C where Gal80<sup>ts</sup> is non-functional. Control neurons were from  
167 flies carrying only the *Gal4/Gal80* (control 1 in Fig. 8K) or only the *Efa6-RNAi* transgene  
168 (control 2).

169

#### 170 Fibroblast cell culture

171 NIH/3T3 fibroblasts were grown in DMEM supplemented with 1% glutamine  
172 (Invitrogen), 1% penicillin/streptomycin (Invitrogen) and 10% FCS in culture dishes (100 mm  
173 with vents; Fisher Scientific UK Ltd) at 37°C in a humidified incubator at 5% CO<sub>2</sub>. Cells were  
174 split every 2-3 d, washed with pre-warmed PBS, incubated with 4 ml of Trypsin-EDTA (T-E) at  
175 37°C for 5 min, then suspended in 7 ml of fresh culture medium and eventually diluted (1/3-  
176 1/20 dilution) in a culture dish containing 10 ml culture media.

177 For transfection of NIH/3T3 cells, 2 ml cell solution (~10<sup>5</sup> cells per ml) were first  
178 transferred to 6-well plates, and grown overnight to double cell density. 2  $\mu$ g of DNA and 2  $\mu$ l  
179 Plus reagent (Invitrogen) were added to 1 ml serum-free media in a centrifuge tube, incubated

180 for 5 mins at RT, then 6  $\mu$ l Lipofectamine (Invitrogen) were added, and incubated at RT for 25  
181 mins. Cells in the 6-well plate were washed with serum-free medium and 25 mins later  
182 DNA/Lipofectamine was mixed into the medium (1/1 dilution). Plates were incubated for 3 hrs  
183 at 37°C, washed with 2 ml PBS, 400  $\mu$ l trypsin were added for 5 mins (37°C), then 3 ml  
184 complete medium; cells were suspended and added in 1 ml aliquots to 35 mm glass-bottom  
185 dishes (MatTek) coated with fibronectin [300  $\mu$ l of 5  $\mu$ g/ml fibronectin (Sigma-Aldrich) placed  
186 in the center of a MatTek dish for 1 hr at 37°C, then washed with PBS]; 1 ml of medium was  
187 added and cells grown for 6 hrs or 24 hrs at 37°C in a CO<sub>2</sub> incubator. For live imaging, the  
188 medium was replaced with 2 ml Ham's F-12 medium + 4% FCS.

189

### 190 Dissection of adult brains

191 To analyse the function of Efa6 in MT bundle integrity in medulla axons *in vivo*, flies were  
192 aged at 29°C. Flies were maintain in groups of up to 20 flies of the same gender (Stefana et  
193 al., 2017) and changed into new tubes every 3-4 days. Brain dissections were performed in  
194 Dulbecco's PBS (Sigma, RNBF2227) after briefly sedating them on ice. Dissected brains with  
195 their laminas and eyes attached were placed into a drop of Dulbecco's PBS on MatTek glass  
196 bottom dishes (P35G1.5-14C), covered by coverslips and immediately imaged with a 3i  
197 Marianas Spinning Disk Confocal Microscope.

198 To measure branching in *ato-Gal4 Drosophila* neurons, adult brains were dissected in  
199 Dulbecco's PBS and fixed with 4% PFA for 15 min. Antibody staining and washes were  
200 performed with PBS supplemented with 0.3% Triton X-100. Specimens were embedded in  
201 Vectashield (VectorLabs).

202

### 203 Immunohistochemistry

204 Primary fly neurons and fibroblasts were fixed in 4% paraformaldehyde (PFA) in 0.05 M  
205 phosphate buffer (PB; pH 7–7.2) for 30 min at room temperature (RT); for anti-Eb1 staining,  
206 ice-cold +TIP fix (90% methanol, 3% formaldehyde, 5 mM sodium carbonate, pH 9; stored at -  
207 80°C and added to the cells) (Rogers et al., 2002) was added for 10 mins. Adult brains were  
208 dissected out of their head case in PBS and fixed with 4% PFA in PBS for 1 hr, followed by a  
209 1hr wash in PBT.

210 Antibody staining and washes were performed with PBT. Staining reagents: anti-  
211 tubulin (clone DM1A, mouse, 1:1000, Sigma; alternatively, clone YL1/2, rat, 1:500, Millipore  
212 Bioscience Research Reagents); anti-DmEb1 (gift from H. Ohkura; rabbit, 1:2000) (Elliott et  
213 al., 2005); anti-Elav (mouse, 1:1000, DHB); anti-GFP (goat, 1:500, Abcam); Cy3-conjugated  
214 anti-HRP (goat, 1:100, Jackson ImmunoResearch); F-actin was stained with Phalloidin  
215 conjugated with TRITC/Alexa647, FITC or Atto647N (1:100 or 1:500; Invitrogen and Sigma).  
216 Specimens were embedded in ProLong Gold Antifade Mountant.

217

### 218 Microscopy and data analysis

219 Standard documentation was performed with AxioCam monochrome digital cameras (Carl  
220 Zeiss Ltd.) mounted on BX50WI or BX51 Olympus compound fluorescent microscopes. For  
221 the analysis of *Drosophila* primary neurons, we used two well established parameters (Alves-  
222 Silva et al., 2012; Sánchez-Soriano et al., 2010): axon length (from cell body to growth cone  
223 tip; measured using the segmented line tool of ImageJ) and the degree of MT disorganisation

224 in axons which was either measured as binary score or ratio (percentage of neurons showing  
225 obvious MT disorganisation in their axons) or as "MT disorganisation index" (MDI) (Qu et al.,  
226 2017): the area of disorganisation was measured using the freehand selection in ImageJ; this  
227 value was then divided by axon length (see above) multiplied by 0.5  $\mu\text{m}$  (typical axon diameter,  
228 thus approximating the expected area of the axon if it were not disorganised). For Eb1::GFP  
229 comet counts, neurons were subdivided into axon shaft and growth cones (GC): the proximal  
230 GC border was set where the axon widens up (broader GCs) or where filopodia density  
231 increases significantly (narrow GCs). MT loss in fibroblasts was assessed on randomly  
232 chosen images of successfully transfected, GFP-expressing fibroblasts, stained for tubulin  
233 and actin. Images were derived from at least 2 independent experimental repeats performed  
234 on different days, for each of which at least 3 independent culture wells were analysed by  
235 taking a minimum of 20 images per well. Due to major differences in plasma membrane  
236 versus cytoplasmic localisation of constructs, their expression strengths could not be  
237 standardised. Assuming a comparable expression strength distribution, we therefore analyse  
238 all transfected cells in the images and assigned them to three categories: MTs intact,  
239 damaged or gone (Fig. 3G-G"). To avoid bias, image analyses were performed blindly, i.e. the  
240 genotype or treatment of specimens was masked. To analyse ruffle formation in fibroblasts,  
241 cells were stained with actin and classified (with or without ruffles).

242 To assess the degree of branching, we measured axonal projections of dorsal cluster  
243 neurons in the medulla, which is part of the optic lobe in the adult brain (Hassan et al., 2000;  
244 Voelzmann et al., 2016b). These neurons were labelled by expressing *UAS-myr-tdTomato* via  
245 the *ato-Gal4* driver either alone (control), together with *UAS-Efa6<sup>RNAi</sup>* or together with *UAS-*  
246 *Efa6-FL-GFP*. We analysed them in young brains (2-5 d after eclosion of flies from their pupal  
247 case) or old brains (15-18 d). Z-stacks of adult fly brains (optic lobe area) were taken with a  
248 Leica DM6000 B microscope and extracted with Leica MM AF Premier software. They were  
249 imaged from anterior and the number of branches was quantified manually. Branches were  
250 defined as the protrusions from the DC neuron axons in the medulla. Branches in fly primary  
251 neurons at 5DIV were also counted manually and defined as MT protrusions from main axon.

252 To measure MT disorganisation in the optic lobe of adult flies, *GMR31F10-Gal4*  
253 (Bloomington #49685) was used to express *UAS- $\alpha$ -tubulin84B-GFP* (Grieder et al., 2000) in a  
254 subset of lamina axons which projects within well-ordered medulla columns (Prokop and  
255 Meinertzhagen, 2006). Flies were left to age for 26-27 days (about half their life expectancy)  
256 and then their brains were dissected out, mounted in Mattek dishes and imaged using a 3i  
257 spinning disk confocal system at the ITM Biomedecial imaging facility at the University of  
258 Liverpool. A section of the medulla columns comprising the 4 most proximal axonal terminals  
259 was used to quantify the number of swellings and regions with disorganised MTs.

260 Time lapse imaging of cultured primary neurons (in Schneider's/FCS) and fibroblasts  
261 (in Ham's F-12/FCS) was performed on a Delta Vision Core (Applied Precision) restoration  
262 microscope using a [*100x/1.40 UPlan SAPO (Oil)*] objective and the Sedat Quad filter set  
263 (*Chroma #89000*). Images were collected using a Coolsnap HQ2 (Photometrics) camera. The  
264 temperature was set to 26°C for fly neurons and 37°C for fibroblasts. Time lapse movies were  
265 constructed from images taken every 2 s for 2 mins. To analyse MT dynamics, Eb1::GFP  
266 comets were tracked manually using the "manual tracking" plug-in of ImageJ.

267 For statistical analyses, Kruskal–Wallis one-way ANOVA with *post hoc* Dunn's test or  
268 Mann–Whitney Rank Sum Tests (indicated as  $P_{\text{MW}}$ ) were used to compare groups, and  $\chi^2$   
269 tests (indicated as  $P_{\chi^2}$ ) were used to compare percentages. All raw data of our analyses are  
270 provided as supplementary Excel/Prism files.

271  
272  
273  
274  
275  
276  
277  
278  
279  
280  
281  
282  
283  
284  
285  
286  
287  
288  
289  
290  
291  
292  
293

**Molecular biology**

EGFP tags are based on pcDNA3-EGFP or pUAST-EGFP. All *Drosophila melanogaster* efa6 constructs are based on cDNA clone IP15395 (Uniprot isoform C, intron removed). *Caenorhabditis elegans* efa-6 (Y55D9A.1a) constructs are derived from pCZGY1125-efa-6-pcr8 (kindly provided by Andrew Chisholm). *Homo sapiens* PSD1 (ENST00000406432.5, isoform 202) constructs were PCR-amplified from pLC32-hu-psd1-pcr8 vector (kindly provided by Andrew Chisholm). *Homo sapiens* PSD2 (ENST00000274710.3, isoform 201, 771aa) constructs were PCR-amplified from pLC33-hu-psd2-pcr8 vector (kindly provided by Andrew Chisholm). *Homo sapiens* PSD3 was PCR-amplified from pLC34 hu-psd3-pcr8 vector (kindly provided Andrew Chisholm). Note that the PSD3 cDNA clone is most closely related to isoform 201 (ENST00000286485.12: 513aa) and therefore lacks the putative N-terminus found in isoform 202 (ENST00000327040.12). However, the putative MTED core sequence is encoded in the C-terminal PH domain (Fig.2C), not the potential N-terminus. *Homo sapiens* PSD4 (ENST00000441564.7, isoform 205) was PCR-amplified from pLC35-hu-psd4-pcr8 vector (kindly provided by Andrew Chisholm). The CAAX motif is derived from human KRAS. The *DmEfa6*-Nterm $\Delta$ SxiP::EGFP (aa1-410) insert was synthesised by GeneArt Express (ThermoFisher). All construct were cloned using standard (SOE) PCR/ligation based methods, and constructs and inserts are detailed in Table T1. To generate transgenic fly lines, *P[acman]M-6-attB-UAS-1-3-4* constructs were integrated into *PBac{yellow[+]attP-3B}VK00031* (Bloomington line #9748) via PhiC31 mediated recombination (outsourced to Bestgene Inc.).

final vector	Source	insert
<i>pcDNA3-EGFP</i>	Addgene	<i>XhoI</i> -EGFP- <i>XbaI</i>
<i>pUAST-Ascl-Pacl-EGFP</i>	this study	<i>KpnI, Ascl, Pacl</i> -EGFP- <i>XbaI</i>
<i>pUAST-DmEfa6FL-EGFP (aa1-1387)</i>	this study	<i>KpnI, Ascl-kozak</i> -Efa6 (aa1-1387)- <b>GSGSGS-EGFP</b> - <i>Pacl, XbaI</i>
<i>P[acman]M-6-attB-UAS-1-3-4-DmEfa6FL-EGFP (aa1-1387)</i>	this study	<i>Ascl-kozak</i> - <i>DmEfa6</i> (aa1-1387)- <b>GSGSGS-EGFP</b> - <i>Pacl</i>
<i>pcDNA3.1-DmEfa6FL-EGFP (aa1-1387)</i>	this study	<i>KpnI, Ascl-kozak</i> - <i>DmEfa6</i> (aa1-1387)- <b>GSGSGS-EGFP</b> - <i>Pacl, XbaI</i>
<i>pUAST-DmEfa6<math>\Delta</math>Cterm-EGFP (aa1-894)</i>	this study	<i>KpnI, Ascl-kozak</i> - <i>DmEfa6<math>\Delta</math>Cterm</i> (aa1-894)- <b>GSGSGS-EGFP</b> - <i>Pacl, XbaI</i>
<i>P[acman]M-6-attB-UAS-1-3-4-DmEfa6<math>\Delta</math>Cterm-EGFP (aa1-894)</i>	this study	<i>Ascl-kozak</i> - <i>DmEfa6<math>\Delta</math>Cterm</i> (aa1-894)- <b>GSGSGS-EGFP</b> - <i>Pacl</i>
<i>pcDNA3.1-DmEfa6<math>\Delta</math>Cterm-EGFP (aa1-894)</i>	this study	<i>KpnI, Ascl-kozak</i> - <i>DmEfa6<math>\Delta</math>Cterm</i> (aa1-894)- <b>GSGSGS-EGFP</b> - <i>Pacl, XbaI</i>
<i>pUAST-DmEfa6-Nterm-EGFP (aa1-410)</i>	this study	<i>KpnI, Ascl-kozak</i> - <i>DmEfa6-Nterm</i> (aa1-410)- <b>GSGSGS-EGFP</b> - <i>Pacl, XbaI</i>
<i>P[acman]M-6-attB-UAS-1-3-4-DmEfa6-Nterm-EGFP (aa1-410)</i>	this study	<i>Ascl-kozak</i> - <i>DmEfa6-Nterm</i> (aa1-410)- <b>GSGSGS-EGFP</b> - <i>Pacl</i>
<i>pcDNA3.1-DmEfa6-Nterm-EGFP (aa1-410)</i>	this study	<i>KpnI, Ascl-kozak</i> - <i>DmEfa6-Nterm</i> (aa1-410)- <b>GSGSGS-EGFP</b> - <i>Pacl, XbaI</i>
<i>pUAST-DmEfa6-Nterm-CAAX-EGFP (aa1-410)</i>	this study	<i>KpnI, Ascl-kozak</i> - <i>DmEfa6-Nterm</i> (aa1-410)- <b>GSGSGS-EGFP-CAAX[KRAS]</b> - <i>Pacl, XbaI</i>
<i>P[acman]M-6-attB-UAS-1-3-4-DmEfa6-Nterm-CAAX-EGFP (aa1-410)</i>	this study	<i>Ascl-kozak</i> - <i>DmEfa6-Nterm</i> (aa1-410)- <b>GSGSGS-EGFP-CAAX[KRAS]</b> - <i>Pacl</i>
<i>pcDNA3.1-DmEfa6-Nterm-CAAX-EGFP (aa1-410)</i>	this study	<i>KpnI, Ascl-kozak</i> - <i>DmEfa6-Nterm</i> (aa1-410)- <b>GSGSGS-EGFP-CAAX[KRAS]</b> - <i>Pacl, XbaI</i>

<b>pUAST-DmEfa6-Nterm<math>\Delta</math>SxiP-EGFP (aa1-410)</b>	this study	<u><i>KpnI, AscI-kozak-DmEfa6-Nterm<math>\Delta</math>SxiP (aa1-410; SQIP&gt;AAAA; SRIP&gt;AAAA)-GSGSGS-EGFP-Pacl, XbaI</i></u>
<b>pcDNA3.1-DmEfa6-Nterm<math>\Delta</math>SxiP-EGFP (aa1-410)</b>	this study	<u><i>KpnI, AscI-kozak-DmEfa6-Nterm<math>\Delta</math>SxiP (aa1-410; SQIP&gt;AAAA; SRIP&gt;AAAA)-GSGSGS-EGFP-Pacl, XbaI</i></u>
<b>pUAST-DmEfa6-Nterm<math>\Delta</math>MTED-EGFP (aa1-300)</b>	this study	<u><i>KpnI, AscI-kozak-DmEfa6-Nterm<math>\Delta</math>MTED (aa1-300)-GSGSGS-EGFP-Pacl, XbaI</i></u>
<b>pcDNA3.1-DmEfa6-Nterm<math>\Delta</math>MTED-EGFP (aa1-300)</b>	this study	<u><i>KpnI, AscI-kozak-DmEfa6-Nterm<math>\Delta</math>MTED (aa1-300)-GSGSGS-EGFP-Pacl, XbaI</i></u>
<b>pUAST-DmEfa6<math>\Delta</math>Nerm-EGFP (aa851-1387)</b>	this study	<u><i>KpnI, AscI-kozak-DmEfa6<math>\Delta</math>Nerm (aa851-1387)-GSGSGS-EGFP-Pacl, XbaI</i></u>
<b>pcDNA3.1-DmEfa6<math>\Delta</math>Nerm-EGFP (aa851-1387)</b>	this study	<u><i>KpnI, AscI-kozak-DmEfa6<math>\Delta</math>Nerm (aa851-1387)-GSGSGS-EGFP-Pacl, XbaI</i></u>
<b>pUAST-DmEfa6-MTED-EGFP (aa322-341)</b>	this study	<u><i>KpnI, AscI-kozak-DmEfa6-MTED (aa322-341)-GSGSGS-EGFP-Pacl, XbaI</i></u>
<b>pcDNA3.1-DmEfa6-MTED-EGFP (aa322-341)</b>	this study	<u><i>KpnI, AscI-kozak-DmEfa6-MTED (aa322-341)-GSGSGS-EGFP-Pacl, XbaI</i></u>
<b>pcDNA3.1-CeEfa6-FL-EGFP (aa1-816)</b>	this study	<u><i>KpnI, AscI-kozak-CeEfa6 (aa1-816)-GSGSGS-EGFP-Pacl, XbaI</i></u>
<b>pcDNA3.1-CeEfa6-Nterm-EGFP (aa1-152)</b>	this study	<u><i>KpnI, AscI-kozak-CeEfa6-Nterm (aa1-152)-GSGSGS-EGFP-Pacl, XbaI</i></u>
<b>pcDNA3.1-CeEfa6-MTED-EGFP (aa24-42)</b>	this study	<u><i>KpnI, AscI-kozak-CeEfa6-MTED (aa24-42)-GSGSGS-EGFP-Pacl, XbaI</i></u>
<b>pcDNA3.1-HsPSD1-FL-EGFP (aa1-1024)</b>	this study	<u><i>KpnI, AscI-kozak-HsPSD1 (aa1-1024)-GSGSGS-NotI-EGFP-Pacl, XbaI</i></u>
<b>pcDNA3.1-HsPSD1-Nterm-EGFP (aa1-280)</b>	this study	<u><i>KpnI, AscI-kozak-HsPSD1-Nterm (aa1-280)-GSGSGS-NotI-EGFP-Pacl, XbaI</i></u>
<b>pcDNA3.1-HsPSD1-MTED-EGFP (aa31-49)</b>	this study	<u><i>KpnI, AscI-kozak-HsPSD1-MTED (aa31-49)-GSGSGS-NotI-EGFP-Pacl, XbaI</i></u>
<b>pcDNA3.1-HsPSD2-FL-EGFP (aa1-771)</b>	this study	<u><i>KpnI, AscI-kozak-HsPSD2 (aa1-771)-GSGSGS-NotI-EGFP-Pacl, XbaI</i></u>
<b>pcDNA3.1-HsPSD3-EGFP (aa515-1047)</b>	this study	<u><i>KpnI, AscI-kozak-HsPSD3 (aa515-1047)-GSGSGS-NotI-EGFP-Pacl, XbaI</i></u>
<b>pcDNA3.1-HsPSD4-FL-EGFP (aa1-1027)</b>	this study	<u><i>KpnI, AscI-kozak-HsPSD4 (aa1-1027)-GSGSGS-NotI-EGFP-Pacl, XbaI</i></u>
<b>pcDNA3.1-co-HsPSD1-MTED-EGFP (aa31-49)</b>	this study	<u><i>KpnI, AscI-kozak-HsPSD1-MTED (aa31-49)-GSGSGS-EGFP-Pacl, XbaI</i></u>
<b>pcDNA3.1-co-CeEfa6-MTED-EGFP (aa24-42)</b>	this study	<u><i>KpnI, AscI-kozak-CeEfa6-MTED (aa24-42)-GSGSGS-EGFP-Pacl, XbaI</i></u>
<b>pcDNA3.1-co-DmEfa6-MTED-EGFP (aa322-341)</b>	this study	<u><i>KpnI, AscI-kozak-DmEfa6-MTED (aa322-341)-GSGSGS-EGFP-Pacl, XbaI</i></u>
<b>pCS107-DmEfa6-Nterm-EGFP</b>	this study	<u><i>NotI-kozak-DmEfa6-Nterm (aa1-410)-GSGSGS-EGFP-StuI</i></u>
<b>RFP (Xenopus injection)</b>	tba	tba
<b>pFastBac-His6-MCAK-EGFP-StrepII</b>	tba	His6-MCAK::EGFP-StrepII
<b>pFastBac-His6-DmEfa6<math>\Delta</math>Cterm-EGFP-StrepII (aa1-894)</b>	this study	His6-DmEfa6 $\Delta$ Cterm::EGFP-StrepII (aa1-894)

294 **Tab. T1.** co=codon optimised; *Dm*=*Drosophila melanogaster*; *Ce*=*Caenorhabditis elegans*;  
 295 *Hs*=*Homo sapiens*

296

297 *In silico* analyses

298 To generate the **phylogenetic tree** of Efa6/PSD full length isoforms and N-terms of different  
 299 species (see Fig. S1), their amino acid sequences were aligned using Muscle or ClustalO  
 300 (Goujon et al., 2010; McWilliam et al., 2013; Sievers et al., 2011). ProtTest (Abascal et al.,



2005; Darriba et al., 2011) was used to determine amino acid frequencies in the protein datasets and to identify the optimal amino acid substitution model to be used for the Bayesian inference (VT+I+G+F). CUDA-Beagle-optimised MrBayes (Ronquist et al., 2012) was run using the VT+I+G+F model [prset statefreqpr=fixed(empirical); lset rates=invgamma] using 5 chains (1 heated) and 9 parallel runs until the runs converged and standard deviation of split frequencies were below 0.015 (0.06 for N-terms); PSRF+ was 1.000 and min ESS was >1300 for the TL, alpha and pinvar parameters. The *Drosophila melanogaster* Sec7-PH domain-containing protein Steppke was used as outgroup in the full length tree. Archaeopteryx (Han and Zmasek, 2009) was used to depict the MrBayes consensus tree showing branch lengths (amino acid substitutions per site) and Bayesian posterior probabilities.

To identify a potential MTED in PSD1, previously identified Efa6 MTED motifs (O'Rourke et al., 2010) of 18 orthologues were aligned to derive an amino acid logo. Further orthologues were identified and used to refine the logo. Invariant sites and sites with restricted amino acid substitutions were determined (most prominently MxG-stretch). Stretches containing the invariant MxG stretch were aligned among vertebrate species to identify potential candidates. Berkley's Weblogo server (Crooks et al., 2004) was used to generate amino acid sequence logos for each phylum using MTED (ExxxMxGE/D) and MTED-like (MxGE/D) amino acid stretches.

319

#### In vitro analyses

**Protein Expression and Purification:** *Drosophila* Efa6- $\Delta$ Cterm was cloned into a modified pFastBac vector containing an N-terminal His6 tag and C-terminal eGFP and StrepII tags. Recombinant protein was expressed in Sf9 insect cells for 72 hours using a *Baculovirus* system. The protein was purified via a two-step protocol of Ni-affinity using a 1ml His-Trap column (GE Healthcare) in Ni-affinity buffer [50 mM Tris pH 7.5, 300 mM NaCl, 1mM Mg Cl<sub>2</sub>, 10 % (v/v) glycerol] and elution with 200mM imidazole, followed by Step-tag affinity chromatography using StepTactin resin (GE Healthcare) in BRB20, 75mM KCl, 0.1% Tween 20, 10% (v/v) glycerol and elution with 5mM desthiobiotin. MTED peptide (Genscript) was shipped as lyophilised powder with a purity of 95.2%. Upon arrival peptide was dissolved in ultrapure water and used directly.

**MT binding assays:** GMPCPP-stabilised, rhodamine-labeled MTs were adhered to the surface of flow chambers (Helenius et al., 2006). 20 nM Efa6- $\Delta$ Cterm::GFP (in BRB20 pH 6.9, 75mM KCl, 0.05% Tween20, 0.1 mg/ml BSA, 1% 2-mercaptoethanol, 40mM glucose, 40 mg/ml glucose oxidase, 16 mg/ml catalase) or 20 nM MCAK::GFP (in the same buffer plus 1 mM ATP and 1 mM taxol) was introduced to the MT-containing channel. Images were recorded using a Zeiss Observer.Z1 microscope equipped with a Zeiss Laser TIRF 3 module, QuantEM 512SC EMCDD camera (Photometrics) and 100x objective (Zeiss, alphaPlanApo/1.46NA oil). Images of rhodamine-labeled MTs using a lamp as the excitation source and GFP fluorescence using TIRF illumination via a 488 nm laser were collected as described (Patel et al., 2016). For both rhodamine and GFP imaging an exposure time of 100 ms was used. The mean GFP intensity on individual MTs was determined from the mean pixel intensity of lines drawn along the long-axis of individual microtubules in Fiji (Schindelin et al., 2012). The rhodamine signal was used to locate the position of MTs in the GFP images. Intensity from a region of background was subtracted.

**MT depolymerisation assays:** GMPCPP-stabilised, rhodamine-labelled MTs were adhered to the surface of flow chambers (Helenius et al., 2006). Images of a field of fluorescent

347 microtubules were recorded using a Zeiss Observer.Z1 microscope, collecting 1 image every  
348 5 s with an exposure time of 100 ms. Efa6- $\Delta$ Cterm::GFP (14 nM), MCAK (40 nM) in solution  
349 (BRB20 pH 6.9, 75mM KCl, 1mM ATP, 0.05% Tween 20, 0.1 mg/ml BSA, 1% 2-  
350 mercaptoethanol, 40mM glucose, 40 mg/ml glucose oxidase, 16 mg/ml catalase) were added  
351 to the channel 1 min after acquisition had commenced. Depolymerisation rates were  
352 determined from plots of the length of individual microtubules versus time, obtained by  
353 thresholding and particle analysis of images using Fiji (Schindelin et al., 2012).

354 **Xenopus oocyte assays:** cytosol extracts from *Xenopus* oocytes were obtained as described  
355 in (Allan and Vale, 1991). **MT depolymerisation** was assessed in a microscopic flow  
356 chamber (Vale and Toyoshima, 1988) where *Xenopus* cytosol (1  $\mu$ l cytosol diluted with 20  $\mu$ l  
357 acetate buffer) was incubated for 20 min to allow MTs to polymerise. Then cytosol was  
358 exchanged by flow through with Efa6- $\Delta$ Cterm::GFP, MCAK or synthetic MTED peptide (all 20  
359 nM in acetate buffer pH 7.4: 100 mM K-Acetate, 3 mM Mg-Acetate, 5 mM EGTA, 10 mM  
360 HEPES), and MT length changes observed by recording 10 random fields via VE-DIC  
361 microscopy (Allan, 1993; Allan and Vale, 1991). **MT polymerisation** was analysed in a  
362 microscope flow cell containing 9  $\mu$ l diluted *Xenopus* cytosol (see above) to which 1  $\mu$ l acetate  
363 buffer was added, either alone or containing 20nM MTED. After 10 min, 20 random fields were  
364 recorded via VE-DIC microscopy for each condition and the numbers of MTs per field counted.

365 For the *in vivo* assay, *Xenopus* embryos were injected in one blastomere at the 4-cell stage  
366 with 200 ng of mRNA encoding Efa6-Nterm::GFP or mCherry alone. The embryos were  
367 imaged at stage 10.25 (Heasman, 2006) with a Leica fluorescent stereoscope.

#### 368 **Microtubule growth assays**

369 30 $\mu$ M porcine brain tubulin (25% rhodamine-labelled) was incubated in 80mM PIPES pH6.9,  
370 5mM MgCl<sub>2</sub>, 1mM EGTA, 5% DMSO and 1mM GTP at 37°C for 30min in the presence of  
371 either no peptide, 30 $\mu$ M MTED peptide or 300 $\mu$ M MTED peptide. The reactions were then  
372 diluted 60-fold into BRB80 buffer (80mM PIPES pH6.9, 1mM MgCl<sub>2</sub>, 1mM EGTA) containing  
373 1mM taxol. Samples were added to channels constructed from poly-lysine coated cover  
374 glasses, washed with BRB80, 1mM taxol and imaged by fluorescence microscopy.

#### 375 **Tubulin pull-down assays**

376 MTED peptide was coupled to cyanogen bromide-activated Sepharose beads (GE  
377 Healthcare). 30 $\mu$ M porcine brain tubulin was incubated with either peptide-coated or uncoated  
378 Sepharose beads in BRB80, 0.2% Tween 20 for 30mins at 20°C. The beads were washed  
379 three times with a 2:1 v/v ratio of BRB80, 0.2% Tween 20 to beads. An equal volume of 2x  
380 Laemmli buffer was added to the washed beads, incubated at 90°C for 5min, spun down and  
381 supernatant run on a 12% SDS-PAGE gel.

382

383

## 384 **Results**

385

### 386 Efa6 is widely expressed in *Drosophila* neurons and restricts axonal growth

387 To evaluate the function of Efa6 in neurons, we first determined its expression in the nervous  
388 system. We used a genomically engineered fly line in which the endogenous *Efa6* gene was  
389 GFP-tagged (*Efa6-GFP*; Huang et al., 2009). These animals widely express Efa6::GFP  
390 throughout the CNS at larval and adult stages (Fig. 1F-I). We cultured primary neurons from

391 this fly line to analyse the subcellular distribution of Efa6. In young neurons at 6 hrs *in vitro*  
392 (6HIV) and in mature neurons at 5 days *in vitro* (5DIV), Efa6 was localised throughout cell  
393 bodies and axons (Fig. 1B, E).

394 We next determined whether *Drosophila* Efa6 has an impact on axon growth, using fly lines  
395 with decreased or abolished Efa6 expression: Efa6 knock-down (*Efa6-RNAi*), overlapping  
396 deficiencies uncovering the entire *Efa6* gene locus (*Efa6<sup>Def</sup>*), or different loss-of-function  
397 mutant alleles generated by genomic engineering (*Efa6<sup>KO#1</sup>*, *Efa6<sup>GX6[w-]</sup>*, *Efa6<sup>GX6[w+]</sup>*). In all  
398 these conditions, axon length at 6 HIV was increased compared to wild-type by at least 20%  
399 (Fig. 2D).

400 We then tested whether over-expression of Efa6 would cause the opposite effect, i.e. axon  
401 shortening or even loss. For this, we generated a transgenic *UAS-Efa6-FL-GFP* line and, in  
402 addition, developed methods to transfect *UAS*-constructs into *Drosophila* primary neurons  
403 (see Methods). When expressed pan-neuronally transgenic or transfected full-length *Efa6-  
404 FL::GFP* localised to cell bodies, axons and growth cones of primary neurons, as similarly  
405 observed with the endogenous protein (Figs.1B,C, S3B). The transgenic expression caused a  
406 ~20% reduction in axon length, which was increased to ~50% upon transfection (likely due to  
407 higher copy numbers of the expression construct ;Fig. 2C, D). Furthermore, we observed an  
408 increase in the number of neurons without axons from ~26% in *UAS-GFP*-transfected controls  
409 to ~43% in *Efa6-FL::GFP*-positive neurons (Fig.3B).

410 Together, these results suggest that Efa6 restricts axonal growth, comparable to reports for *C.  
411 elegans* Efa6 (*CeEfa6*; Chen et al., 2015; Chen et al., 2011). The loss of whole axons upon  
412 *Efa6-FL::GFP* over-expression might suggest that Efa6 performs its morphogenetic roles by  
413 inhibiting MTs.

414

#### 415 Efa6 eliminates peripheral or even entire MT networks in mouse fibroblasts

416 To assess whether the negative impact of Efa6 on axon outgrowth might be through inhibiting  
417 MTs, we used NIH3T3 mouse fibroblasts as a heterologous cell system known to provide  
418 meaningful readouts for functional studies of *Drosophila* MT regulators (Alves-Silva et al.,  
419 2012; Beaven et al., 2015). When fibroblasts were analysed 24 hrs after transfection with  
420 *Efa6-FL-GFP*, we found a graded depletion of MT networks depending on *Efa6-FL::GFP*  
421 protein levels (shown and quantified in Fig.S5). At moderate expression levels, *Efa6-FL::GFP*  
422 localised along the circumference and in areas of membrane folds (open arrow heads in  
423 Figs.S5B), and MTs tended to be lost predominantly from the cell fringes (curved arrows in  
424 Figs.S5B and S7B). At high expression levels, *Efa6-FL::GFP* became detectable in the  
425 cytoplasm and even nucleus (double-chevrons in Fig.S5C), suggesting that membrane-  
426 association might become saturated. In these cases, MTs were completely absent (Fig.S5C).  
427 When quantifying these MT phenotypes across all transfected fibroblasts, there was a strong  
428 increase in MT network defects and depletion upon *Efa6-FL::GFP* expression as compared to  
429 *GFP* controls (Fig. 3B).

430 When performing live analyses, we consistently observed that growing MTs labelled with  
431 EB3::mCherry extended to the very cell fringes of control fibroblasts (Suppl. Movie M1),  
432 whereas MTs in fibroblasts transfected with *Efa6-FL::GFP* showed a very different behaviour:  
433 hardly any MTs polymerised into areas along the rim where Efa6 was enriched but stopped at  
434 the border, often accompanied by *Efa6-FL::GFP* accumulation at MT plus ends at the  
435 invasion site (Suppl. Movie M2).

436 Taken together, also these data suggest that Efa6 inhibits MTs. The fibroblast experiments  
437 suggest that Efa6 is membrane-associated and excludes MTs from this position, and the  
438 studies in fly neurons indicate the relevance of such functions for neuronal morphogenesis.  
439 The combined use of mouse fibroblasts and *Drosophila* primary neurons provides therefore a  
440 robust system with informative readouts for MT loss - ideal to carry out a systematic structure-  
441 function analysis of Efa6.

442

#### 443 The N-terminal 18aa motif of Efa6 is essential for microtubule-inhibiting activity of Efa6

444 A detailed analysis of the domain structures of Efa6 proteins from 30 species revealed that C-  
445 termini of almost all species contain a putative pleckstrin homology domain (PH; potentially  
446 membrane-associating; Macia et al., 2008), a Sec7 domain (potentially activating Arf  
447 GTPases; D'Souza-Schorey and Chavrier, 2006; Huang et al., 2009) and a coiled-coil (CC)  
448 domain (Franco et al., 1999; Figs.3A, S2). In contrast, the N-termini are mainly unstructured  
449 and reveal enormous length differences among species. Accordingly, phylogenetic  
450 relationship analyses comparing either full-length or N-terminal Efa6, show that chordate  
451 proteins are rather distant from invertebrates, and that arthropods form a clear subgroup  
452 within the invertebrates (Fig. S1A,B). None of the identifiable N-terminal domains/motifs is  
453 particularly well conserved (details in Fig.S2). For example, the *Drosophila* N-terminus  
454 contains (1) a putative PDZ domain (aa16-88; mainly found in insect versions of Efa6), (2) two  
455 SxIP motifs (aa 233-6 and 262-5; found primarily in Efa6 of flies, some other insects and  
456 molluscs; some vertebrate/mammalian species display derived SxLP motifs), and (3) a motif  
457 of 18aa displaying 89% similarity with a motif in the N-terminus of CeEfa6 suggested to be  
458 involved in MT inhibition (O'Rourke et al., 2010; conserved in nematodes, arthropods and  
459 molluscs).

460 To assess potential roles of the *Drosophila* 18aa motif (from now on referred to as MT  
461 elimination domain, MTED), we generated a series of GFP-tagged N-terminal constructs  
462 (Fig.3B): *Efa6-ΔCterm-GFP* (encoding the entire N-terminal half upstream of the Sec7  
463 domain), *Efa6-Nterm-GFP* (restricting to the N-terminal part containing all the identified  
464 functional domains), *Efa6-Nterm<sup>ΔMTED</sup>-GFP* (lacking the MTED) and *Efa6-MTED-GFP*  
465 (encoding only the MTED). All these N-terminal Efa6 variants showed the same localisation  
466 pattern throughout neurons (Fig.S3C,D,F,G), and in the cytoplasm and nucleus of fibroblasts  
467 (Fig.S4C,D,F,G). Cytoplasmic and nuclear localisations occurred even at low expression  
468 levels, indicating that the absent C-terminus (and likely PH domain within) usually mediates  
469 membrane association. This nuclear localisation occurs in the absence of any predicted N-  
470 terminal nuclear localisation sequences (Figs.3A, S2A), likely reflecting a known artefact of  
471 GFP-tagged proteins (Alves-Silva et al., 2012; Seibel et al., 2007).

472 In spite of their very similar localisation patterns, the functional impact of these constructs was  
473 clearly MTED-dependent: only constructs containing the MTED (*Efa6-ΔCterm::GFP*, *Efa6-  
474 Nterm::GFP* and *Efa6-MTED::GFP*) caused strong axon loss in neurons and MT network  
475 depletion in fibroblasts, whereas *Efa6-Nterm<sup>ΔMTED</sup>::GFP* behaved like GFP controls (Figs.3B;  
476 S3C,D,F,G; S7C,D,G,H).

477 In addition, we assessed potential roles of the two SxIP sites predicted to bind EB proteins  
478 (Honnappa et al., 2009; Fig.3A). Accordingly, we found that *Efa6-Nterm::GFP* tip-tracks and  
479 that *Efa6-FL::GFP* accumulates at sites where EB3-enriched MTs get in contact (Suppl. Mov.  
480 M2 and 3). Such binding to EBs at MT plus ends, might enhance Efa6's ability to capture MTs  
481 for inhibition. However, when replacing each of the two SxIP motifs by four alanines (*Efa6-*

482 Nterm<sup>ΔSxIP</sup>::GFP), the construct still induced a strong axon loss and MT network depletion in  
483 fibroblasts (Figs.3B, S3E, S4E, S7F). Similar observations were reported for Kif2C, which  
484 clearly tip-tracks MTs through binding EB1, but does not require this property for its MT  
485 depolymerising activity (Moore et al., 2005).

486 Taken together, our results pinpoint the MTED as the key mediator of MT-depleting functions  
487 of *Drosophila* Efa6, suggesting this function to be conserved between flies and *C. elegans*.

488

#### 489 The MTED is a good predictor of MT-inhibiting function directly affecting MT polymerisation

490 To assess whether the MTED motif is a good predictor for MT-inhibiting capabilities of Efa6  
491 family members, we used 12 different constructs comprising: full length versions of (1)  
492 CeEfa6, (2) *Drosophila* Efa6 and (3-6) all four human PSDs (Fig. 3C), as well as N-terminal  
493 versions of (7) CeEfa6, (8) fly Efa6 and (9) human PSD1 (Fig. 3D). Furthermore, we deduced  
494 a MTED consensus sequence from 39 Efa6 genes (details in Fig. S2C), identified the most  
495 likely human MTED-like sequence (position 31-49aa of PSD1; MTED-core in Fig. 3A) and  
496 synthesised codon-optimised versions of (10) this human as well as the (11) fly and (12) worm  
497 MTEDs (Figs. S2B,C). When transfected into fibroblasts, we found that all 6 fly/worm  
498 constructs had strong MT-inhibiting properties, whereas none of the 6 human constructs  
499 (PSD1-4 full length, PSD1-Nterm, PSD1-MTED-like) showed MT collapse (Fig.3C-E).  
500 Therefore, the presence of a well conserved canonical MTED seems to be a good predictor  
501 for MT-inhibiting capabilities of Efa6 proteins.

502 To gain insights into the mechanisms through which MTEDs might act, we carried out a series  
503 of *in vitro* experiments. Purified Efa6-Nterm::GFP clearly associated with MTs *in vitro* (Fig.  
504 S8A), but failed to reconstitute any MT-inhibiting activity (Fig. S8B). We therefore tested the  
505 same protein in *Xenopus* oocyte extract to assess potential co-factor requirements, but saw  
506 again no activity (Fig. S8C) - in spite of the fact that injection of a corresponding mRNA into  
507 *Xenopus* oocytes caused strong cell division phenotypes (Fig. S8D,E). We suspected  
508 problems with recombinant expression of the protein, which is predicted to have large  
509 disordered regions, and instead used synthetic MTED peptide. We found that MTED-coated  
510 sepharose beads pulled down unpolymerised tubulin (Fig.4B), indicating a direct interaction of  
511 the peptide with tubulin. Furthermore, addition of synthetic MTED peptide to a MT growth  
512 assay, resulted in strong suppression of MT polymerisation in a dose-dependent manner  
513 (Fig.4A).

514 Taken together, the MTED exists primarily in Efa6 homologues of invertebrate species and its  
515 presence correlates with MT-inhibiting properties of these proteins. This conclusion is strongly  
516 supported by our finding that *Drosophila* MTED directly interferes with MT polymerisation,  
517 which can explain why MTs fail to enter Efa6-enriched areas in fibroblasts (Suppl. Mov. M2).

518

#### 519 The C-terminal domain restricts the microtubule-inhibiting activity of Efa6 to the cortex

520 Our structure-function analyses strongly suggested that Efa6 is membrane-associated. This is  
521 further supported by a membrane ruffle phenotype we observed in fibroblasts when  
522 expressing Efa6-FL::GFP or the C-terminal derivative Efa6-ΔNterm::GFP (Figs.3B; curved  
523 open arrows in Figs.S4B,H and S6B,D). Efa6-ΔNterm::GFP had no obvious effects on MT  
524 networks (Fig. S7I), and its membrane ruffling phenotype likely reflects an evolutionarily  
525 conserved function of the Efa6 C-terminus through its Sec7, PH and/or CC domains (Derrien  
526 et al., 2002; Franco et al., 1999; Macia et al., 2008). Accordingly, we find the same membrane

527 ruffling when expressing PSD1-FL::GFP (curved open arrows in Fig. S6E).

528 However, even if the C-terminus plays no active role in the MT inhibition process, it still  
529 regulates this function. This is suggested by the Efa6- $\Delta$ Cterm::GFP and Efa6-Nterm::GFP  
530 variants which lack the C-terminus (Fig.3B), fail to associate with the cortex (Fig.S4C,D,F,G),  
531 do not cause ruffling (Fig.S6C), but induce MT phenotypes far stronger than Efa6-FL::GFP  
532 does (Figs.3B; S7C,D,H vs B). To assess whether lack of membrane tethering could explain  
533 this phenotypic difference, we generated the Efa6-Nterm::GFP::CAAX variant (Fig.3B) where  
534 Efa6-Nterm::GFP is fused to the membrane-associating CAAX domain (Hancock et al., 1991);  
535 this addition of CAAX changed the properties of Efa6-Nterm::GFP back to Efa6-FL::GFP-like  
536 behaviours (Figs.3B; S4B,I; S7B,E): the hybrid protein localised to the cortex in fibroblasts  
537 and had only a moderate MT phenotype, and also the axon loss phenotype was mild. Also in  
538 live analyses, the CAAX construct reproduced the effect of excluding MTs from Efa6-N-  
539 term::GFP::CAAX-enriched areas (Suppl. Mov. M4). These findings confirm membrane  
540 tethering as an important regulatory feature restricting Efa6 function.

541 Taken together, our structure-function data clearly establish *Drosophila* Efa6 as a cortical  
542 collapse factor: its N-terminal MTED blocks polymerisation which of MTs at the cortex via the  
543 Efa6 C-terminus.

544

#### 545 Efa6 negatively regulates MT polymerisation at the growth cone membrane and in filopodia

546 We next asked how Efa6's cortical collapse function relates to the observed axon growth  
547 phenotypes. For this, we focussed on growth cones (GCs) as the sites where axons extend;  
548 this extension requires the splaying of MTs from the axonal bundle tip at the base of GCs to  
549 explore the actin-rich periphery (Dent et al., 2011; Lowery and van Vactor, 2009; Prokop et al.,  
550 2013).

551 In GCs of primary neurons at 6 HIV, loss of Efa6 caused an increase in MT polymerisation  
552 events: the total number of Eb1 comets was increased as compared to wild-type controls (Fig.  
553 5I). Eb1::GFP comets in *Efa6* mutant neurons frequently persisted when reaching the GC  
554 periphery, where they could occasionally be observed to undergo curved extensions along the  
555 periphery (Suppl. Mov. M7 and SM8). Comet velocity was unaffected ( $\sim 0.3 \mu\text{m/s}$ ), but the  
556 lifetime of Eb1::GFP comets was  $\sim 1.4$  times longer in mutant GCs, with the dwell time of Eb1  
557 comets at the tip of filopodia being increased from  $2.10\text{s} \pm 0.24 \text{ s}$  in wild-type to  $6.26\text{s} \pm$   
558  $0.40 \text{ s}$  in *Efa6* mutant neurons (Fig. 5M); we even observed cases where comets at the tips of  
559 filopodia were moving backwards, seemingly pushed back by the retracting filopodial tip  
560 (Suppl. Mov. M7 and M8). In agreement with the increased lifetime, more microtubules  
561 invaded growth cone filopodia in *Efa6* mutant neurons, as quantified by counting filopodia that  
562 contained EB1 comets or MTs (Fig.5D,E,J,K; note that the total number of filopodia per GC  
563 was in the range of 10-11 for both wild-type and *Efa6*; not shown). Transgenically expressed  
564 Efa6-FL::GFP caused the opposite effect, i.e. a reduction in the number of GC filopodia  
565 containing Eb1 comets or MTs (Fig. 5G-L; green columns).

566 Next, we investigated MT dynamics in axon shafts. In contrast to GCs, MTs in the axon shaft  
567 are organised into bundles, hence kept away from the membrane. Accordingly, neither loss-  
568 nor gain-of-function had an obvious effect on Eb1 comet numbers, lifetimes, velocities and  
569 directionalities (Fig. 6A-D). However, like in GCs, there was a strong increase in filopodia  
570 along the shaft that contained MTs when Efa6 was absent, and a strong decrease when over-  
571 expressing Efa6-FL::GFP (Fig. 6E-G).

572 Taken together, our data are consistent with a model in which *Efa6* primarily inhibits  
573 explorative MTs that leave the axon bundle in either GCs or axon shafts and polymerise  
574 towards the cell membrane or into filopodia. Surplus MTs in the periphery of GCs can explain  
575 the extra axonal growth we observed (Fig.2).

576

#### 577 *Efa6* negatively influences axon branching

578 We hypothesised that an increase in explorative MTs could also cause a rise in axon  
579 branching (see Introduction), either by inducing GC splitting through parallel growth events in  
580 the same GC (Acebes and Ferrus, 2000), or by seeding new collateral branches along the  
581 axon shaft (Kalil and Dent, 2014; Lewis et al., 2013). To test this possibility, we studied mature  
582 primary neurons at 5 days *in vitro* (DIV). We found that *Efa6*<sup>KO#1</sup> homozygous mutant neurons  
583 showed almost double the number of collateral branches as observed in wild-type neurons,  
584 whereas expression of *Efa6*-FL::GFP reduced branching by 21% (Fig.7A-C,E). This reduction  
585 is mediated by the *Efa6* N-terminus, since expression of *Efa6*-Nterm::GFP::CAAX caused a  
586 similar degree in branch reduction (Fig.7D,E).

587 To extend these studies to neurons *in vivo*, we studied dorsal cluster neurons, a subset of  
588 neurons with stereotypic axonal projections in the optic lobe of adult brains (Fig.7F-K, see  
589 Methods; Hassan et al., 2000; Voelzmann et al., 2016b). To manipulate *Efa6* levels in these  
590 neurons, either *Efa6*-RNAi or *Efa6*-FL-GFP was co-expressed with the membrane marker  
591 *myr-tdTomato*. Their axon branches were assessed in brains of young and old flies (2-5 d and  
592 15-18 d after eclosure from the pupal case, respectively; Figs.7F-K). We found that *Efa6*  
593 knock-down in dorsal cluster neurons caused a significant increase in branch numbers by 29%  
594 in young and by 38% in old brains, whereas over-expression of *Efa6*::GFP strongly decreased  
595 branch numbers by 33% in young and 28% in old brains, respectively (Fig.7L).

596 In these experiments, *Efa6*-FL::GFP expression had an intriguing further effect: Only 57% of  
597 young brains had any axons in the medulla region, compared to 88% in controls (Figs.7H,M,  
598 S9B). However, in the older *Efa6*-FL::GFP expressing fly brains, the axons were eventually  
599 present (Fig.7K,M, S9D). We concluded that this phenotype reflected delayed outgrowth,  
600 which is also consistent with the decrease in axon growth observed upon *Efa6* over-  
601 expression in primary neurons (green bars in Fig.2D).

602 Taken together, our data indicate a physiologically relevant role of *Efa6* as negative regulator  
603 of axonal branching, mediated through its N-terminus, most likely via its function as cortical  
604 collapse factor.

605

#### 606 *Efa6* maintains axonal MT bundle integrity in cultured neurons

607 Apart from changes in growth and branching, we noticed that a significant amount of *Efa6*-  
608 depleted neurons displayed axons with swellings where MTs lost their bundled conformation  
609 and were arranged into intertwined, criss-crossing curls instead (Fig.S10; arrowheads in Fig.  
610 8D-F). To quantify the strength of this phenotype, we measured the area of MT  
611 disorganisation relative to axon length (referred to as 'MT disorganisation index', MDI; Qu et  
612 al., 2017). MDI measurements in *Efa6* mutant neurons revealed a mild 1.3 fold increase in MT  
613 disorganisation in young neurons which gradually worsened to 2.3 fold at 5 DIV and ~4 fold at  
614 10 DIV (Fig.8A-F,I; all normalised to controls).

615 The observed gradual increase in phenotype could be the result of a genuine function of *Efa6*  
616 not only during axon growth but also their subsequent maintenance. Alternatively, it could be

617 caused by maternal gene product deposited in the mutant embryos by their heterozygous  
618 mothers (Prokop, 2013b); such maternal *Efa6* could mask mutant phenotypes at early stages  
619 so that they become apparent only after most Efa6 has degraded. To assess the latter  
620 possibility, we used a pre-culture strategy to remove potential maternal Efa6 (see Methods;  
621 Prokop et al., 2012; Sánchez-Soriano et al., 2010). When plating neurons after 5 days of pre-  
622 culture, we still found a low amount of MT disorganisation in young neurons and a subsequent  
623 gradual increase to severe phenotypes over the following days (Fig.8J).

624 This finding argues for a continued role of Efa6 in preventing MT disorganisation during  
625 development as well as in mature neurons. To further test this possibility, we used a  
626 temperature-based conditional knock-down technique (*elav-GAL4 UAS-Efa6-RNAi UAS-*  
627 *Gal80<sup>ts</sup>* abbreviated to *elav/Efa6<sup>IR</sup>/Gal80<sup>ts</sup>*; see Methods): the *elav/Efa6<sup>IR</sup>/Gal80<sup>ts</sup>* neurons  
628 were grown without knock-down (19°C) for 3 days, a stage at which they have long undergone  
629 synaptic differentiation (Küppers-Munther et al., 2004; Prokop et al., 2012); at that point, we  
630 found no difference in MT disorganisation between non-induced construct-bearing cells and  
631 control neurons (Fig. 8K). After this period, cells were grown for another four days under  
632 knock-down conditions (27°C), and then fixed on day seven. At this point, MT disorganisation  
633 in the *elav/Efa6<sup>IR</sup>/Gal80<sup>ts</sup>* neurons was significantly increased over control neurons (Fig. 8K),  
634 indicating that Efa6 is not only required during development but also during later maintenance  
635 to prevent MT disorganisation.

636 In contrast to increased MT disorganisation upon functional loss of Efa6, expression of Efa6-  
637 FL::GFP or Efa6-Nterm::GFP::CAAX showed a tendency to reduce MT disorganisation even  
638 below the baseline levels measured in control cells (cultured in parallel without the expression  
639 construct; Fig.8I), arguing that also this role of Efa6 is likely due to the cortical collapse  
640 function of Efa6 (see Discussion).

641

#### 642 *Efa6* maintains axonal MT bundle integrity *in vivo*

643 We then assessed whether a role of Efa6 in MT bundle maintenance is relevant *in vivo*. For  
644 this, we studied a subset of lamina neurons, which project prominent axons in the medulla of  
645 the adult optic lobe (Prokop and Meinertzhagen, 2006). We labelled MTs in these axons by  
646 expressing *α-tubulin84B-GFP* either alone (*GMR-tub* controls), or together with *Efa6<sup>RNAi</sup>* to  
647 knock down *Efa6* specifically in these neurons (*GMR-tub-Efa6<sup>IR</sup>*; see Methods for details).

648 When analysing aged flies at 26-27 days, we found that *Efa6* knock-down caused a doubling  
649 in the occurrence of axonal swellings with disorganised axonal MTs: the average of total  
650 swellings per column section was increased from 0.3 in controls to 0.65 swellings upon Efa6  
651 knock-down; about a third of these contained disorganised MTs (*GMR-tub-Efa6<sup>IR</sup>*: 0.23 per  
652 column section; *GMR-tub*: 0.13; Fig.9). These data demonstrated that our findings in cultured  
653 neurons are relevant *in vivo*.

654 We propose therefore that Efa6 provides a quality control mechanism that prevents MT  
655 disorganisation by inhibiting only MTs that have escaped axonal bundles. This model would  
656 also be consistent with the slow onset and gradual increase of MT disorganisation we  
657 observed upon Efa6 deficiency (Fig.8I,J).

658

#### 659 Efa6 and Shot promote MT bundles through complementary mechanisms

660 If Efa6 provides a quality control mechanism that "cleans up" explorative MTs, it should act



661 complementary to other factors that "prevent" explorative MTs by actively keeping them in  
662 axonal bundles. Very powerful preventive factors in both mammals and fly are the  
663 spectraplakins (Bernier and Kothary, 1998; Dalpe et al., 1998; Voelzmann et al., 2017). In  
664 *Drosophila*, spectraplakins are represented by the single *shot stop* (*shot*) gene; *shot*  
665 deficiency causes a severe increase in axonal off-track MTs and MT disorganisation (Alves-  
666 Silva et al., 2012; Qu et al., 2017; Sánchez-Soriano et al., 2009).

667 To study potential mutual enhancement of *Efa6* and *shot* mutant phenotypes, we first  
668 determined numbers of MTs in axonal shaft filopodia: both single-mutant conditions showed a  
669 strong enhancement of filopodial MTs (blue vs. orange bars in Fig.6F,G); this phenotype was  
670 substantially further increased in *shot*<sup>3</sup> *Efa6*<sup>GX6[w-]</sup> double-mutant neurons (orange/blue bars in  
671 Fig. 6F,G). *Vice versa*, when transfecting *Efa6-FL-GFP* to boost the hypothesised "cleaning-  
672 up" function, the *shot*<sup>3</sup> mutant phenotype was significantly improved (Fig. 6G).

673 We then tested whether this increase in off-track MTs would correlate with more MT  
674 disorganisation. At 6 HIV, *shot*<sup>3</sup> mutant neurons displayed a 2.4-fold, and *Efa6*<sup>GX6[w-]</sup> mutant  
675 neurons a 1.55-fold increase in MDI (normalised to wild-type); this value was dramatically  
676 increased to 6.16 fold in *shot*<sup>3</sup> *Efa6*<sup>GX6[w-]</sup> double mutant neurons (Fig. 8M). This strongly  
677 suggests that *Efa6* and *Shot* do not act through the same mechanism, but perform  
678 complementary roles in regulating and maintaining axonal MTs and MT bundles. This  
679 conclusion was further confirmed by our finding that transfection of *Efa6-FL-GFP* into *shot*<sup>3</sup>  
680 mutant neurons could alleviate the MDI phenotype (Fig. 8N).

681 Finally, we assessed whether these complementary relationships between *Shot* and *Efa6* are  
682 relevant *in vivo*. Since complete loss of *Shot* is an embryonically lethal condition, we first  
683 tested this in culture whether the lack of just one copy of *shot* has an enhancing effect on *Efa6*  
684 deficiency. We found that MT disorganisation phenotypes of *Efa6-RNAi* (blue bar in Fig.8L)  
685 and of *shot*<sup>3/+</sup> heterozygous mutant neurons (orange bar) at 6 HIV were clearly enhanced  
686 when both genetic manipulations were combined (orange/blue bar). When testing the same  
687 genetic constellations in our optic lobe model, we found that the originally observed increase  
688 in MT disorganisation caused by cell-autonomous knock-down of *Efa6* (black arrows and blue  
689 bar in Fig.9B,E) was also further enhanced when the same experiment was carried out in a  
690 *shot*<sup>3/+</sup> heterozygous mutant background (black arrows and orange/blue bar in Fig.9C,E).

691 These findings support our conclusion that there is a correlation between off-track MTs and  
692 MT disorganisation. Furthermore, they are consistent with a scenario where both *Shot* and  
693 *Efa6* regulate axonal MTs but through independent and complementary pathways: *Efa6*  
694 inhibits MTs at the cortex (with peripheral MTs persisting for longer if *Efa6* is absent), whereas  
695 *Shot* actively maintains MTs in bundles (with more MTs going off-track if *Shot* is absent) - and  
696 both these functions complement each other during MT bundle maintenance (see further  
697 details in the Discussion).

698

## 699 Discussion

### 700 Cortical collapse factors are important microtubule regulators relevant for axon morphology

701 Axons are the structures that wire our brain and body and are therefore fundamental to  
702 nervous system function. To understand how axons are formed during development, can be  
703 maintained in a plastic state thereafter, and why they deteriorate in pathological conditions, we  
704 need to improve our knowledge of axonal cell biology (Hahn et al., 2019). The MT bundles  
705 that form the core of axons are an essential aspect of this cell biology, and understanding how

706 these bundles are regulated and contribute to axon morphogenesis will provide essential  
707 insights into axon development and maintenance (Voelzmann et al., 2016a). Here we have  
708 addressed fundamental contributions made by cortical collapse factors. We started from  
709 reports that two such factors from distinct protein families both negatively impact on axon  
710 growth in species as diverse as *C. elegans* (CeEfa6; Chen et al., 2015; Chen et al., 2011) and  
711 mouse (Kif21A; van der Vaart et al., 2013).

712 We found that *DmEfa6* likewise acts as a negative regulator of axon growth. We demonstrate  
713 that fly Efa6 is a cortical collapse factor, inhibiting MTs primarily via the 18 aa long MTED.  
714 Since the MTED is the only shared motif with CeEfa6 in an otherwise entirely divergent N-  
715 terminus (Fig. 3C), this clearly demonstrates that the MTED is functionally conserved between  
716 both species (Chen et al., 2015; Chen et al., 2011; O'Rourke et al., 2010).

717 Capitalising on *Drosophila* neurons as a conceptually well-established model (Prokop et al.,  
718 2013; Voelzmann et al., 2016a), we went on to demonstrate two novel roles for Efa6: as a  
719 negative regulator of axon branching and a quality control factor maintaining MT bundle  
720 organisation. To perform these functions, Efa6 does not affect the dynamics of MTs contained  
721 within the central axonal bundles, but it inhibits mainly those MTs that leave these bundles  
722 (Fig.10A). By inhibiting explorative MTs in GCs, it negatively impacts on a key event  
723 underlying axon growth (explained below; yellow arrows in Fig.10C). By inhibiting off-track  
724 MTs in the axon shaft, it tones down the machinery that seeds new interstitial branches (red  
725 arrow in Fig.10C), but also prevents these MTs from going astray and cause MT  
726 disorganisation (curled MTs in Fig.10C).

727 Therefore, our work provides conceptual understanding of cortical collapse factors, which can  
728 explain how their molecular functions and subcellular roles in MT regulation link to their  
729 reported axonal growth phenotypes during development and regeneration (Chen et al., 2015;  
730 Chen et al., 2011; Heidary et al., 2008; van der Vaart et al., 2013), and to their additional  
731 functions in axon branching and maintenance reported here. Apart from existing links of  
732 cortical collapse factors to neurodevelopmental disorders (Heidary et al., 2008; Tiab et al.,  
733 2004; van der Vaart et al., 2013), we would therefore predict future links also to  
734 neurodegeneration.

735

### 736 Roles of Efa6 during axonal growth

737 During axon growth, MTs constantly polymerise towards the periphery of GCs; the advance of  
738 many of these MTs is inhibited at the leading edge, and our work shows that cortical collapse  
739 factors are key mediators to this end. Only a fraction of MTs enters filopodia, potentially  
740 helped by active guidance mechanisms such as MT-actin cross-linkage (e.g. through  
741 spectraplakins, tau, drebrin-EB3 ;Alves-Silva et al., 2012; Biswas and Kalil, 2018; Geraldo et  
742 al., 2008). The widely accepted protrusion-engorgement-consolidation model of axon growth  
743 proposes that stabilised MTs in filopodia can seed axon elongation events (Aletta and Greene,  
744 1988; Goldberg and Burmeister, 1986; Prokop et al., 2013). This model is consistent with our  
745 findings for Efa6. Thus loss of Efa6 can contribute to enhanced axon growth in two ways:  
746 firstly, through allowing more MTs to enter filopodia; secondly, by allowing them to dwell in  
747 filopodia for longer, thus enhancing the likelihood of their stabilisation (yellow arrows in  
748 Fig.10C). This scenario can explain why loss of *Efa6* in *C. elegans* improves axon re-growth  
749 after injury and growth overshoot during development (Chen et al., 2015; Chen et al., 2011),  
750 and why the upregulation of Kif21A levels in GCs causes stalled axon growth (van der Vaart  
751 et al., 2013).

752

753 Roles of Efa6 during axonal branching

754 As explained in the introduction, axon branching can occur via GC split, in that diverging MTs  
755 get stabilised in parallel in the same GC (Acebes and Ferrus, 2000; yellow arrows in Fig.10C).  
756 Alternatively, it can occur through interstitial branching which involves the active generation  
757 (e.g. through MT severing) and then stabilisation of off-track MTs (Kalil and Dent, 2014; Lewis  
758 et al., 2013; Tymanskyj et al., 2017; Yu et al., 2008). Both models agree with our observations  
759 in Efa6-deficient/over-expressing neurons: we find greater/lower numbers of MTs in GC and  
760 shaft filopodia at 6 HIV, which then correlate with enhanced/reduced axonal branch numbers  
761 in mature neurons (red arrow in Fig.10C).

762 If interstitial branch formation is negatively regulated by *Efa6*, this poses the question as to  
763 whether Efa6 has to be actively down-regulated in healthy neurons for branching to occur;  
764 Efa6 could either be physically removed from future branch points (Chen et al., 2015) or its  
765 MT inhibition function could be switched off. We believe that no such regulation is required  
766 because Efa6 seems to be in a well-balanced equilibrium. Enough Efa6 appears to be present  
767 to inhibit occasional, likely accidental off-track MTs; this capacity is surpassed when the  
768 number of off-track MTs is actively increased, for example through MT severing proteins  
769 during axonal branch formation (Yu et al., 2008). Such a saturation model is supported by our  
770 experiments with *shot* (Fig.6F,G): filopodial MT numbers are elevated in *shot* mutant neurons,  
771 although Efa6 is present and functional (as demonstrated by the further increase in filopodial  
772 MT numbers in *shot Efa6* double-mutant neurons; Fig.10D,E). This strongly suggests that  
773 Efa6 function occurs at a level that is easily saturated when increasing the number of  
774 explorative MTs.

775

776 Roles of Efa6 during axonal MT bundle maintenance

777 Axonal MT disorganisation in Efa6-deficient neurons occurs gradually and can even be  
778 induced by knock-down of Efa6 at mature stages (Fig.8K). Therefore, Efa6 appears to prevent  
779 MT disorganisation during axon development and maintenance, as is consistent with its  
780 continued expression in the nervous system (Fig.1). Such a continued role makes sense in a  
781 scenario where MT bundles remain highly dynamic throughout a neuron's lifetime, constantly  
782 undergoing polymerisation to drive renewal processes that prevent senescence (Hahn et al.,  
783 2019; Voelzmann et al., 2016a).

784 Based on these findings, we propose Efa6 to act as a quality control or maintenance factor  
785 within our model of "local axon homeostasis" (Hahn et al., 2019; Voelzmann et al., 2016a).  
786 This model states that MTs in the force-enriched environment of axons have a tendency to go  
787 off-track and curl up (Pearce et al., 2018), thus potentially seeding MT disorganisation.  
788 Different classes of MT-binding regulators, amongst them spectraplakins, prevent this by  
789 actively promoting the bundled conformation (Voelzmann et al., 2017). We propose that  
790 cortical collapse factors act complementary in that they do not actively maintain MTs in  
791 bundles, but inhibit those MTs that have escaped the bundling mechanisms (Hahn et al.,  
792 2019).

793 In this scenario, MTs are protected from cortical collapse as long as they are actively  
794 maintained in axonal bundles; this can explain the long known conundrum of how axonal MTs  
795 extend hundreds of micrometres in relative proximity to the cell cortex in axons, whereas in  
796 non-neuronal cells cortical proximity of MTs tends to trigger either their inhibition or tethered

797 stabilisation (Fukata et al., 2002; Kaverina et al., 1998).

798

### 799 Evolutionary and mechanistic considerations of Efa6 function

800 We found that the MTED motif correlates well with MT inhibiting functions of Efa6 family  
801 members, whereas the rest of the N-terminus bears no obvious further reminiscence. Our  
802 experiments with N-terminal protein and synthetic MTED peptide, both reveal association with  
803 MTs/tubulin. The MTED strongly interferes with MT polymerisation. Future co-crystallisation  
804 experiments are required to reveal how the MTED works. Given its small size we hypothesise  
805 that it simply blocks assembly, rather than acting via more complex mechanisms such as  
806 active promotion of depolymerisation (e.g. kinesin-8 and -13, XMap215; Al-Bassam and  
807 Chang, 2011; Brouhard and Rice, 2014) or severing (e.g. spastin, katanin, fidgetin; McNally  
808 and Roll-Mecak, 2018; Sharp and Ross, 2012).

809 In any case, the small size of MTEDs might come in handy as experimental tools to inhibit  
810 MTs, potentially displaying complementary properties to existing genetic tools such as the  
811 kinesin-13 Kif2C (Moore et al., 2005; Schimizzi et al., 2010), stathmin (Marklund et al., 1996)  
812 or spastin (Eckert et al., 2012). Importantly, the experiments with the CAAX domain have  
813 shown that Efa6's MT inhibiting function can be targeted to specific subcellular compartments  
814 clearing them of MTs, thus opening up a wide range of future applications.

815 Interestingly, the MT-inhibiting role of Efa6 seems not to be conserved in chordates (Fig.2A).  
816 However, roles of cortical collapse factors in neurons seem to have been taken over by other  
817 proteins such as the kinesin-4 family member Kif21A. The CFEOM1-linked Kif21A<sup>R954W</sup>  
818 mutation causes the protein to relocate from the axon shaft to the growth cone of cultured  
819 hippocampal neurons (van der Vaart et al., 2013). In consequence, increased Kif21A levels in  
820 GCs cause reduced axon growth - and we observed the same with Efa6 over-expression  
821 (green bars in Fig.2D). The decreased levels of Kif21A in proximal axons correlate with a local  
822 increase in side branches - and we observed the same with Efa6 loss of function (blue bars in  
823 Fig.7E, L).

824 Finally, we found that the C-terminal domains of Efa6 might display some degree of functional  
825 conservation. So far, work on mammalian PSDs has revealed functions for C-terminal  
826 domains in regulating ARF6, ARF1 or ARL14 during actin cytoskeletal reorganisation and  
827 membrane ruffling, tumour formation and immune regulation (Derrien et al., 2002; Paul et al.,  
828 2011; Pils et al., 2005). Our finding that PSD1 and C-terminal Efa6 constructs cause similar  
829 membrane ruffling phenotypes in fibroblasts (Figs.S4 and S6), suggests that some conserved  
830 functions reside in this region and might further contribute, together with N-terminally  
831 mediated MT inhibition, to the neuronal or non-neuronal defects that cause semi-lethality  
832 displayed by *Efa6* mutant flies (data not shown).

833

### 834 Conclusions and future perspectives

835 We propose that Efa6 acts as a cortical collapse factor which is important for the regulation of  
836 axonal MTs and relevant for axon growth, maintenance and branching. Although this function  
837 of Efa6 is evolutionarily not widely conserved, our findings provide a helpful paradigm for  
838 studies of other classes of cortical collapse factors also in mammalian neurons. Promising  
839 research avenues will be to refine our mechanistic understanding of how Efa6 blocks MT  
840 polymerisation, not only to better understand how it can be regulated in axons, but also to  
841 better exploit MTEDs as molecular tools in cell biological research.

842

## 843 Acknowledgements

844 This work was made possible through support by the BBSRC to A.P (BB/I002448/1,  
845 BB/P020151/1, BB/L000717/1, BB/M007553/1) to N.S.S. (BB/M007456/1) and KD  
846 (BB/J005983/1), by parents as well as the Faculty of Life Sciences to Y.Q., by the Leverhulme  
847 Trust to I.H. (ECF-2017-247) and by the German Research Council (DFG) to A.V. (VO  
848 2071/1-1). The Manchester Bioimaging Facility microscopes used in this study were  
849 purchased with grants from the BBSRC, The Wellcome Trust and The University of  
850 Manchester Strategic Fund. The Fly Facility has been supported by funds from The University  
851 of Manchester and the Wellcome Trust (087742/Z/08/Z). We thank Tom Millard and Marvin  
852 Bentley for very helpful comments on the manuscript, Simon Lowell for advice on the  
853 phylogenetic analyses, Hiro Ohkura for kindly providing DmEb1 antibody and Andrew  
854 Chisholm for the *C.elegans* Efa6 and human PSD constructs. Stocks obtained from the  
855 Bloomington *Drosophila* Stock Center (NIH P40OD018537) were used in this study.

856

## 857 References

858

- 859 Abascal, F., Zardoya, R., and Posada, D. (2005). ProtTest: selection of best-fit models of  
860 protein evolution. *Bioinformatics* 21, 2104-2105.
- 861 Acebes, A., and Ferrus, A. (2000). Cellular and molecular features of axon collaterals and  
862 dendrites. *Trends Neurosci* 23, 557-565.
- 863 Adalbert, R., and Coleman, M.P. (2012). Axon pathology in age-related neurodegenerative  
864 disorders. *Neuropathol Appl Neurobiol* 39, 90–108.
- 865 Al-Bassam, J., and Chang, F. (2011). Regulation of microtubule dynamics by TOG-domain  
866 proteins XMAP215/Dis1 and CLASP. *Trends Cell Biol* 21, 604-614.
- 867 Aletta, J.M., and Greene, L.A. (1988). Growth cone configuration and advance: a time-lapse  
868 study using video-enhanced differential interference contrast microscopy. *J Neurosci* 8,  
869 1425-1435.
- 870 Allan, V.J. (1993). Assay of membrane motility in interphase and metaphase *Xenopus*  
871 extracts. *Methods Cell Biol* 39, 203-226.
- 872 Allan, V.J., and Vale, R.D. (1991). Cell cycle control of microtubule-based membrane  
873 transport and tubule formation in vitro. *J Cell Biol* 113, 347-359.
- 874 Alves-Silva, J., Sánchez-Soriano, N., Beaven, R., Klein, M., Parkin, J., Millard, T., Bellen, H.,  
875 Venken, K.J.T., Ballestrem, C., Kammerer, R.A., et al. (2012). Spectraplakins promote  
876 microtubule-mediated axonal growth by functioning as structural microtubule-associated  
877 proteins and EB1-dependent +TIPs (Tip Interacting Proteins). *J Neurosci* 32, 9143-9158.
- 878 Beaven, R., Dzhindzhev, N.S., Qu, Y., Hahn, I., Dajas-Bailador, F., Ohkura, H., and Prokop,  
879 A. (2015). *Drosophila* CLIP-190 and mammalian CLIP-170 display reduced microtubule  
880 plus end association in the nervous system. *Mol Biol Cell* 26, 1491-1508.
- 881 Bernier, G., and Kothary, R. (1998). Prenatal onset of axonopathy in *Dystonia musculorum*  
882 mice. *Dev Genet* 22, 160-168.
- 883 Bettencourt da Cruz, A., Schwarzel, M., Schulze, S., Niyiyati, M., Heisenberg, M., and  
884 Kretschmar, D. (2005). Disruption of the MAP1B-related protein FUTSCH leads to  
885 changes in the neuronal cytoskeleton, axonal transport defects, and progressive  
886 neurodegeneration in *Drosophila*. *Mol Biol Cell* 16, 2433-2442.
- 887 Biswas, S., and Kalil, K. (2018). The microtubule-associated protein tau mediates the  
888 organization of microtubules and their dynamic exploration of actin-rich lamellipodia and  
889 filopodia of cortical growth cones. *J Neurosci* 38, 291-307.

- 890 Brouhard, G.J., and Rice, L.M. (2014). The contribution of  $\alpha\beta$ -tubulin curvature to microtubule  
891 dynamics. *J Cell Biol* 207, 323-334.
- 892 Calkins, D.J. (2013). Age-Related Changes in the Visual Pathways: Blame It on the AxonAge-  
893 Related Changes in the Visual Pathways. *Invest Ophthalmol Vis Sci* 54, ORSF 37-41.
- 894 Chen, L., Chuang, M., Koorman, T., Boxem, M., Jin, Y., and Chisholm, A.D. (2015). Axon  
895 injury triggers EFA-6 mediated destabilization of axonal microtubules via TACC and  
896 doublecortin like kinase. *eLife* 4, e08695.
- 897 Chen, L., Wang, Z., Ghosh-Roy, A., Hubert, T., Yan, D., O'Rourke, S., Bowerman, B., Wu, Z.,  
898 Jin, Y., and Chisholm, A.D. (2011). Axon regeneration pathways identified by systematic  
899 genetic screening in *C. elegans*. *Neuron* 71, 1043-1057.
- 900 Conde, C., and Caceres, A. (2009). Microtubule assembly, organization and dynamics in  
901 axons and dendrites. *Nat Rev Neurosci* 10, 319-332.
- 902 Crooks, G.E., Hon, G., Chandonia, J.M., and Brenner, S.E. (2004). WebLogo: a sequence  
903 logo generator. *Genome Res* 14, 1188-1190.
- 904 D'Souza-Schorey, C., and Chavrier, P. (2006). ARF proteins: roles in membrane traffic and  
905 beyond. *Nature Rev Molec Cell Biol* 7, 347.
- 906 Dalpe, G., Leclerc, N., Vallee, A., Messer, A., Mathieu, M., De Repentigny, Y., and Kothary, R.  
907 (1998). Dystonin is essential for maintaining neuronal cytoskeleton organization. *Mol Cell*  
908 *Neurosci* 10, 243-257.
- 909 Darriba, D., Taboada, G.L., Doallo, R., and Posada, D. (2011). ProtTest 3: fast selection of  
910 best-fit models of protein evolution. *Bioinformatics* 27, 1164-1165.
- 911 Debanne, D., Campanac, E., Bialowas, A., Carlier, E., and Alcaraz, G. (2011). Axon  
912 physiology. *Physiol Rev* 91, 555-602.
- 913 Dent, E.W., Gupton, S.L., and Gertler, F.B. (2011). The growth cone cytoskeleton in axon  
914 outgrowth and guidance. *Cold Spring Harb Perspect Biol* 3, a001800.
- 915 Derrien, V., Couillault, C., Franco, M., Martineau, S., Montcourrier, P., Houlgatte, R., and  
916 Chavrier, P. (2002). A conserved C-terminal domain of EFA6-family ARF6-guanine  
917 nucleotide exchange factors induces lengthening of microvilli-like membrane protrusions.  
918 *Journal of cell science* 115, 2867-2879.
- 919 Eckert, T., Le, D.T.-V., Link, S., Friedmann, L., and Woehlke, G. (2012). Spastin's  
920 microtubule-binding properties and comparison to katanin. *PLoS One* 7, e50161.
- 921 Elliott, S.L., Cullen, C.F., Wrobel, N., Kernan, M.J., and Ohkura, H. (2005). EB1 is essential  
922 during *Drosophila* development and plays a crucial role in the integrity of chordotonal  
923 mechanosensory organs. *Mol Biol Cell* 16, 891-901.
- 924 Fang, Y., and Bonini, N.M. (2012). Axon degeneration and regeneration: insights from  
925 *Drosophila* models of nerve injury. *Annu Rev Cell Dev Biol* 28, 575-597.
- 926 Franco, M., Peters, P.J., Boretto, J., van Donselaar, E., Neri, A., D'Souza-Schorey, C., and  
927 Chavrier, P. (1999). EFA6, a sec7 domain-containing exchange factor for ARF6,  
928 coordinates membrane recycling and actin cytoskeleton organization. *EMBO J* 18, 1480-  
929 1491.
- 930 Fukata, M., Watanabe, T., Noritake, J., Nakagawa, M., Yamaga, M., Kuroda, S., Matsuura, Y.,  
931 Iwamatsu, A., Perez, F., and Kaibuchi, K. (2002). Rac1 and Cdc42 capture microtubules  
932 through IQGAP1 and CLIP-170. *Cell* 109, 873-885.
- 933 Geraldo, S., Khanzada, U.K., Parsons, M., Chilton, J.K., and Gordon-Weeks, P.R. (2008).  
934 Targeting of the F-actin-binding protein drebrin by the microtubule plus-tip protein EB3 is  
935 required for neuritegenesis. *Nat Cell Biol* 10, 1181-1189.
- 936 Goldberg, D.J., and Burmeister, D.W. (1986). Stages in axon formation: observations of  
937 growth of *Aplysia* axons in culture using video-enhanced contrast-differential interference  
938 contrast microscopy. *J Cell Biol* 103, 1921-1931.

- 939 Goujon, M., McWilliam, H., Li, W., Valentin, F., Squizzato, S., Paern, J., and Lopez, R. (2010).  
940 A new bioinformatics analysis tools framework at EMBL-EBI. *Nucleic Acids Res* 38, W695-  
941 699.
- 942 Grieder, N.C., de Cuevas, M., and Spradling, A.C. (2000). The fusome organizes the  
943 microtubule network during oocyte differentiation in *Drosophila*. *Development* 127, 4253-  
944 4264.
- 945 Hahn, I., Fuss, B., Peters, A., Werner, T., Sieberg, A., Gosejacob, D., and Hoch, M. (2013).  
946 The *Drosophila* Arf GEF Steppke controls MAPK activation in EGFR signaling. *Journal of*  
947 *cell science* 126, 2470-2479.
- 948 Hahn, I., Voelzmann, A., Liew, Y.-T., Costa-Gomes, B., and Prokop, A. (2019). The model of  
949 local axon homeostasis - explaining the role and regulation of microtubule bundles in axon  
950 maintenance and pathology bioRxiv, 10.1101/577320
- 951 Han, M.V., and Zmasek, C.M. (2009). phyloXML: XML for evolutionary biology and  
952 comparative genomics. *BMC Bioinformatics* 10, 356.
- 953 Hancock, J.F., Cadwallader, K., Paterson, H., and Marshall, C.J. (1991). A CAAX or a CAAL  
954 motif and a second signal are sufficient for plasma membrane targeting of ras proteins.  
955 *EMBO J* 10, 4033-4039.
- 956 Hassan, B.A., Bermingham, N.A., He, Y., Sun, Y., Jan, Y.N., Zoghbi, H.Y., and Bellen, H.J.  
957 (2000). *atonal* regulates neurite arborization but does not act as a proneural gene in the  
958 *Drosophila* brain. *Neuron* 25, 549-561.
- 959 Heasman, J. (2006). Patterning the early *Xenopus* embryo. *Development* 133, 1205-1217.
- 960 Heidary, G., Engle, E.C., and Hunter, D.G. (2008). Congenital Fibrosis of the Extraocular  
961 Muscles. *Seminars in Ophthalmology* 23, 3-8.
- 962 Helenius, J., Brouhard, G., Kalaidzidis, Y., Diez, S., and Howard, J. (2006). The  
963 depolymerizing kinesin MCAK uses lattice diffusion to rapidly target microtubule ends.  
964 *Nature* 441, 115-119.
- 965 Hinrichs, M.H., Jalal, A., Brenner, B., Mandelkow, E., Kumar, S., and Scholz, T. (2012). Tau  
966 protein diffuses along the microtubule lattice. *J Biol Chem* 287, 38559-38568.
- 967 Hoffman, P.N. (1995). Review : The Synthesis, Axonal Transport, and Phosphorylation of  
968 Neurofilaments Determine Axonal Caliber in Myelinated Nerve Fibers. *The Neuroscientist*  
969 1, 76-83.
- 970 Honnappa, S., Gouveia, S.M., Weisbrich, A., Damberger, F.F., Bhavesh, N.S., Jawhari, H.,  
971 Grigoriev, I., van Rijssel, F.J., Buey, R.M., Lawera, A., et al. (2009). An EB1-binding motif  
972 acts as a microtubule tip localization signal. *Cell* 138, 366-376.
- 973 Huang, J., Zhou, W., Dong, W., Watson, A.M., and Hong, Y. (2009). From the Cover:  
974 Directed, efficient, and versatile modifications of the *Drosophila* genome by genomic  
975 engineering. *Proc Natl Acad Sci U S A* 106, 8284-8289.
- 976 Kalil, K., and Dent, E.W. (2014). Branch management: mechanisms of axon branching in the  
977 developing vertebrate CNS. *Nat Rev Neurosci* 15, 7-18.
- 978 Kaverina, I., Rottner, K., and Small, J.V. (1998). Targeting, capture, and stabilization of  
979 microtubules at early focal adhesions. *J Cell Biol* 142, 181-190.
- 980 Kolodziej, P.A., Jan, L.Y., and Jan, Y.N. (1995). Mutations that affect the length, fasciculation,  
981 or ventral orientation of specific sensory axons in the *Drosophila* embryo. *Neuron* 15, 273-  
982 286.
- 983 Krieg, M., Stühmer, J., Cueva, J.G., Fetter, R., Spilker, K., Cremers, D., Shen, K., Dunn, A.R.,  
984 and Goodman, M.B. (2017). Genetic defects in  $\beta$ -spectrin and tau sensitize *C. elegans*  
985 axons to movement-induced damage via torque-tension coupling. *Elife* 6, e20172.
- 986 Küppers-Munther, B., Letzkus, J., Lüer, K., Technau, G., Schmidt, H., and Prokop, A. (2004).  
987 A new culturing strategy optimises *Drosophila* primary cell cultures for structural and  
988 functional analyses. *Dev Biol* 269, 459-478.

- 989 Lewis, T.L., Jr., Courchet, J., and Polleux, F. (2013). Cell biology in neuroscience: Cellular  
990 and molecular mechanisms underlying axon formation, growth, and branching. *J Cell Biol*  
991 *202*, 837-848.
- 992 Lowery, L.A., and van Vactor, D. (2009). The trip of the tip: understanding the growth cone  
993 machinery. *Nat Rev Mol Cell Biol* *10*, 332-343.
- 994 Luo, L., Liao, Y.J., Jan, L.Y., and Jan, Y.N. (1994). Distinct morphogenetic functions of similar  
995 small GTPases: *Drosophila* Drac1 is involved in axonal outgrowth and myoblast fusion.  
996 *Genes Dev* *8*, 1787-1802.
- 997 Macia, E., Partisani, M., Favard, C., Mortier, E., Zimmermann, P., Carlier, M.F., Gounon, P.,  
998 Luton, F., and Franco, M. (2008). The pleckstrin homology domain of the Arf6-specific  
999 exchange factor EFA6 localizes to the plasma membrane by interacting with  
1000 phosphatidylinositol 4,5-bisphosphate and F-actin. *J Biol Chem* *283*, 19836-19844.
- 1001 Marklund, U., Larsson, N., Gradin, H.M., Brattsand, G., and Gullberg, M. (1996). Oncoprotein  
1002 18 is a phosphorylation-responsive regulator of microtubule dynamics. *EMBO J* *15*, 5290-  
1003 5298.
- 1004 Marner, L., Nyengaard, J.R., Tang, Y., and Pakkenberg, B. (2003). Marked loss of myelinated  
1005 nerve fibers in the human brain with age. *J Comp Neurol* *462*, 144-152.
- 1006 McNally, F.J., and Roll-Mecak, A. (2018). Microtubule-severing enzymes: From cellular  
1007 functions to molecular mechanism. *J Cell Biol* *217*, 4057-4069.
- 1008 McWilliam, H., Li, W., Uludag, M., Squizzato, S., Park, Y.M., Buso, N., Cowley, A.P., and  
1009 Lopez, R. (2013). Analysis Tool Web Services from the EMBL-EBI. *Nucleic Acids Res* *41*,  
1010 W597-600.
- 1011 Medana, I.M., and Esiri, M.M. (2003). Axonal damage: a key predictor of outcome in human  
1012 CNS diseases. *Brain* *126*, 515-530.
- 1013 Moore, A.T., Rankin, K.E., von Dassow, G., Peris, L., Wagenbach, M., Ovechkina, Y.,  
1014 Andrieux, A., Job, D., and Wordeman, L. (2005). MCAK associates with the tips of  
1015 polymerizing microtubules. *J Cell Biol* *169*, 391-397.
- 1016 O'Rourke, S.M., Christensen, S.N., and Bowerman, B. (2010). *Caenorhabditis elegans* EFA-6  
1017 limits microtubule growth at the cell cortex. *Nat Cell Biol* *12*, 1235-1241.
- 1018 Patel, J.T., Belsham, H.R., Rathbone, A.J., Wickstead, B., Gell, C., and Friel, C.T. (2016). The  
1019 family-specific alpha4-helix of the kinesin-13, MCAK, is critical to microtubule end  
1020 recognition. *Open Biol* *6*.
- 1021 Paul, P., van den Hoorn, T., Jongasma, Marlieke L.M., Bakker, Mark J., Hengeveld, R.,  
1022 Janssen, L., Cresswell, P., Egan, David A., van Ham, M., ten Brinke, A., et al. (2011). A  
1023 Genome-wide Multidimensional RNAi Screen Reveals Pathways Controlling MHC Class II  
1024 Antigen Presentation. *Cell* *145*, 268-283.
- 1025 Pearce, S.P., Heil, M., Jensen, O.E., Jones, G.W., and Prokop, A. (2018). Curvature-sensitive  
1026 kinesin binding can explain microtubule ring formation and reveals chaotic dynamics in a  
1027 mathematical model. *Bull Math Biol* *80*, 3002-3022.
- 1028 Pils, D., Horak, P., Gleiss, A., Sax, C., Fabjani, G., Moebus, V.J., Zielinski, C., Reinthaller, A.,  
1029 Zeillinger, R., and Krainer, M. (2005). Five genes from chromosomal band 8p22 are  
1030 significantly down-regulated in ovarian carcinoma. *Cancer* *104*, 2417-2429.
- 1031 Ponting, C.P., Phillips, C., Davies, K.E., and Blake, D.J. (1997). PDZ domains: targeting  
1032 signalling molecules to sub-membranous sites. *Bioessays* *19*, 469-479.
- 1033 Prokop, A. (2013a). The intricate relationship between microtubules and their associated  
1034 motor proteins during axon growth and maintenance. *Neur Dev* *8*, 17.
- 1035 Prokop, A. (2013b). A rough guide to *Drosophila* mating schemes. figshare,  
1036 [dx.doi.org/10.6084/m6089.figshare.106631](https://doi.org/10.6084/m6089.figshare.106631).
- 1037 Prokop, A. (2016). Fruit flies in biological research. *Biological Sciences Review* *28*, 10-14.



- 1038 Prokop, A., Beaven, R., Qu, Y., and Sánchez-Soriano, N. (2013). Using fly genetics to dissect  
1039 the cytoskeletal machinery of neurons during axonal growth and maintenance. *J Cell Sci*  
1040 126, 2331-2341.
- 1041 Prokop, A., Küppers-Munther, B., and Sánchez-Soriano, N. (2012). Using primary neuron  
1042 cultures of *Drosophila* to analyse neuronal circuit formation and function. In *The making*  
1043 *and un-making of neuronal circuits in Drosophila*, B.A. Hassan, ed. (New York, Humana  
1044 Press), pp. 225-247.
- 1045 Prokop, A., and Meinertzhagen, I.A. (2006). Development and structure of synaptic contacts in  
1046 *Drosophila*. *Semin Cell Dev Biol* 17, 20-30.
- 1047 Qu, Y., Hahn, I., Webb, S.E.D., Pearce, S.P., and Prokop, A. (2017). Periodic actin structures  
1048 in neuronal axons are required to maintain microtubules. *Mol Biol Cell* 28 296-308.
- 1049 Rogers, S.L., Rogers, G.C., Sharp, D.J., and Vale, R.D. (2002). *Drosophila* EB1 is important  
1050 for proper assembly, dynamics, and positioning of the mitotic spindle. *J Cell Biol* 158, 873-  
1051 884.
- 1052 Ronquist, F., Teslenko, M., van der Mark, P., Ayres, D.L., Darling, A., Höhna, S., Larget, B.,  
1053 Liu, L., Suchard, M.A., and Huelsenbeck, J.P. (2012). MrBayes 3.2: efficient Bayesian  
1054 phylogenetic inference and model choice across a large model space. *Syst Biol* 61, 539-  
1055 542.
- 1056 Sánchez-Soriano, N., Gonçalves-Pimentel, C., Beaven, R., Haessler, U., Ofner, L.,  
1057 Ballestrem, C., and Prokop, A. (2010). *Drosophila* growth cones: a genetically tractable  
1058 platform for the analysis of axonal growth dynamics. *Dev Neurobiol* 70, 58-71.
- 1059 Sánchez-Soriano, N., Tear, G., Whittington, P., and Prokop, A. (2007). *Drosophila* as a genetic  
1060 and cellular model for studies on axonal growth. *Neural Develop* 2, 9.
- 1061 Sánchez-Soriano, N., Travis, M., Dajas-Bailador, F., Goncalves-Pimentel, C., Whitmarsh, A.J.,  
1062 and Prokop, A. (2009). Mouse ACF7 and *Drosophila* Short stop modulate filopodia  
1063 formation and microtubule organisation during neuronal growth. *Journal of cell science* 122,  
1064 2534-2542.
- 1065 Schimizzi, G.V., Currie, J.D., and Rogers, S.L. (2010). Expression levels of a kinesin-13  
1066 microtubule depolymerase modulates the effectiveness of anti-microtubule agents. *PLoS*  
1067 *One* 5, e11381.
- 1068 Schindelin, J., Arganda-Carreras, I., Frise, E., Kaynig, V., Longair, M., Pietzsch, T., Preibisch,  
1069 S., Rueden, C., Saalfeld, S., Schmid, B., et al. (2012). Fiji: an open-source platform for  
1070 biological-image analysis. *Nat Methods* 9, 676-682.
- 1071 Seibel, N.M., Eljouni, J., Nalaskowski, M.M., and Hampe, W. (2007). Nuclear localization of  
1072 enhanced green fluorescent protein homomultimers. *Analytical Biochemistry* 368, 95-99.
- 1073 Sharp, D.J., and Ross, J.L. (2012). Microtubule-severing enzymes at the cutting edge. *Journal*  
1074 *of cell science* 125, 2561-2569.
- 1075 Sievers, F., Wilm, A., Dineen, D., Gibson, T.J., Karplus, K., Li, W., Lopez, R., McWilliam, H.,  
1076 Remmert, M., Soding, J., et al. (2011). Fast, scalable generation of high-quality protein  
1077 multiple sequence alignments using Clustal Omega. *Mol Syst Biol* 7, 539.
- 1078 Stefana, M.I., Driscoll, P.C., Obata, F., Pengelly, A.R., Newell, C.L., MacRae, J.I., and Gould,  
1079 A.P. (2017). Developmental diet regulates *Drosophila* lifespan via lipid autotoxins. *Nat*  
1080 *Commun* 8, 1384.
- 1081 Tiab, L., Manzi, V.d.A., Borruat, F.-X., Munier, F., and Schorderet, D. (2004). Mutation  
1082 analysis of KIF21A in congenital fibrosis of the extraocular muscles (CFEOM) patients.  
1083 *Ophthalmic Genetics* 25, 241-246.
- 1084 Tymanskyj, S.R., Yang, B., Falnikar, A., Lepore, A.C., and Ma, L. (2017). MAP7 regulates  
1085 axon collateral branch development in dorsal root ganglion neurons. *J Neurosci* 37, 1648-  
1086 1661.
- 1087 Vale, R.D., and Toyoshima, Y.Y. (1988). Rotation and translocation of microtubules in vitro  
1088 induced by dyneins from *Tetrahymena* cilia. *Cell* 52, 459-469.

- 1089 van der Vaart, B., van Riel, Wilhelmina E., Doodhi, H., Kevenaer, Josta T., Katrukha,  
1090 Eugene A., Gummy, L., Bouchet, Benjamin P., Grigoriev, I., Spangler, Samantha A., Yu,  
1091 Ka L., *et al.* (2013). CFEOM1-associated kinesin KIF21A is a cortical microtubule growth  
1092 inhibitor. *Developmental Cell* 27, 145-160.
- 1093 Voelzmann, A., Hahn, I., Pearce, S., Sánchez-Soriano, N.P., and Prokop, A. (2016a). A  
1094 conceptual view at microtubule plus end dynamics in neuronal axons. *Brain Res Bulletin*  
1095 126, 226-237.
- 1096 Voelzmann, A., Liew, Y.-T., Qu, Y., Hahn, I., Melero, C., Sánchez-Soriano, N., and Prokop, A.  
1097 (2017). *Drosophila* Short stop as a paradigm for the role and regulation of spectraplakins.  
1098 *Sem Cell Dev Biol* 69, 40-57.
- 1099 Voelzmann, A., Okenve-Ramos, P., Qu, Y., Chojnowska-Monga, M., del Caño-Espinel, M.,  
1100 Prokop, A., and Sánchez-Soriano, N. (2016b). Tau and spectraplakins promote synapse  
1101 formation and maintenance through Jun kinase and neuronal trafficking. *eLife* 5, e14694.
- 1102 Wang, J.T., Medress, Z.A., and Barres, B.A. (2012). Axon degeneration: molecular  
1103 mechanisms of a self-destruction pathway. *J Cell Biol* 196, 7-18.
- 1104 Yu, W., Qiang, L., Solowska, J.M., Karabay, A., Korulu, S., and Baas, P.W. (2008). The  
1105 microtubule-severing proteins spastin and katanin participate differently in the formation of  
1106 axonal branches. *Mol Biol Cell* 19, 1485-1498.
- 1107 Zeidler, M.P., Tan, C., Bellaiche, Y., Cherry, S., Hader, S., Gayko, U., and Perrimon, N.  
1108 (2004). Temperature-sensitive control of protein activity by conditionally splicing inteins.  
1109 *Nat Biotech* 22, 871-876.
- 1110 Zschätzsch, M., Oliva, C., Langen, M., De Geest, N., Ozel, M.N., Williamson, W.R., Lemon,  
1111 W.C., Soldano, A., Munck, S., Hiesinger, P.R., *et al.* (2014). Regulation of branching  
1112 dynamics by axon-intrinsic asymmetries in Tyrosine Kinase Receptor signaling. *Elife* 3,  
1113 e01699.

1114

## 1115 **Figures**

1116

### 1117 **Fig. 1** Efa6 is expressed throughout neurons at all developmental stages

1118 A-E) Images of primary *Drosophila* neurons at 6HIV or 5DIV (at indicated bottom right),  
1119 stained for tubulin (magenta) and GFP (green); control neurons are wild-type (wt) or express  
1120 *elav-Gal4*-driven nuclear GFP (*elav / nl-GFP*), whereas further neurons are either derived  
1121 from the endogenously tagged Efa6::GFP line or express Efa6-FL::GFP under the control of  
1122 *sca-Gal4* (*sca / Efa6-FL::GFP*); asterisks indicate cell bodies and arrow the axon tips. F-I)  
1123 Late larval CNSs at about 4d of development from egg lay (L3; F,G) and adult CNSs from 10d  
1124 old flies (H,I) derived from control wild-type animals (wt) or the Efa6::GFP line (*Efa6::GFP*),  
1125 stained for GFP and actin (Phalloidin, only larval preparations); OL, optic lobe; Br, central  
1126 brain; vNC, ventral nerve cord. Scale bar in A represent 15 $\mu$ m in A-C, 25 $\mu$ m in D and E, 75 $\mu$ m  
1127 in F and G, 130 $\mu$ m in H and I.

1128

1129 **Fig. 2.** Efa6 regulates axonal length in primary *Drosophila* neurons. Examples of primary  
1130 *Drosophila* neurons at 6HIV (A-C), all stained for actin (magenta) and tubulin (green); neurons  
1131 are either wild-type controls (A), Efa6-deficient (B), expressing Efa6-FL::GFP (C); asterisks  
1132 indicate cell bodies, arrows point at axon tips; the scale bar in C represents 10 $\mu$ m.  
1133 Quantification of axon lengths at 6HIV (D); different genotypes are colour-coded: grey, wild-  
1134 type controls; blue, different Efa6 loss-of-function conditions; green, neurons over-expressing  
1135 Efa6 variants; data represent fold-change relative to wild-type controls (indicated as horizontal  
1136 dashed "ctrl" line); they are shown as single data points and a bar indicating mean  $\pm$  SEM

1137 data; P values from Mann-Whitney tests are given above each column, sample numbers at  
1138 the bottom of each bar. For raw data see T2, which can be downloaded here:  
1139 [w.prokop.co.uk/Qu+al/RawData.zip](http://w.prokop.co.uk/Qu+al/RawData.zip).

1140  
1141 **Fig. 3.** Efa6 domain and motif requirements for MT inhibition in neurons and fibroblasts. A)  
1142 Schematics of *Drosophila melanogaster* (*Dm*) Efa6 (isoform C, CG31158), *Caenorhabditis*  
1143 *elegans* (*Ce*) Efa6 (isoform Y55D9A.1a) and *Homo sapiens* (human) PSD1 (isoform 201/202,  
1144 NP\_002770.3), illustrating the positions (numbers indicate first and last residues) of the  
1145 putative PSD95-Dlg1-ZO1 domain [PDZ; expected to anchor to transmembrane proteins  
1146 (Ponting et al., 1997), but not mediating obvious membrane association in fibroblasts:  
1147 Figs.S4C,D], SxIP/SxLP motifs (SRIP, SQIP, SALP, SSLP), the MT-binding domain (MTED),  
1148 SEC7 domain, plekstrin homology (PH) domain and coiled-coil domain (CC). B) Schematics  
1149 on the left follow the same colour code and show the *Dm*Efa6 constructs used in this study  
1150 (dashed red lines indicate the last/first residue before/behind the truncation). Bar graphs on  
1151 the right show the impact that transfection of these constructs had on axon loss in primary  
1152 *Drosophila* neurons (dark grey in left graph) and on MT loss in fibroblasts (dark grey or black  
1153 as indicated; for respective images see F and G below). Analogous fibroblast experiments as  
1154 performed with *Drosophila* constructs were performed with full length constructs of *C. elegans*  
1155 Efa6 and human PSDs (C), with N-terminal constructs (D) or synthetic MTEDs (E) of *Dm* and  
1156 *Ce*Efa6 and of human PSD1. Throughout this figure, construct names are highlighted in red  
1157 for *Drosophila*, light blue for *C. elegans* and yellow for *Homo sapiens*; all graph bars indicate  
1158 percentages of neurons with/without axons (light/dark grey) and of fibroblasts with normal,  
1159 reduced or absent MTs (light, medium, dark grey, respectively); numbers in the left end of  
1160 each bar indicate sample numbers, on the right end the P values from  $\chi^2$  tests relative to  
1161 GFP controls; numbers on the right of bars in B compare some constructs to Efa6-FL::GFP,  
1162 as indicated by black lines. F-F'') Primary neurons expressing Efa6-FL::GFP transgenically  
1163 and stained for tubulin (asterisks, cell bodies; white arrows, axon tips; open arrow, absent  
1164 axon). G-G'') Fibroblasts expressing Efa6-FL::GFP and stained for tubulin; curved arrows  
1165 indicate areas where MTs are retracted from the cell periphery; grey dots in F-G'' indicate the  
1166 phenotypic categories for each neuron and fibroblasts, as used for quantitative analyses in the  
1167 graphs above. Scale bar at bottom of F refers to 10 $\mu$ m in F and 25 $\mu$ m in G. For raw data see  
1168 T3, which can be downloaded here: [w.prokop.co.uk/Qu+al/RawData.zip](http://w.prokop.co.uk/Qu+al/RawData.zip).

1169  
1170 **Fig. 4.** EFA6 peptide interacts directly with  $\alpha/\beta$ -tubulin and inhibits microtubule growth. A) End  
1171 point of microtubule growth assay in the presence of no MTED peptide, or a 1:1 and 10:1  
1172 molar ratio of MTED peptide to tubulin. Scale bar in A refers to 10  $\mu$ m. B) Pull-down of tubulin  
1173 by sepharose beads coated with MTED peptide via cyanogen bromide coupling and control  
1174 beads with no MTED peptide attached.

1175  
1176 **Fig. 5.** Efa6 regulates MT behaviours in GCs. A-H') Examples of primary neurons at 6HIV  
1177 which are either wild-type controls (top), Efa6-deficient (middle) or expressing Efa6-FL::GFP  
1178 (bottom); neurons were either imaged live for Eb1::GFP (green in A,D) or fixed and labelled  
1179 for Eb1 and tubulin (B,E,G; as colour-coded) or actin and tubulin (C,F,H; as colour coded;  
1180 tubulin shown as single channel image on the right); asterisks indicate cell bodies, white  
1181 arrows the tips of GCs, open arrows the tips of MT bundles and arrow heads MTs or Eb1  
1182 comets in filopodial processes; the GC in G is outlined with a white dashed line; scale bar in D

1183 represents 5µm in all images. I-M) Quantitative analyses of MT behaviours in GCs of such  
1184 neurons as indicated above each graph. Different genotypes are colour-coded: grey, wild-type  
1185 controls; blue, different *Efa6* loss-of-function conditions; green, neurons over-expressing Efa-  
1186 FL. The graph in L shows percentages of neurons without any MTs in shaft filopodia (dark  
1187 shade) versus neurons with MTs in at least one filopodium (light shade; P values above bars  
1188 assessed via  $\chi^2$  tests), whereas all other graphs show single data points and a bar  
1189 indicating mean  $\pm$  SEM, all representing fold-increase relative to wild-type controls (indicated  
1190 as horizontal dashed "ctrl" line; P values above columns from Mann-Whitney tests. The  
1191 control values in M (dashed line) equate to an Eb1 comet life-time of 2.10s  $\pm$  0.24SEM in  
1192 filpododia and 5.04s  $\pm$  0.60SEM in growth cones, and a comet velocity of 0.136  $\mu$ m/s  $\pm$   
1193 0.01SEM. Throughout the figure, sample numbers are shown at the bottom of each bar and  
1194 data obtained from live analyses with Eb1::GFP are framed in red. For raw data see T4,  
1195 which can be downloaded here: [w.prokop.co.uk/Qu+al/RawData.zip](http://w.prokop.co.uk/Qu+al/RawData.zip).

1196

1197 **Fig. 6.** Loss of Efa6 promotes MT entry into axon shaft filopodia. Quantitative analyses of MT  
1198 behaviours in axon shafts, as indicated above each graph; bars are colour-coded: grey,  
1199 controls; blue, different *Efa6* mutant alleles; green, neurons over-expressing Efa-FL::GFP or  
1200 Efa6::CAAX::GFP; orange, *shot* mutant allele; red outlines indicate live imaging data, all  
1201 others were obtained from fixed specimens; numbers at the bottom of bars indicate sample  
1202 numbers, above bars P values. A-C,G) Fold-changes relative to wild-type controls (indicated  
1203 as horizontal dashed "ctrl" line) shown as single data points and a bar indicating mean  $\pm$  SEM;  
1204 P values were obtained via Mann-Whitney tests; control values (dashed line) in B and C  
1205 equate to an Eb1 comet lifetime of 7.18 s  $\pm$  0.35 SEM and a velocity of 0.169  $\mu$ m/s  $\pm$   
1206 0.01SEM. D-F) Binary parameters (light versus dark shades as indicated) provided as  
1207 percentages; P values were obtained via  $\chi^2$  tests. For raw data see T5, which can be  
1208 downloaded here: [w.prokop.co.uk/Qu+al/RawData.zip](http://w.prokop.co.uk/Qu+al/RawData.zip).

1209

1210 **Fig. 7.** Efa6 regulates axon branching in in primary *Drosophila* neurons and adult fly brains.  
1211 Examples of primary *Drosophila* neurons at 5DIV (A-D), all stained for actin (magenta) and  
1212 tubulin (green); neurons are either wild-type controls (A), Efa6-deficient (B), expressing Efa6-  
1213 FL::GFP (C), or expressing Efa6-Nterm-CAAX::GFP (D); asterisks indicate cell bodies, arrows  
1214 point at axon tips, arrow heads at axon branches, the curved arrow at an area of MT  
1215 disorganisation; the scale bar in C represents 20µm. Quantification of axonal branch numbers  
1216 (E); different genotypes are colour-coded: grey, wild-type controls; blue, different *Efa6* loss-of-  
1217 function conditions; green, neurons over-expressing Efa6 variants; data represent fold-change  
1218 relative to wild-type controls (indicated as horizontal dashed "ctrl" line); they are shown as  
1219 single data points and a bar indicating mean  $\pm$  SEM data; P values from Mann-Whitney tests  
1220 are given above each column, sample numbers at the bottom of each bar. F-K) Brains  
1221 (medulla region of the optic lobe in oblique view) of young (2-5 d after eclosure; top) and old  
1222 flies (15-18 d; bottom) driving *UAS-myr-tdTomato* via the *ato-Gal4* driver in dorsal cluster  
1223 neurons (example neurons are traced in magenta for axons and green for side branches); flies  
1224 are either wild-type controls (left) or display *ato-Gal4*-driven knock-down of Efa6 (middle) or  
1225 over-expression of Efa6-FL::GFP (right). L,M) Quantification of data for wild-type (wt; grey),  
1226 Efa6 knock-down (blue) and Efa6-FL::GFP over-expression (green): L) shows the number of  
1227 primary branches per axon as fold-change relative to wild-type controls (indicated as  
1228 horizontal dashed "ctrl" line; data are shown as bars indicating mean  $\pm$  SEM accompanied by  
1229 single data points, all normalised to wt); M) displays the number of medullas with axons (light

1230 colours) or without axons (dark colours) shown as a percentages in young and old flies. In all  
1231 graphs, sample numbers at the bottom (in L number of medullas before and number of axons  
1232 after slash) and P values from Mann-Whitney (G) or  $\chi^2$  tests (H) above each column. Scale  
1233 bar in D represents 60 $\mu$ m in all figures. For raw data see T6, which can be downloaded here:  
1234 [w.prokop.co.uk/Qu+al/RawData.zip](http://w.prokop.co.uk/Qu+al/RawData.zip).

1235  
1236 **Fig. 8.** Efa6 helps to maintain axonal MT bundles in *Drosophila* neurons. A-H) Images of  
1237 primary neurons at 6HIV (left), 5DIV (middle) and 10DIV (right), stained for tubulin (green) and  
1238 actin (magenta), derived from embryos that were either wild-type (wt, A-C), *Efa6* null mutant  
1239 (D-F), homozygous for *shot*<sup>3</sup> (G) or *shot*<sup>3</sup> *Efa6*<sup>GX6[w-]</sup> double-mutant (shot Efa6, H); arrows  
1240 point at axon tip, arrow heads at areas of MT disorganisation, and asterisks indicate the cell  
1241 bodies; the scale bar in A represents 10 $\mu$ m for 6HIV neurons and 25 $\mu$ m for 5DIV and 10DIV  
1242 neurons. I-N) Quantitative analyses of MT disorganisation (measured as MT disorganisation  
1243 index, MDI) in different experimental contexts (as indicated above graphs); different  
1244 genotypes are colour-coded: grey, wild-type controls; blue, *Efa6* loss-of-function; light/dark  
1245 orange, *shot*<sup>3</sup> in hetero-/homozygosis; green, neurons over-expressing Efa-FL::GFP or Efa6-  
1246 NtermCAAX::GFP; data are shown as single data points and a bar indicating mean  $\pm$  SEM, all  
1247 representing fold-change relative to wild-type controls (indicated as horizontal dashed "ctrl"  
1248 line); P values from Mann-Whitney tests in I, J) and Kruskal–Wallis one-way ANOVA with *post*  
1249 *hoc* Dunn's test in K-N) are given above each column, sample numbers at the bottom of each  
1250 bar. Control 1 in (K) is *tub-Gal80*, *elav-Gal4* alone and control 2 *UAS-Efa6RNAi*. For raw data  
1251 see T7, which can be downloaded here: [w.prokop.co.uk/Qu+al/RawData.zip](http://w.prokop.co.uk/Qu+al/RawData.zip).

1252  
1253 **Fig. 9** Efa6 is required for axonal MT bundle maintenance in adult fly brains. A-C) Medulla  
1254 region of adult brains at 26-27 days after eclosure, all carrying the *GMR31F10-Gal4* driver and  
1255 *UAS- $\alpha$ -tubulin84B-GFP* (*GMR-tub*) which together stain MTs in a subset of lamina neuron  
1256 axons that terminate in the medulla. The other specimens co-express *Efa6-RNAi* either alone  
1257 (*GMR-tub-Efa6<sup>IR</sup>* in B) or combined with a *shot*<sup>3/+</sup> heterozygous mutant background (*GMR-tub-*  
1258 *Efa6<sup>IR</sup> shot<sup>3/+</sup>* in C). White/black arrows indicate axonal swellings without/with MT  
1259 disorganisation; rectangles outlined by red dashed lines are shown as 2.5 fold magnified  
1260 insets where white arrow heads point at disorganised MTs; the scale bar in A represents  
1261 15 $\mu$ m in all images. D, E) Quantitative analyses of all axonal swelling (D) or swellings with MT  
1262 disorganisation (E); different genotypes are colour-coded as indicated; bars show mean  $\pm$   
1263 SEM, all representing fold-change relative to wild-type controls (indicated as horizontal  
1264 dashed line); P values from Kruskal–Wallis one-way tests are given above each column,  
1265 sample numbers at the bottom of each bar. For raw data see table T8, which can be  
1266 downloaded here: [w.prokop.co.uk/Qu+al/RawData.zip](http://w.prokop.co.uk/Qu+al/RawData.zip).

1267  
1268 **Fig. 10.** A model of the suggested roles of Efa6. **A)** The model of local axon homeostasis  
1269 (Prokop, 2016; Voelzmann et al., 2016a) states that axonal MTs (green bars) are actively kept  
1270 in bundles; for example, their continued polymerisation (1) mediated by plus end machinery  
1271 (blue circle) is guided by spectraplakins (here Shot) along cortical actin into parallel bundles  
1272 (2), or MTs are kept together through cross-linkage (brown "L"; 4) (Bettencourt da Cruz et al.,  
1273 2005; Krieg et al., 2017); here we propose that MTs accidentally leaving the bundle become  
1274 vulnerable (orange circles) through inhibition (red "T") by cortically anchored Efa6. **B)** In  
1275 normal neurons, polymerising MTs in bundles (dark blue circles) are protected by Shot

1276 (marine lines) and MT-MT cross-linkers (brown rectangles), whereas MTs approaches the  
1277 membrane (orange arrow heads) either by splaying out in GCs or leaving the bundle in the  
1278 shaft (orange arrow heads) become vulnerable (orange circles) to inhibition by Efa6 (light  
1279 green/red dashes) both along the cortex and in filopodia **C**) Upon Efa6 deficiency, MTs  
1280 leaving bundles or entering GCs are no longer subjected to Efa6-mediated cortical inhibition  
1281 (blue arrow heads) and can cause gradual build-up of MT disorganisation; when entering shaft  
1282 filopodia they can promote interstitial branch formation (red arrow), when entering GC  
1283 filopodia they can promote axon growth or even branching through GC splitting (yellow  
1284 arrows). **D**) Far more MTs leave the bundles in *shot* mutant neurons, but a good fraction of  
1285 them is inhibited by Efa6 (increased number of orange arrow heads). **E**) In the absence of  
1286 both Shot and Efa6, more MTs leave the bundles, but there is no compensating cortical  
1287 inhibition (increased number of blue arrow heads), so that the MT disorganisation phenotype  
1288 worsens.

1289

1290

1291 **Supplementary materials**

1292

1293 **Fig. S1.** Phylogentic tree analysis of Efa6. Bayesian phylogenetic analysis of full length (A) or  
1294 N-termini (B) of Efa6 orthologues. Sequences were aligned using Muscle or ClustalO and  
1295 posterior probabilities and branch lengths calculated using MrBayes. Branch length scale is  
1296 indicated; blue numbers show posterior probabilities of each branch split. For the full length  
1297 tree, *Drosophila steppke* (*step*) was used as outgroup (Hahn et al., 2013). In both full length  
1298 and N-terminus analyses, chordates (cream colour) split off very early from Efa6 versions of  
1299 other species, in line with an early speciation event separating both groups before the  
1300 vertebrate multiplication events took place. Phyla are highlighted in different colours, gene  
1301 symbols and/or accession numbers are given after the species names.

1302

1303 **Fig. S2.** Efa6 N-terminal domains vary amongst different phyla. A) Domain annotations in 56  
1304 Efa6 orthologues via EMBL SMART and Uniprot. Phyla are colour-coded as in Fig.S1. Note  
1305 that there is a strong variation of lengths and domain composition in particular of the N-  
1306 terminus. The putative PDZ domain seems to be a feature mainly of insect versions of Efa6  
1307 and is absent from any analysed chordate orthologues; MTED and MTED-like sequences  
1308 cannot be consistently identified in all Efa6 orthologues and are very divergent in chordate  
1309 Efa6/PSD versions. SxIP/SxLP sites [flanked by positive charges as would be expected of  
1310 functional motifs (Honnappa et al., 2009)] are found in the N-terminal half of only a subset of  
1311 Efa6 versions in nematodes (e.g. *C. elegans*), insects (in particular flies, e.g. *D. melanogaster*)  
1312 and molluscs, and even fewer in chordates; in mouse, alpaca and cat SxIP/SxLP sites are  
1313 flanked by negative charges. B) To determine a potential MTED consensus sequence, 37  
1314 sequences of molluscs, nematodes, arthropods and putative MTED sequences of mammalian  
1315 PSD1-4 were grouped according to phylum; consensus sequences were depicted using  
1316 Berkley's Weblogo online server (default colour scheme). Amino acid positions identical to *D.*  
1317 *melanogaster* and *C. elegans* MTED are highlighted (faint yellow).

1318

1319 **Fig.S3.** Localisation of Efa6 constructs in primary neurons. Images show transfected primary  
1320 *Drosophila* neurons at 18HIV stained for tubulin (magenta) and GFP (green and in greyscale  
1321 below the colour image). Cell bodies are indicated by asterisks, axon tips by arrows. The  
1322 transfected constructs are indicated top right following the nomenclature explained in Fig.3B.  
1323 Scale bar in A represents 10µm for all figures shown.

1324

1325 **Fig.S4.** Efa6 constructs localisations in fibroblasts. Images show fibroblasts which are all  
1326 stained for GFP (green) and either for actin or MTs (magenta); GFP and actin/MTs shown as  
1327 single channels in greyscale below the colour image, 24hrs after transfection with control  
1328 (GFP) or Efa6-derived constructs (nomenclature as explained in Fig.3B, but leaving out the  
1329 "Efa6"-prefix and "::GFP"-postfix, as indicated top right. Double chevrons indicate nuclear  
1330 localisation, arrow heads membrane localisation apparent at cell edges and curved arrows  
1331 membrane ruffles. Scale bar in A represents 10µm in all images.

1332

1333 **Fig.S5.** MT inhibition by Efa6-FL is concentration-dependent in fibroblasts. **A-C)**  
1334 Representative images of fibroblasts stained for GFP and tubulin (green and magenta,  
1335 respectively; both shown as single channels in greyscale below the colour image). Images

1336 were taken 24hrs after transfection with *Efa6-FL::GFP*, assessed for GFP intensity (plotted on  
1337 the ordinate in **D**; examples for low, moderate and high expression are given in the left, middle  
1338 and right columns, respectively) and then grouped with respect to their MT phenotypes into  
1339 “MTs intact” (light grey), “mild MT defects” (medium grey) or “MTs gone” (black), as indicated  
1340 by greyscale circles in the lowest row of A-C and the abscissa of D. Arrow heads point at GFP  
1341 accumulation at membrane edges, white curved arrows indicate areas of the cell from where  
1342 MTs have retracted, open arrows point at retraction fibres and the double chevron indicates  
1343 the nucleus position and signs of nuclear GFP localisation. Scale bar in A represents 10µm in  
1344 all images. For raw data see T9, which can be downloaded here:  
1345 [w.prokop.co.uk/Qu+al/RawData.zip](http://w.prokop.co.uk/Qu+al/RawData.zip).

1346  
1347 **Fig. S6.** Conserved functions of the Efa6 C-terminus in membrane ruffle formation. **A-E)**  
1348 Representative images of fibroblasts stained for GFP and actin (green and magenta,  
1349 respectively; both shown as single channels in greyscale below the colour image). Images  
1350 were taken 24hrs after transfection with different constructs (indicated top right): control vector  
1351 (GFP; A), Efa6-derived constructs (B-D; nomenclature as explained in Fig.3B, but leaving out  
1352 the “Efa6“-prefix and “::GFP“-postfix) or PSD1-FL::GFP (E). To the right of each image, a  
1353 selected area is displayed with 2.5-fold magnification, showing dotted actin- and GFP-stained  
1354 ruffles (curved open arrows) in B, D and E, but not A and C; ruffle formation has been  
1355 quantified and is shown as a bar graph in **F**. All graph bars indicate percentages of fibroblasts  
1356 with/without membrane ruffles (dark/light grey); P values on top of bars are from Chi<sup>2</sup> tests  
1357 relative to GFP controls. As shown, ruffle phenotype were never observed with any N-terminal  
1358 Efa6 variants but are reproduced with the Efa6-ΔNterm::GFP variant (comprising the C-  
1359 terminal Sec7, PH and CC domains; Fig. 3B). Scale bar in the top image of A represents 10  
1360 µM for all fibroblasts shown. For raw data see T10, which can be downloaded here:  
1361 [w.prokop.co.uk/Qu+al/RawData.zip](http://w.prokop.co.uk/Qu+al/RawData.zip).

1362  
1363 **Fig. S7.** Representative MT phenotypes induced by the different constructs in transfected  
1364 fibroblasts. Fibroblasts 24hrs after transfection with different control (GFP) or Efa6-derived  
1365 constructs as indicated top right in each image (nomenclature as explained in Fig.3B, but  
1366 leaving out the “Efa6“-prefix and “::GFP“-postfix). Cells were stained for tubulin (black; images  
1367 shown as inverted greyscale) and classified as “no MT defects” (light grey), “mild MT defects”  
1368 (medium grey) or “MTs gone” (black), as indicated by greyscale boxes bottom left of each  
1369 image; curved arrows indicate peripheral MT depletion. Each image represents the most  
1370 prominent phenotype for each respective construct. Scale bar at the bottom right in H  
1371 represents 25µm in all images.

1372  
1373 **Fig. S8.** *In vitro* attempts to resolve the MT inhibition mechanism of Efa6. A) To determine  
1374 whether Efa6 directly affects MT stability, we recombinantly expressed Efa6-ΔCterm::GFP in  
1375 Sf9 cells, purified the protein and observed its interaction with MTs using total internal  
1376 reflection fluorescence (TIRF) microscopy in a low ionic strength buffer (BRB20, 75mM KCl);  
1377 images on the left show three examples of kymographs of MT lattices decorated with Efa6-  
1378 ΔCterm::GFP, which displays a mixture of stationary molecules and diffusive interactions  
1379 typical of non-translocating MT-associated proteins (Helenius et al., 2006; Hinrichs et al.,  
1380 2012); bar charts (right) show quantification of the amount of interacting protein: background  
1381 signal from MTs alone, Efa6-ΔCterm::GFP (20nM) and the non-translocating kinesin



1382 MCAK::GFP (20nM) as positive control; at the same protein concentration, over 2-fold more  
1383 molecules of MKAC typically interact with MTs; all graphs in this figure show individual data  
1384 points and bars representing mean  $\pm$  SEM; numbers above bars show P values obtained from  
1385 Mann–Whitney Rank Sum statistical analyses, numbers in bars the respective sample  
1386 numbers. B) Kymographs (left) show individual fluorescently-labelled GMPCPP-stabilised MTs  
1387 *in vitro* (Patel et al., 2016), either alone (MTs only; basal depolymerisation rate, n=7) or in the  
1388 presence of 14 nM Efa6- $\Delta$ Cterm::GFP (n=8) or 40nM MCAK::GFP (n=18); the bar chart (right)  
1389 quantifies the induced depolymerisation rates; using two different purifications of Efa6-  
1390  $\Delta$ Cterm::GFP on three separate occasions, we saw no evidence of MT depolymerisation  
1391 above the basal level of depolymerisation typically observed in these assays, whereas parallel  
1392 control experiments with mitotic centromere-associated kinesin/MCAK showed MT  
1393 depolymerisation rates typical of this kinesin. C) To assess whether MT destabilisation might  
1394 require additional cytoplasmic factors, we used *Xenopus* oocyte extracts: phase contrast  
1395 images show MTs in *Xenopus* oocyte extracts (after they had been allowed to polymerise for  
1396 20 min) and then showing stills from before, 10s after and 120s after washing in 20nM  
1397 MCAK::GFP (as positive control) or 20nM Efa6- $\Delta$ Cterm::GFP; squares outlined by dashed  
1398 white lines are shown magnified in insets revealing MTs; MTs clearly vanish upon treatment  
1399 with MCAK, but counts of MTs did not reveal any obvious effects on MTs with Efa6-  
1400  $\Delta$ Cterm::GFP. D,E) *RFP* controls and *Efa6-Nterm::GFP* expression constructs were injected  
1401 into *Xenopus* embryos at the 4-cell stage and analysed 24 hrs later; only the *Efa6* construct  
1402 caused a strong suppression of cell division, as indicated by the presence of very large cells  
1403 (arrows) and pigmentation defects (curved arrows) at the site of injection, suggesting that  
1404 Efa6-Nterm::GFP is functional when expressed in the *Xenopus* context. Scale bar (in top left  
1405 image) represents 3  $\mu$ m in C (2.5 fold magnified insets), and 1400  $\mu$ m / 350  $\mu$ m / 140  $\mu$ m in  
1406 left / middle / right images of D and E, respectively. For raw data see T11, which can be  
1407 downloaded here: [w.prokop.co.uk/Qu+al/RawData.zip](http://w.prokop.co.uk/Qu+al/RawData.zip).

1408  
1409 **Fig. S9.** *ato-Gal4*-driven Efa-FL::GFP expression in adult brains. Brains (region of the optic  
1410 lobe in oblique view; white dashed line indicating the lower edge of the medulla) of young (2-5  
1411 d after eclosure; top) and old flies (15-18 d; bottom) which are either from wild-type controls or  
1412 from flies driving *UAS-myr-dtTomato* and *UAS-Efa6-FL-GFP* via the *ato-Gal4* driver in dorsal  
1413 cluster neurons; specimens are stained for GFP and arrows point at stained; for myr-dtTomato  
1414 staining of brains from these experiments see Fig.7F-K. Scale bar in D represents 60 $\mu$ m in all  
1415 images.

1416 **Fig. S10.** Efa6 mutant primary neurons show MT disorganisation. Quantitative analyses of MT  
1417 disorganisation measured as binary score: percentages of neurons with bundled MTs  
1418 throughout (light colour) or showing obvious MT disorganisation in their axons (dark colour) in  
1419 different *Efa6* mutant alleles (control value indicated as horizontal dashed "ctrl" line); P values  
1420 from  $\chi^2$  tests are given above the bars. For raw data see T12, which can be downloaded  
1421 here: [w.prokop.co.uk/Qu+al/RawData.zip](http://w.prokop.co.uk/Qu+al/RawData.zip).

1422  
1423 **Suppl. Mov. M1.** MT behaviours in control fibroblasts transfected with GFP. Eb3 (green) was  
1424 used to visualise MT polymerisation, GFP (magenta) localises throughout the cell; MTs clearly  
1425 polymerise to the very fringe of the transfected cell. Movies were taken at one frame per  
1426 second; the scale bar corresponds to 25 $\mu$ m, close ups are twofold magnified. Movie available  
1427 at [w.prokop.co.uk/Qu+al/SupplMov.html](http://w.prokop.co.uk/Qu+al/SupplMov.html).

1428 **Suppl. Mov. M2.** MT behaviours in fibroblasts transfected with Efa6-FL::GFP. Eb3 (green)  
1429 was used to visualise MT polymerisation, which is prevented from entering areas of high Efa6-  
1430 FL::GFP (magenta), with Efa6 often accumulating where MTs enter the area. Movies were  
1431 taken at one frame per second; the scale bar corresponds to 25µm, close ups are twofold  
1432 magnified. Movie available at [w.prokop.co.uk/Qu+al/SupplMov.html](http://w.prokop.co.uk/Qu+al/SupplMov.html).

1433 **Suppl. Mov. M3.** Eb1::GFP in mouse NHTH3 fibroblast about 6 hours after transfection.  
1434 Pictures for the movie were taken at 2 s intervals. Scale bar indicates 10 µm. Movie available  
1435 at [w.prokop.co.uk/Qu+al/SupplMov.html](http://w.prokop.co.uk/Qu+al/SupplMov.html).

1436 **Suppl. Mov. M4.** MT behaviours in fibroblasts transfected with Efa6-Nterm::GFP::CAAX. Eb3  
1437 (green) was used to visualise MT polymerisation, which is prevented from entering areas of  
1438 high Efa6-FL::GFP (magenta), with Efa6 often accumulating where MTs enter the area.  
1439 Movies were taken at one frame per second; the scale bar corresponds to 25µm, close ups  
1440 are twofold magnified. Movie available at [w.prokop.co.uk/Qu+al/SupplMov.html](http://w.prokop.co.uk/Qu+al/SupplMov.html).

1441 **Suppl. Mov. M5.** Eb1::GFP in a growth cone of a wild-type *Drosophila* primary neuron at 6  
1442 HIV. Arrows indicate positions where individual Eb1::GFP comets terminate. Pictures of the  
1443 movie were taken at 2 s intervals. Scale bar indicates 10 µm. Movie available at  
1444 [w.prokop.co.uk/Qu+al/SupplMov.html](http://w.prokop.co.uk/Qu+al/SupplMov.html).

1445 **Suppl. Mov. M6.** Eb1::GFP in a growth cone of a wild-type *Drosophila* primary neuron at 6  
1446 HIV. Arrows indicate positions where individual Eb1::GFP comets terminate. Pictures of the  
1447 movie were taken at 2 s intervals. Scale bar indicates 10 µm. Movie available at  
1448 [w.prokop.co.uk/Qu+al/SupplMov.html](http://w.prokop.co.uk/Qu+al/SupplMov.html).

1449 **Suppl. Mov. M7.** Eb1::GFP in a growth cone of an *Efa6*<sup>GX6[w-]</sup> mutant *Drosophila* primary  
1450 neuron at 6 HIV. The arrow heads follow individual Eb1::GFP comets illustrating either their  
1451 trajectories adjacent to the membrane or prolonged dwell time at filopodial tips. Pictures for  
1452 the movie were taken at 2 s intervals. Scale bar indicates 10 µm. Movie available at  
1453 [w.prokop.co.uk/Qu+al/SupplMov.html](http://w.prokop.co.uk/Qu+al/SupplMov.html).

1454 **Suppl. Mov. M8.** Eb1::GFP in a growth cone of an *Efa6*<sup>GX6[w-]</sup> mutant *Drosophila* primary  
1455 neuron at 6 HIV. The arrow heads follow individual Eb1::GFP comets illustrating either their  
1456 trajectories adjacent to the membrane or prolonged dwell time at filopodial tips. Pictures for  
1457 the movie were taken at 2 s intervals. Scale bar indicates 10 µm. Movie available at  
1458 [w.prokop.co.uk/Qu+al/SupplMov.html](http://w.prokop.co.uk/Qu+al/SupplMov.html).

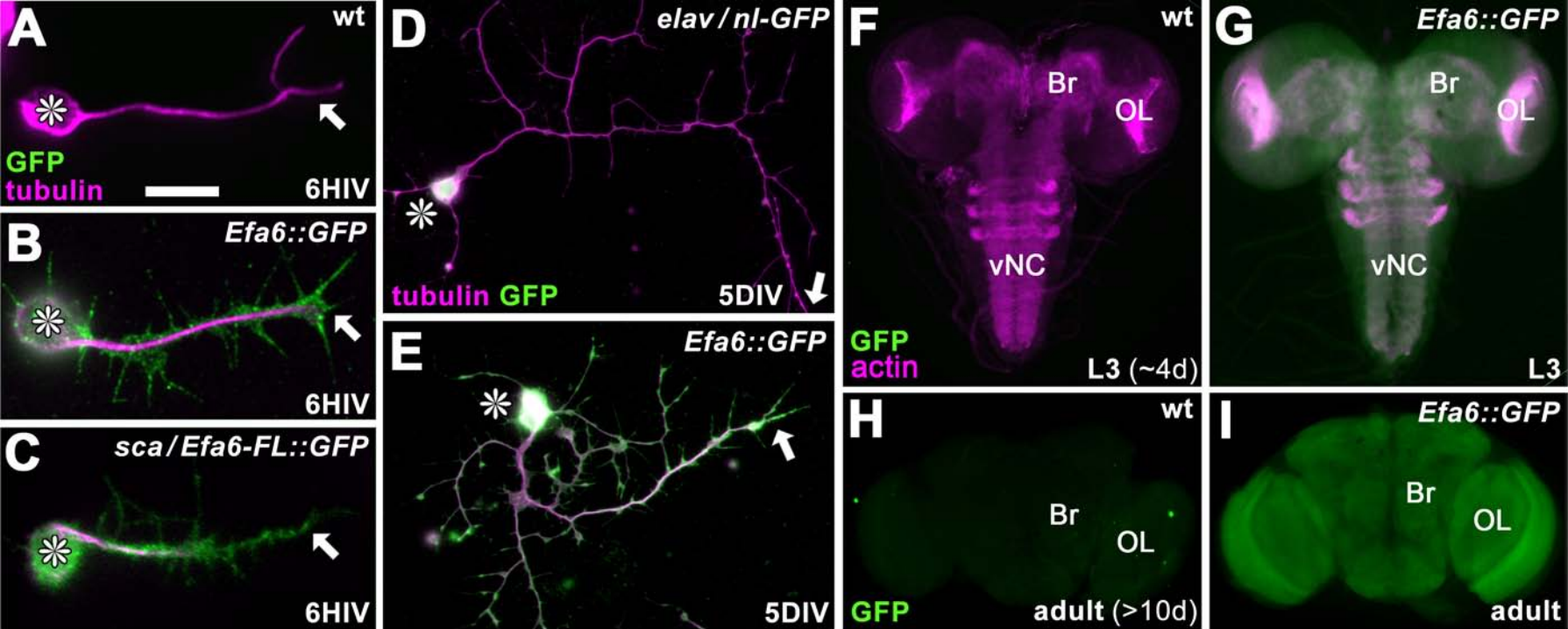


**Fig.1** Qu et al.

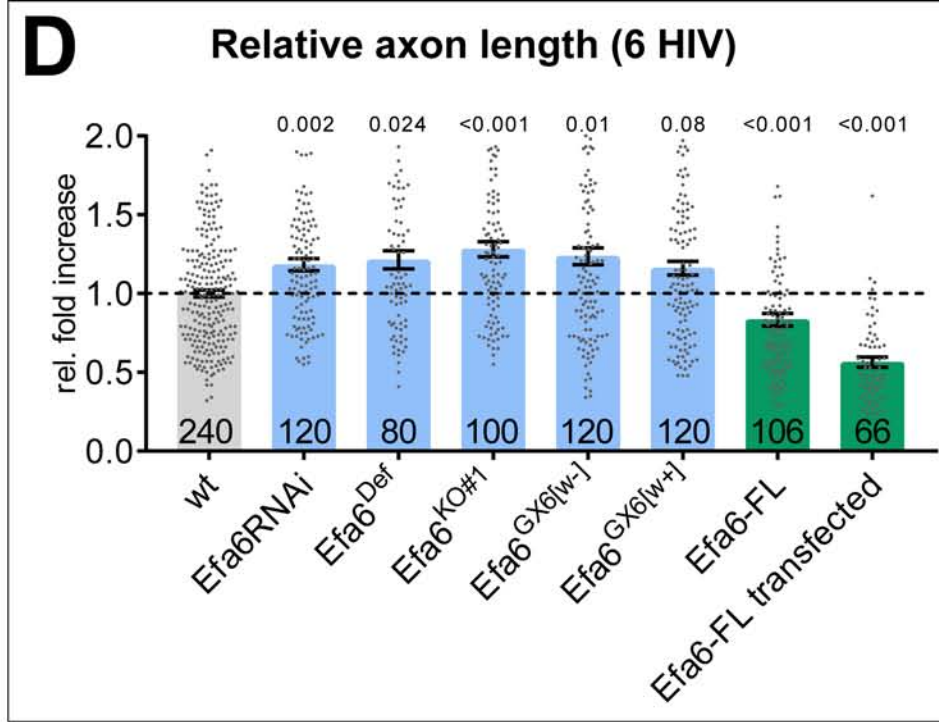
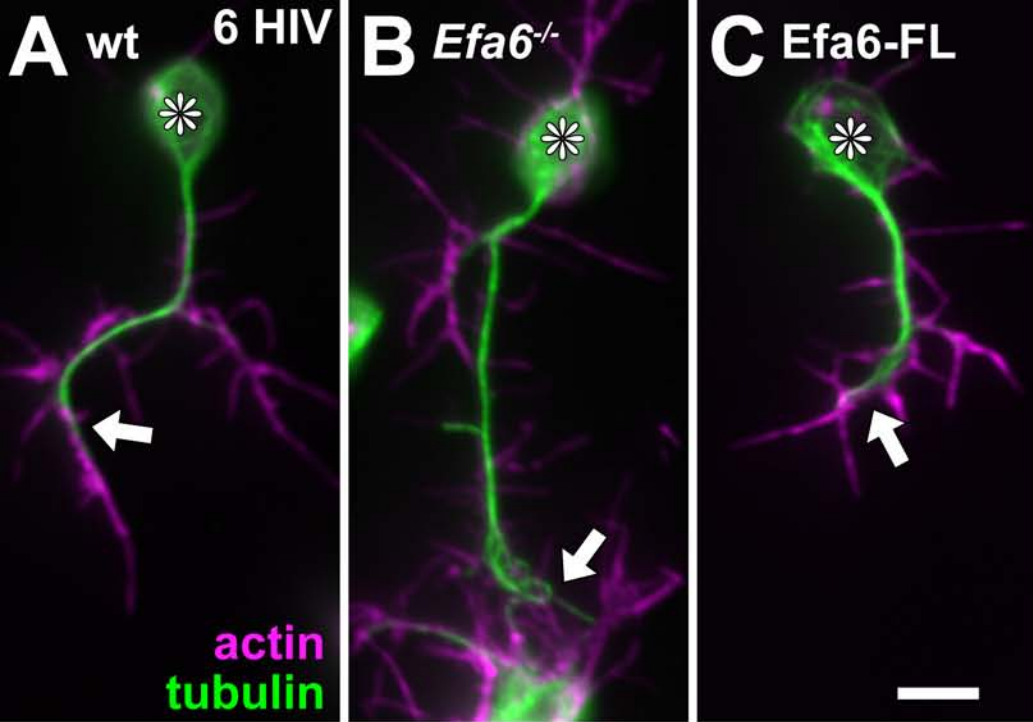


**Fig. 2** Qu et al.

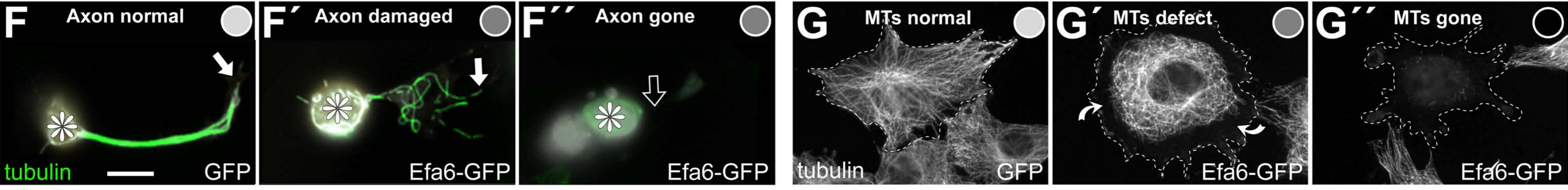
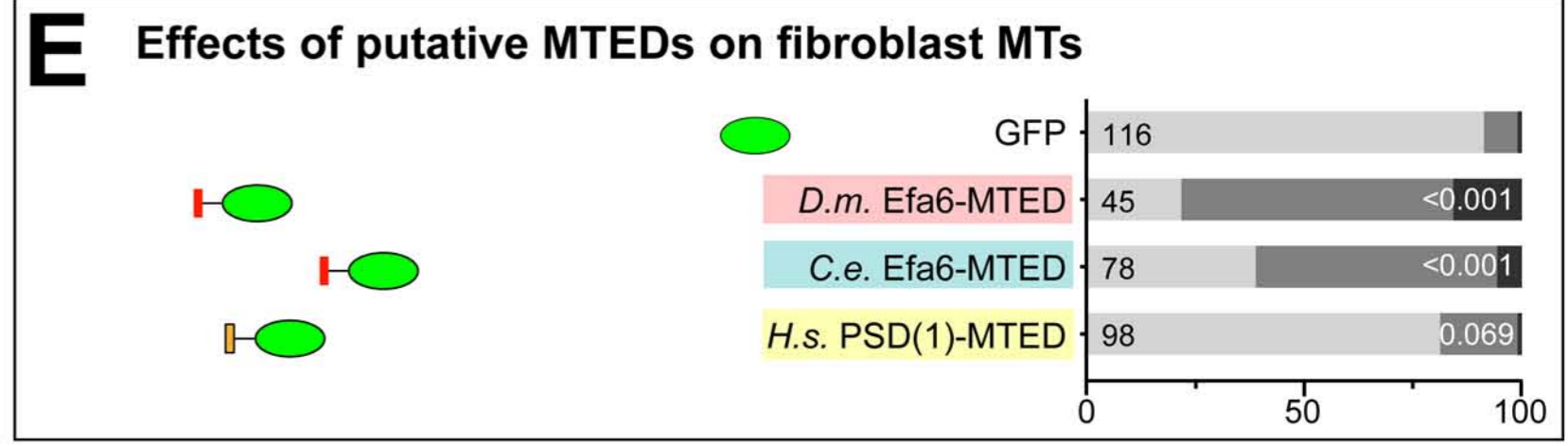
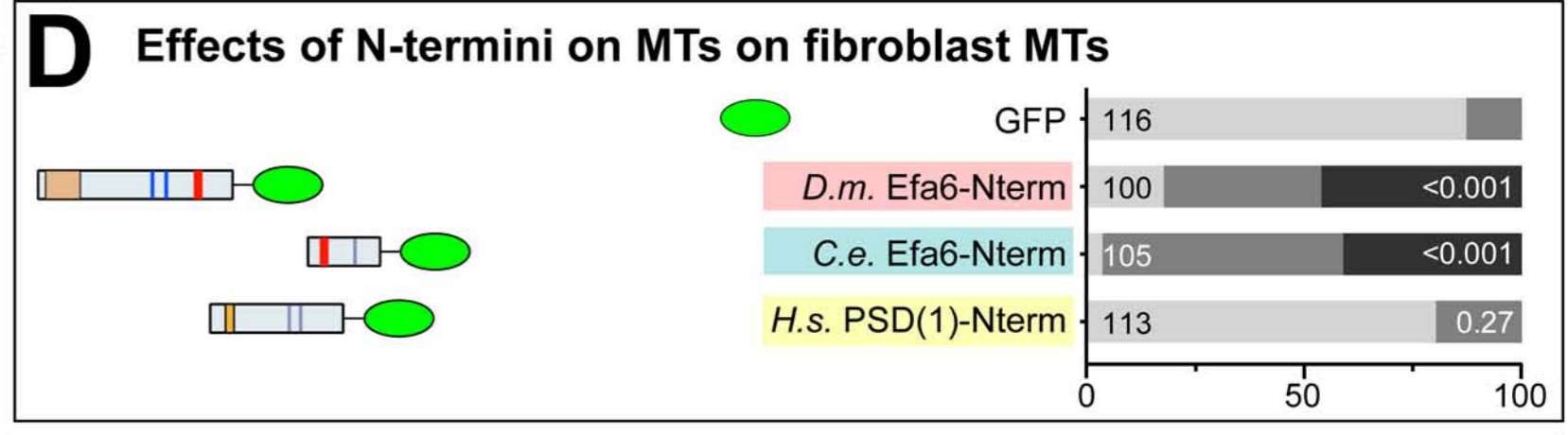
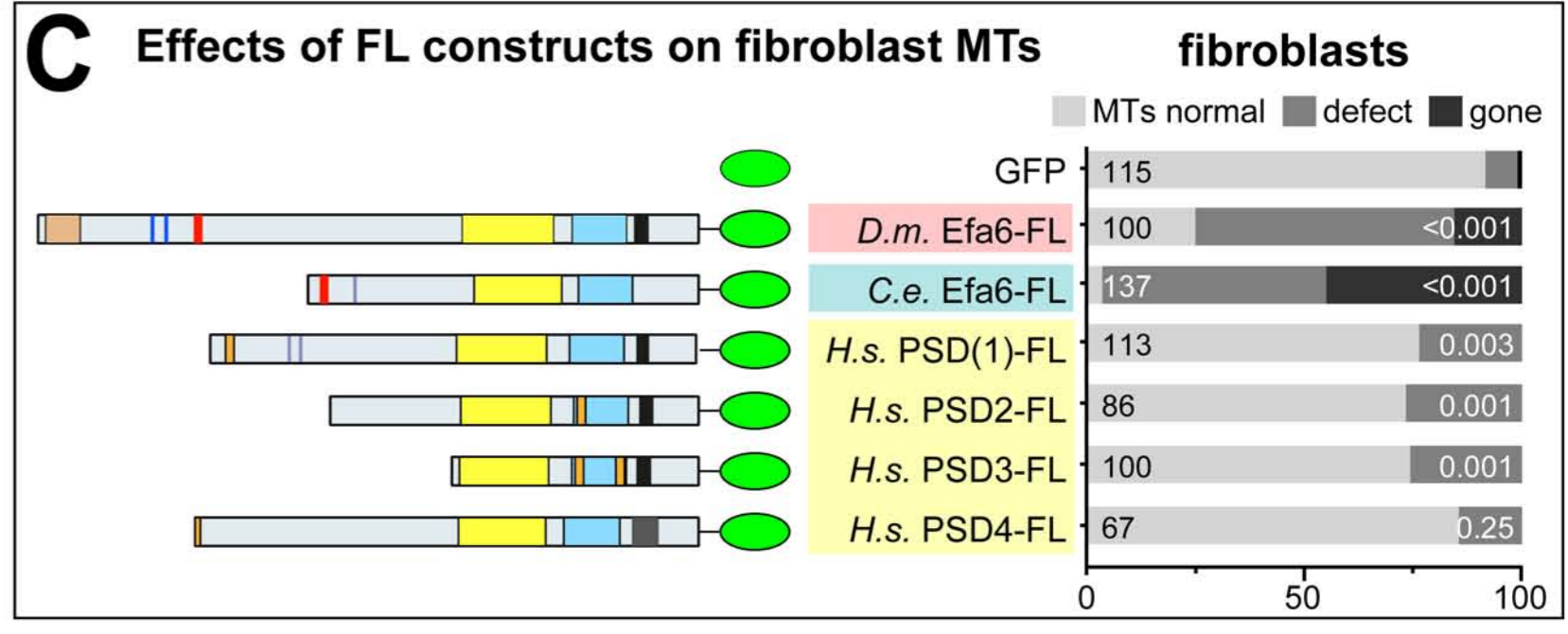
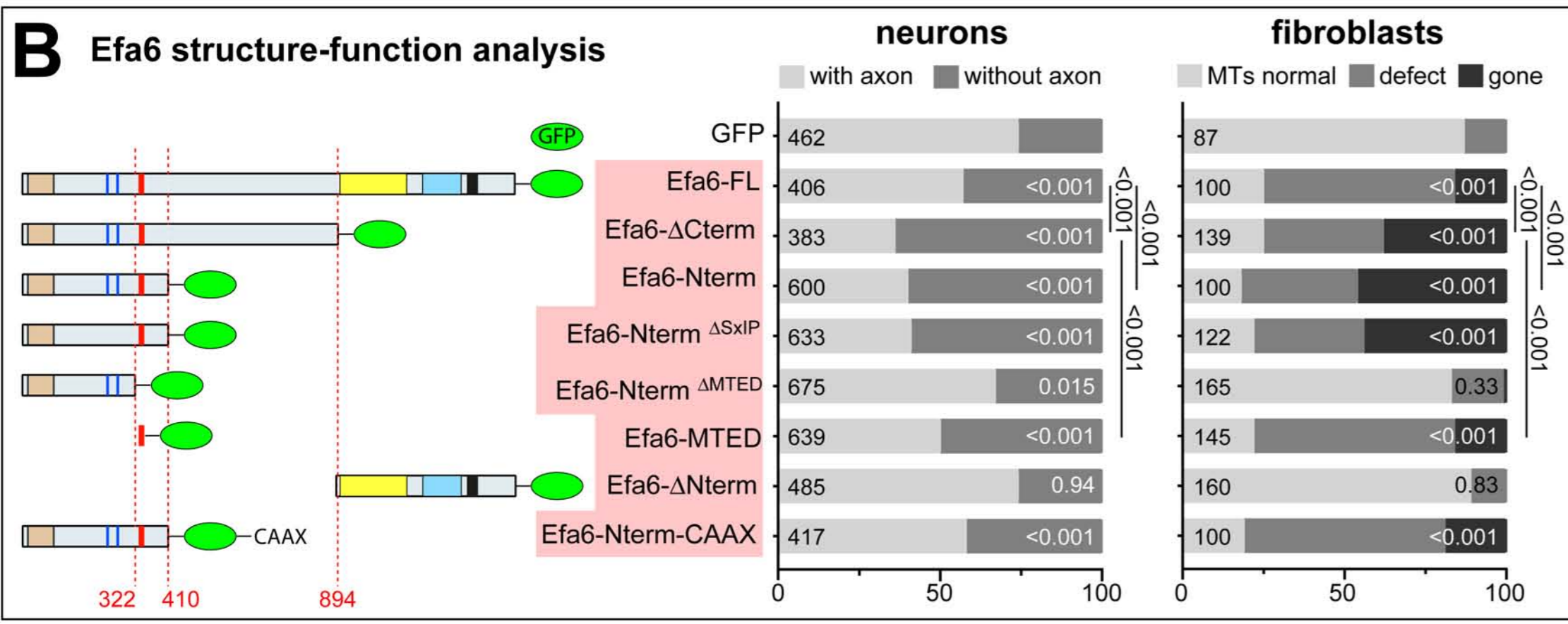
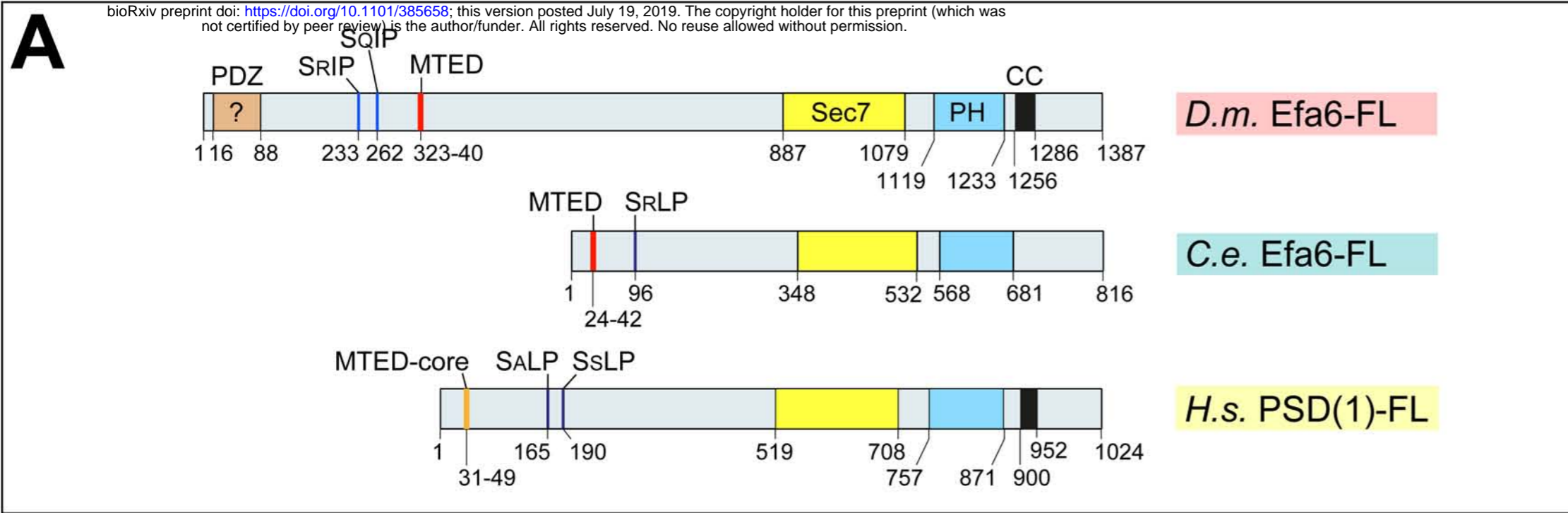


**Fig. 3 Qu et al.**

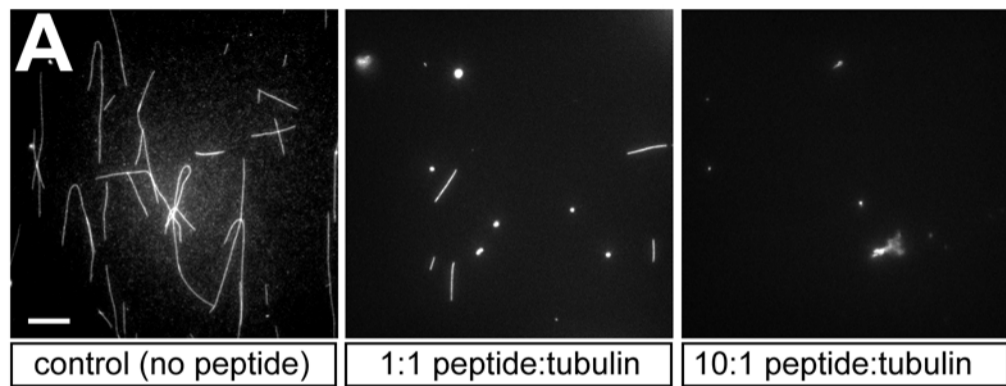


**Fig. 4** Qu et al.

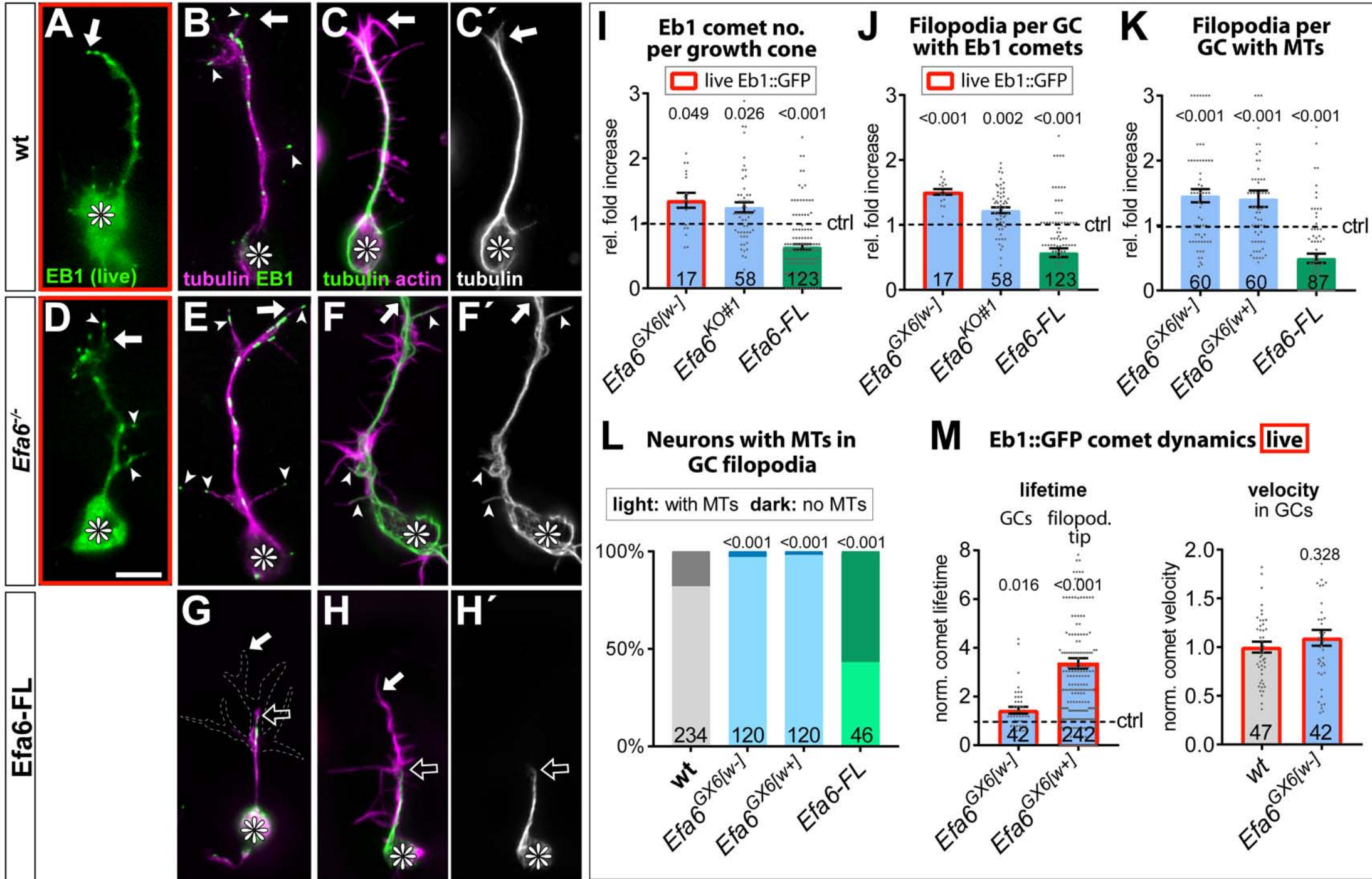


**Fig. 5** Qu et al.

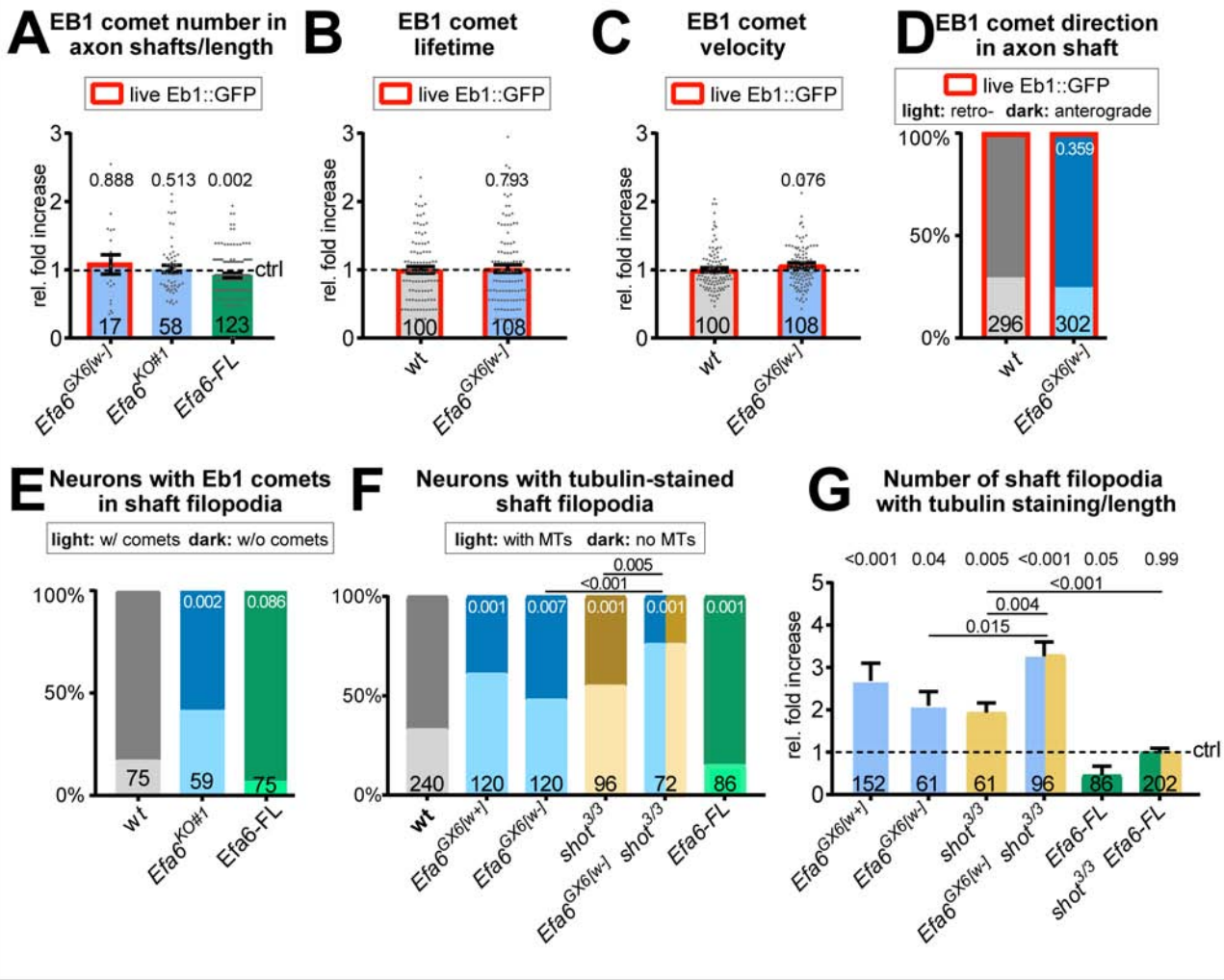
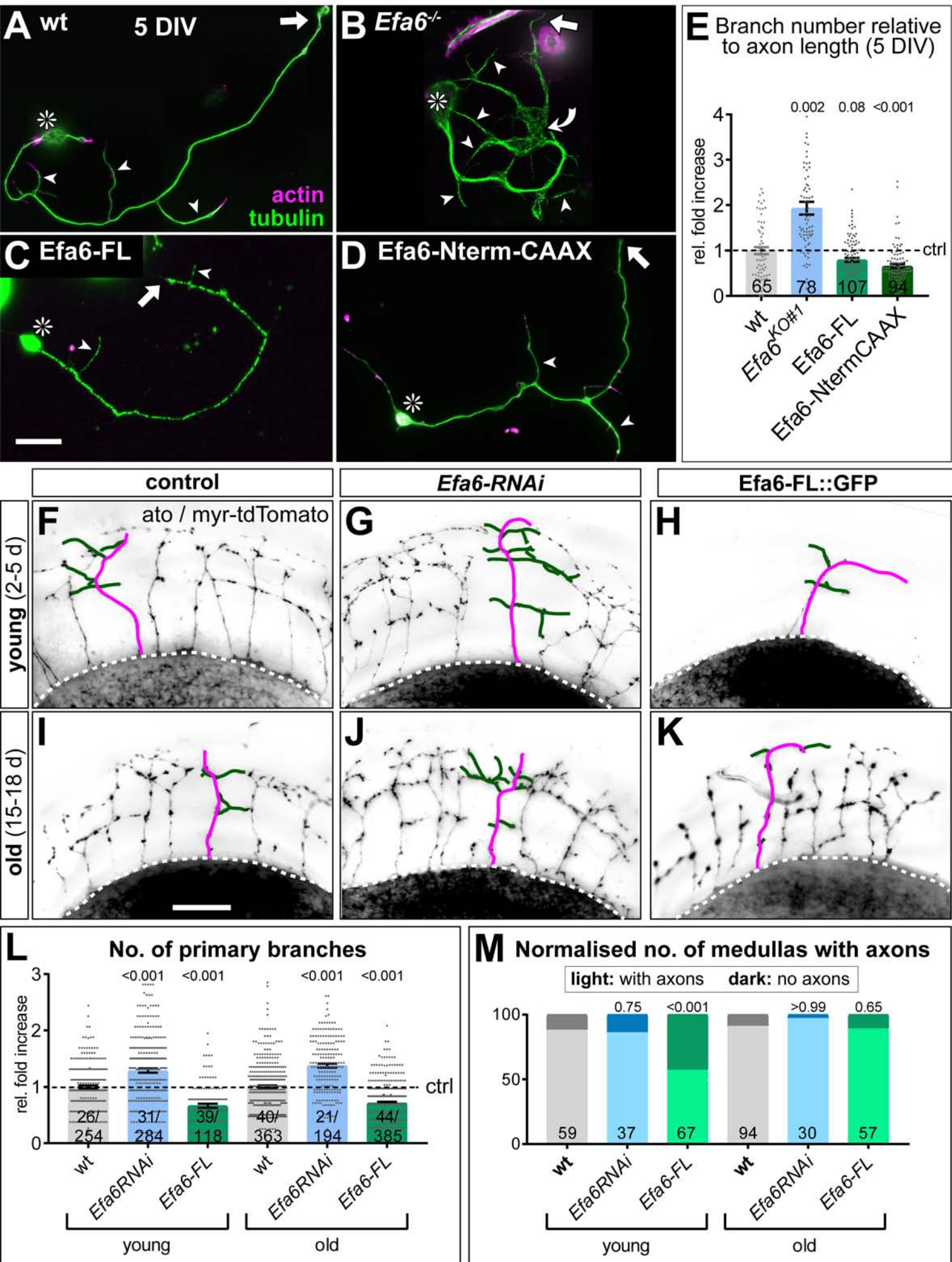
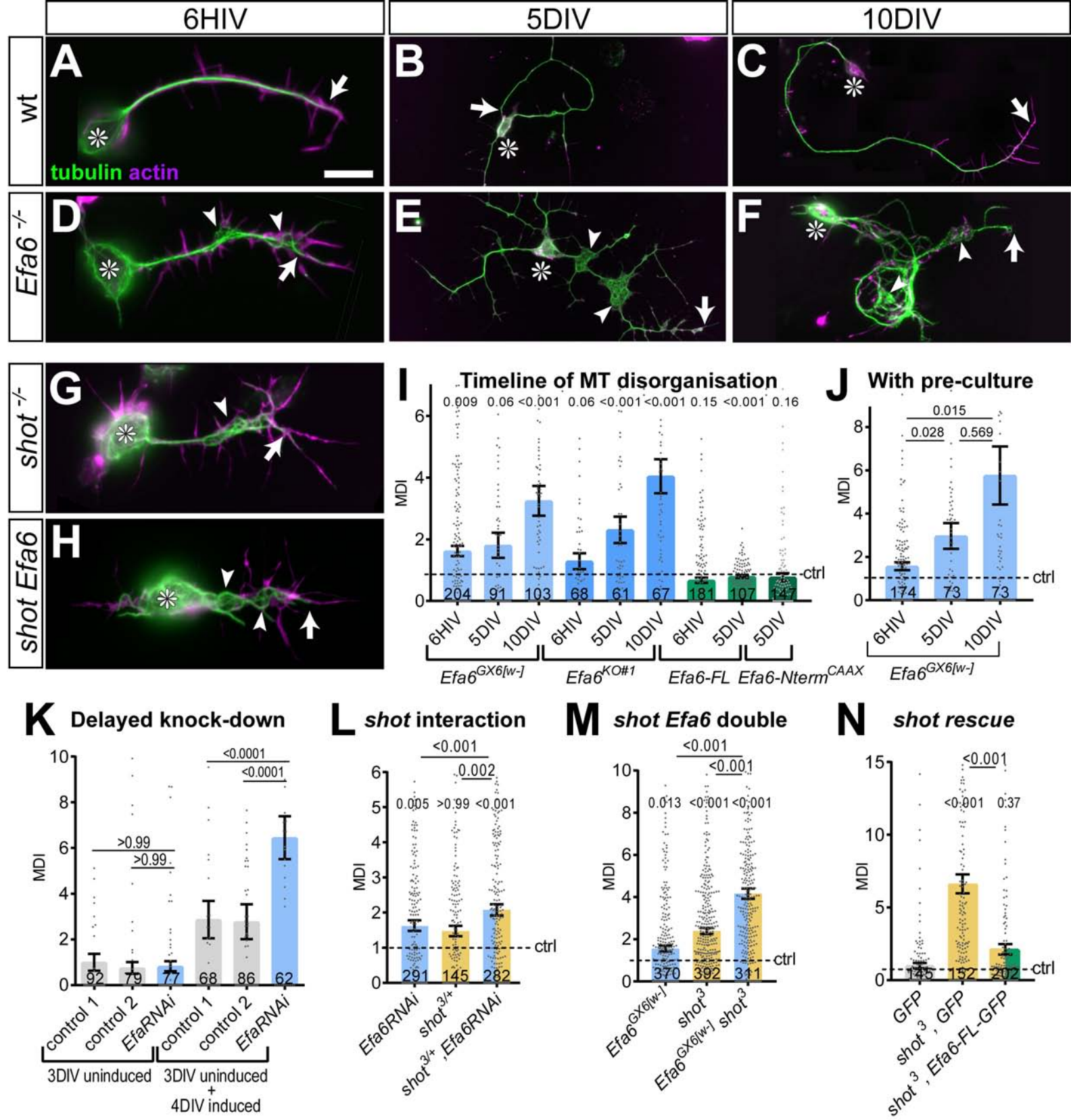


Fig. 6 Qu et al.





**Fig. 7** Qu et al.



**Fig. 8** Qu et al.

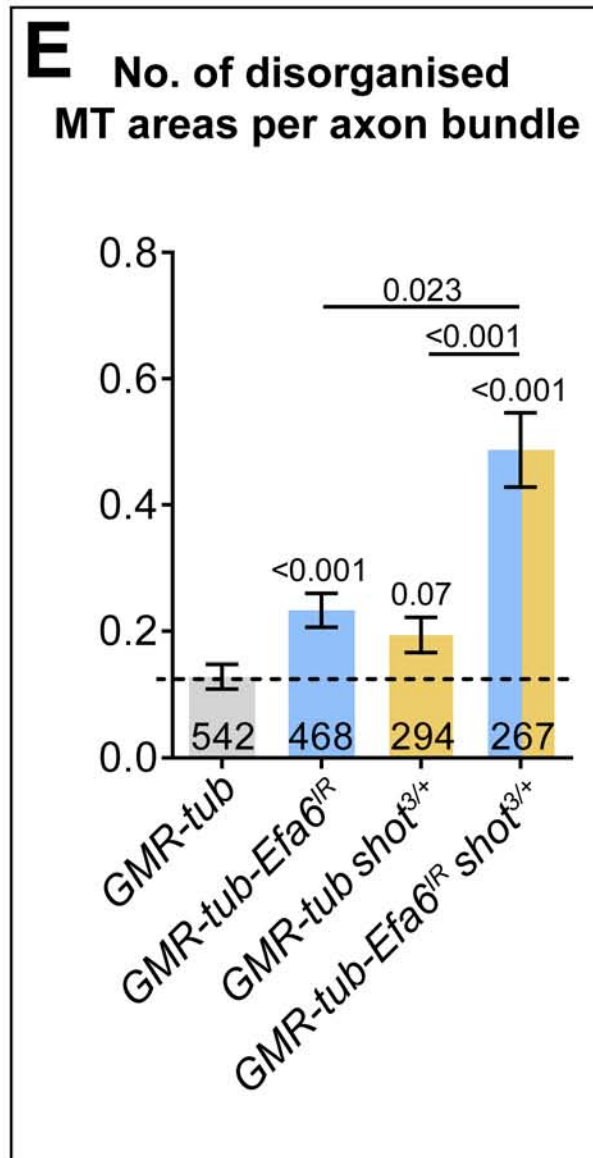
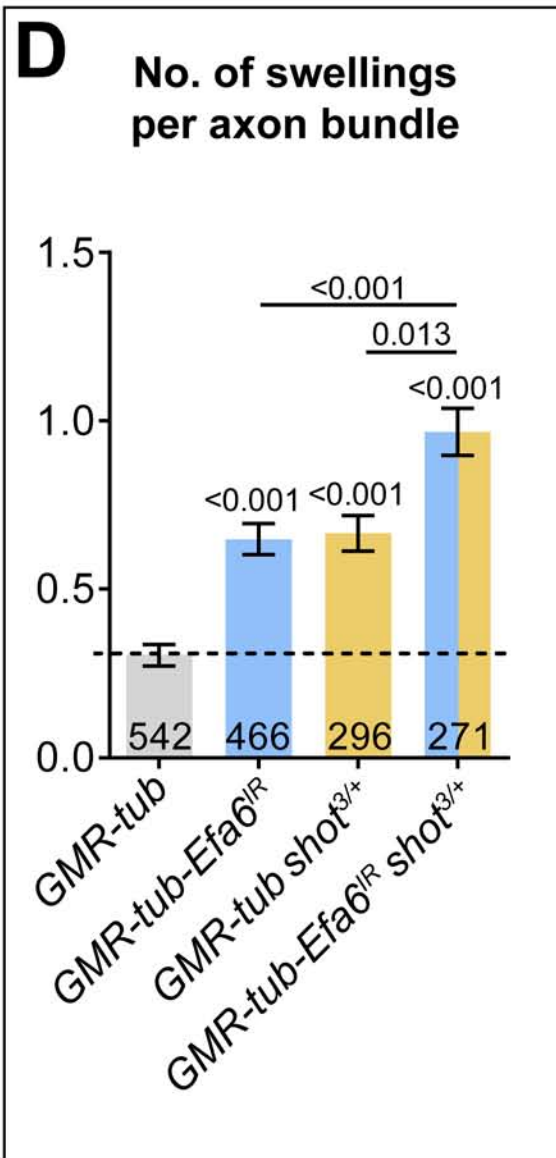
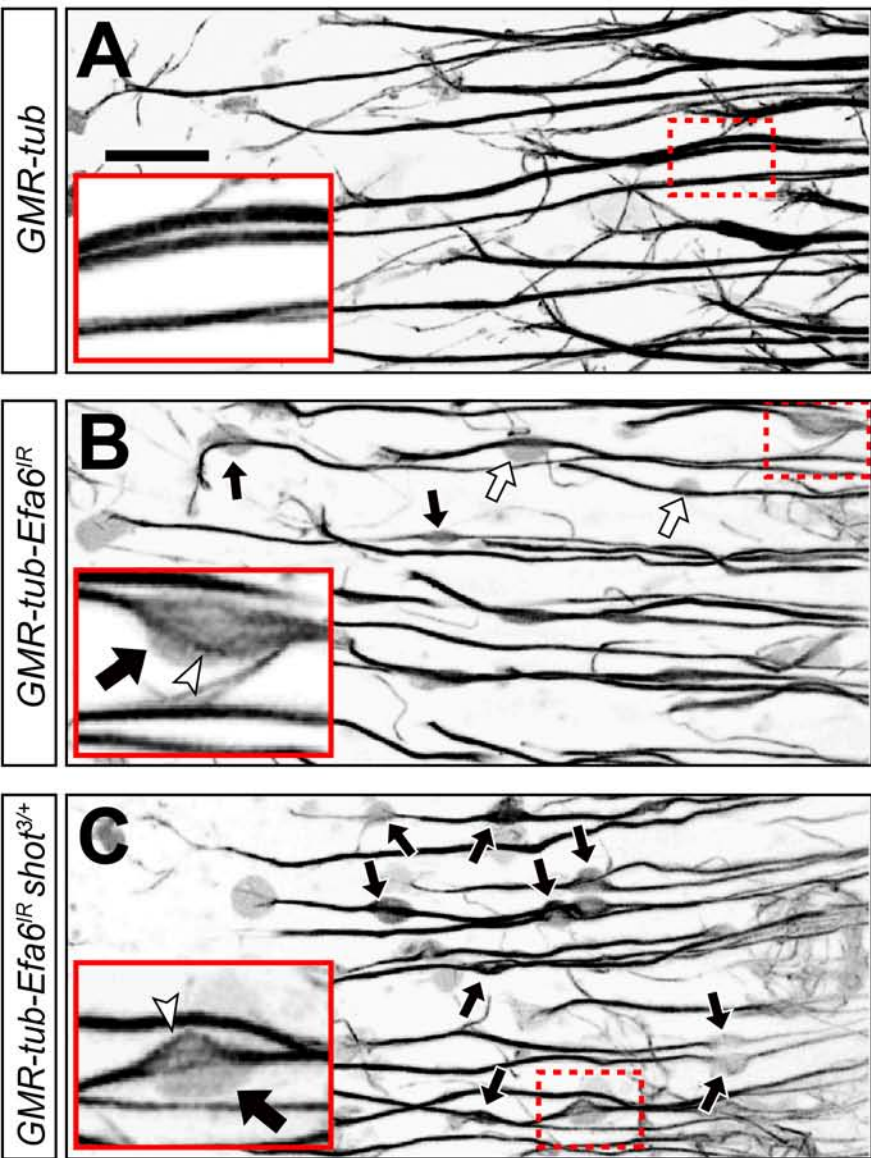


**Fig. 9** Qu et al.

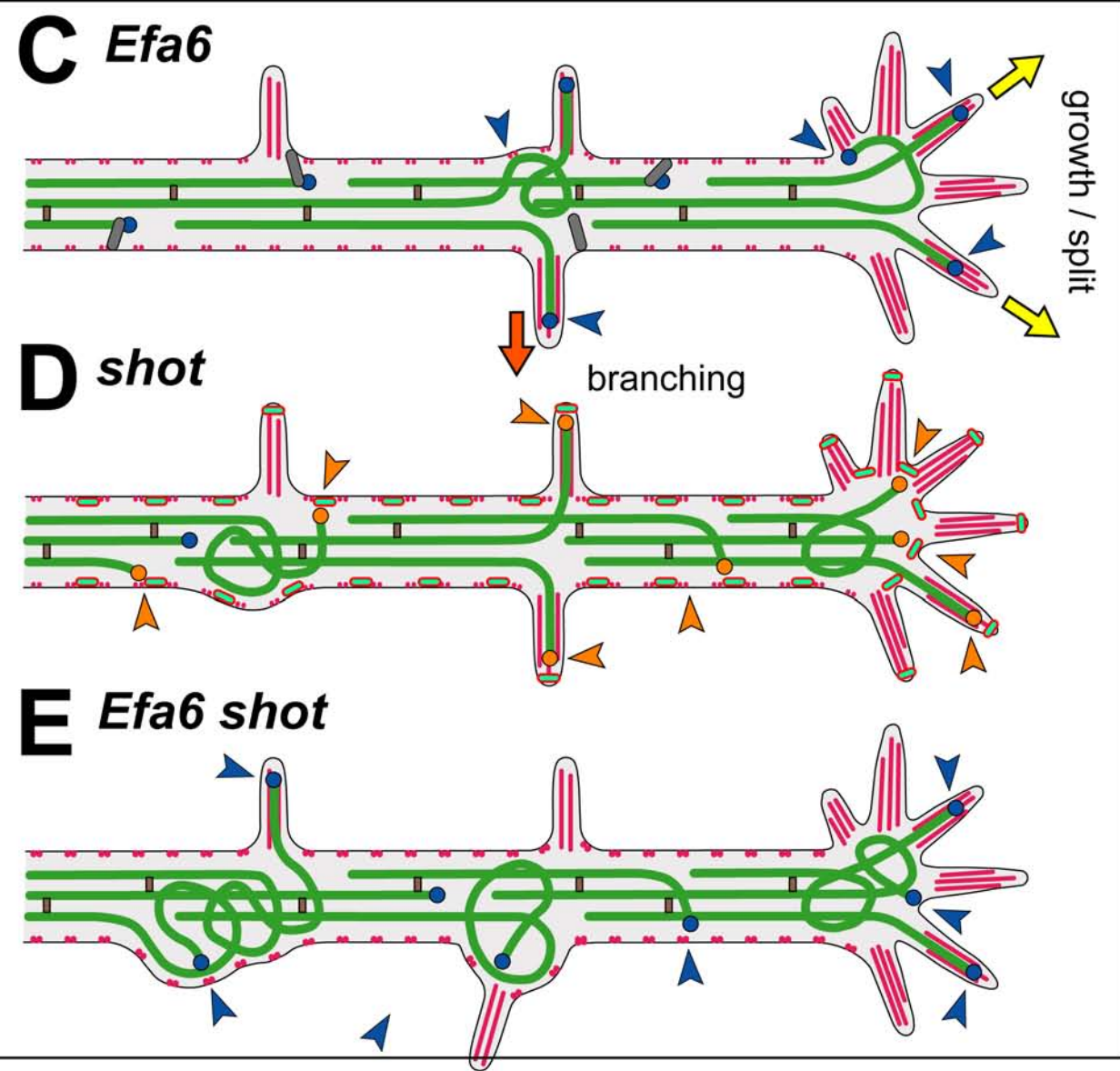
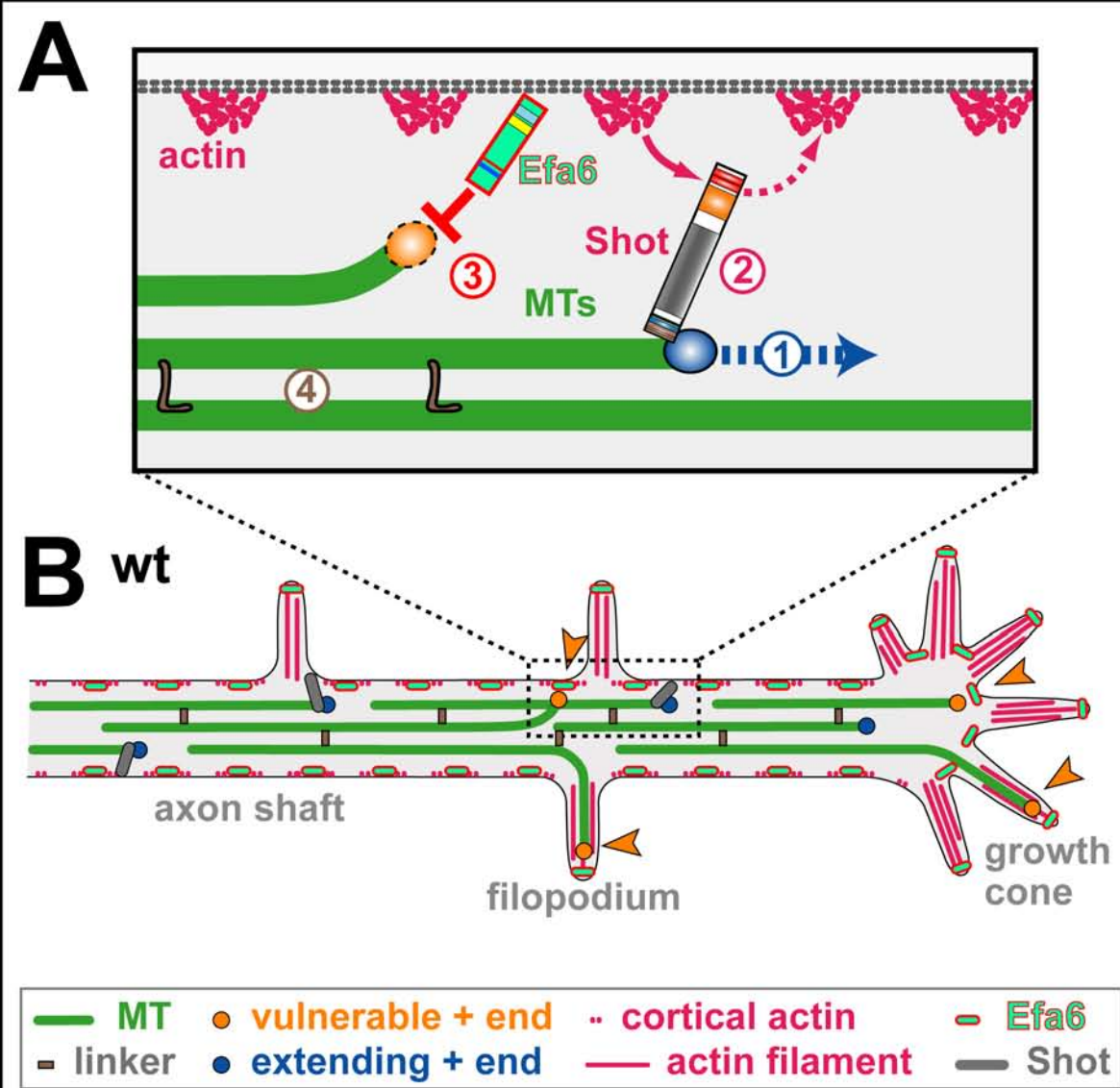
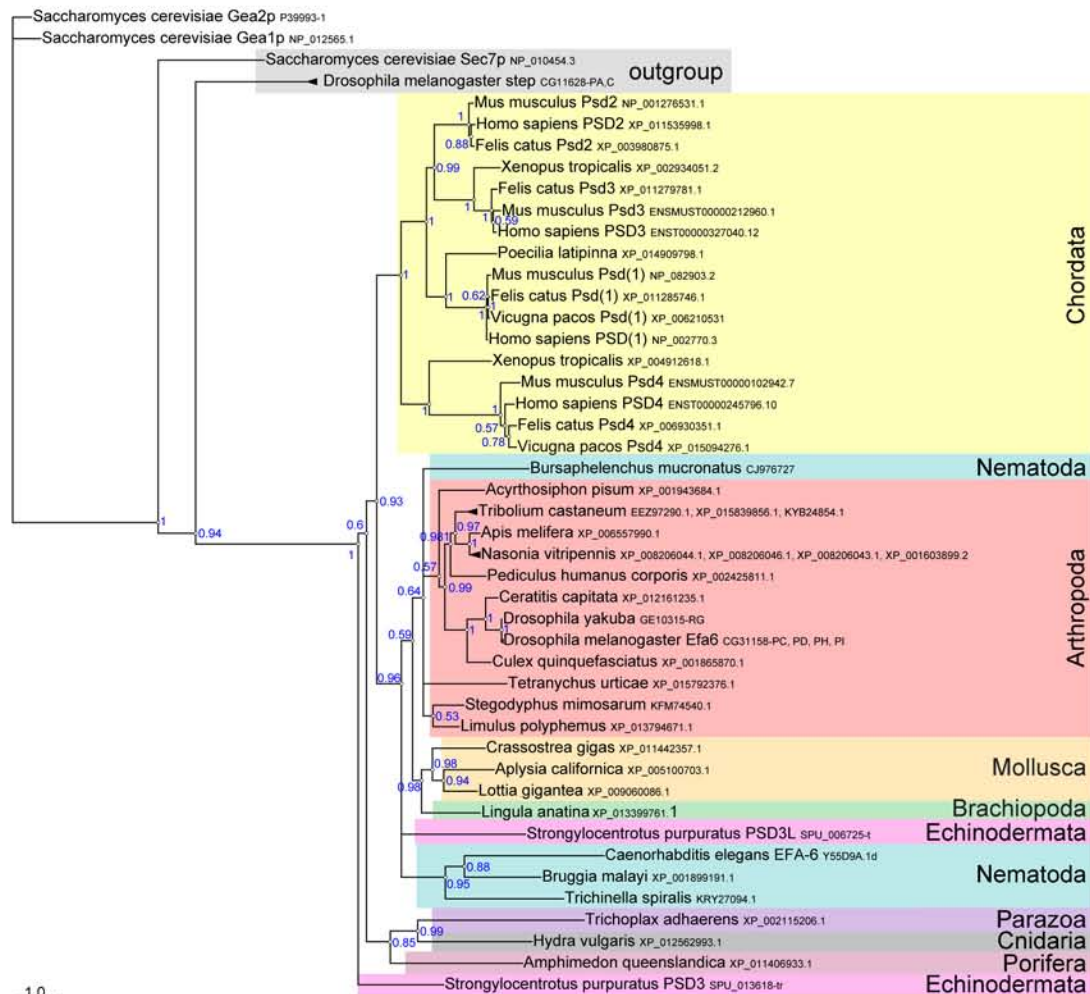


Fig. 10 Qu et al.

## A Full length EFA6 orthologs



## B N-termini of EFA6 orthologs

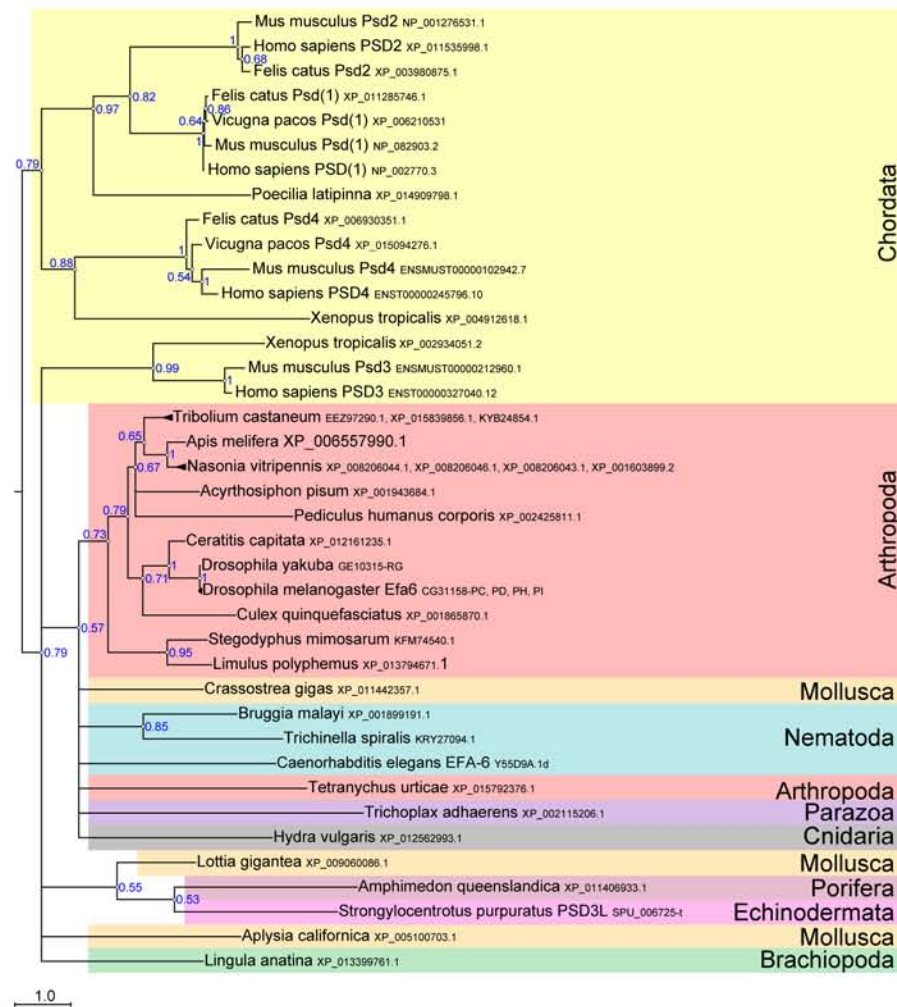


Fig. S1 Qu et al.

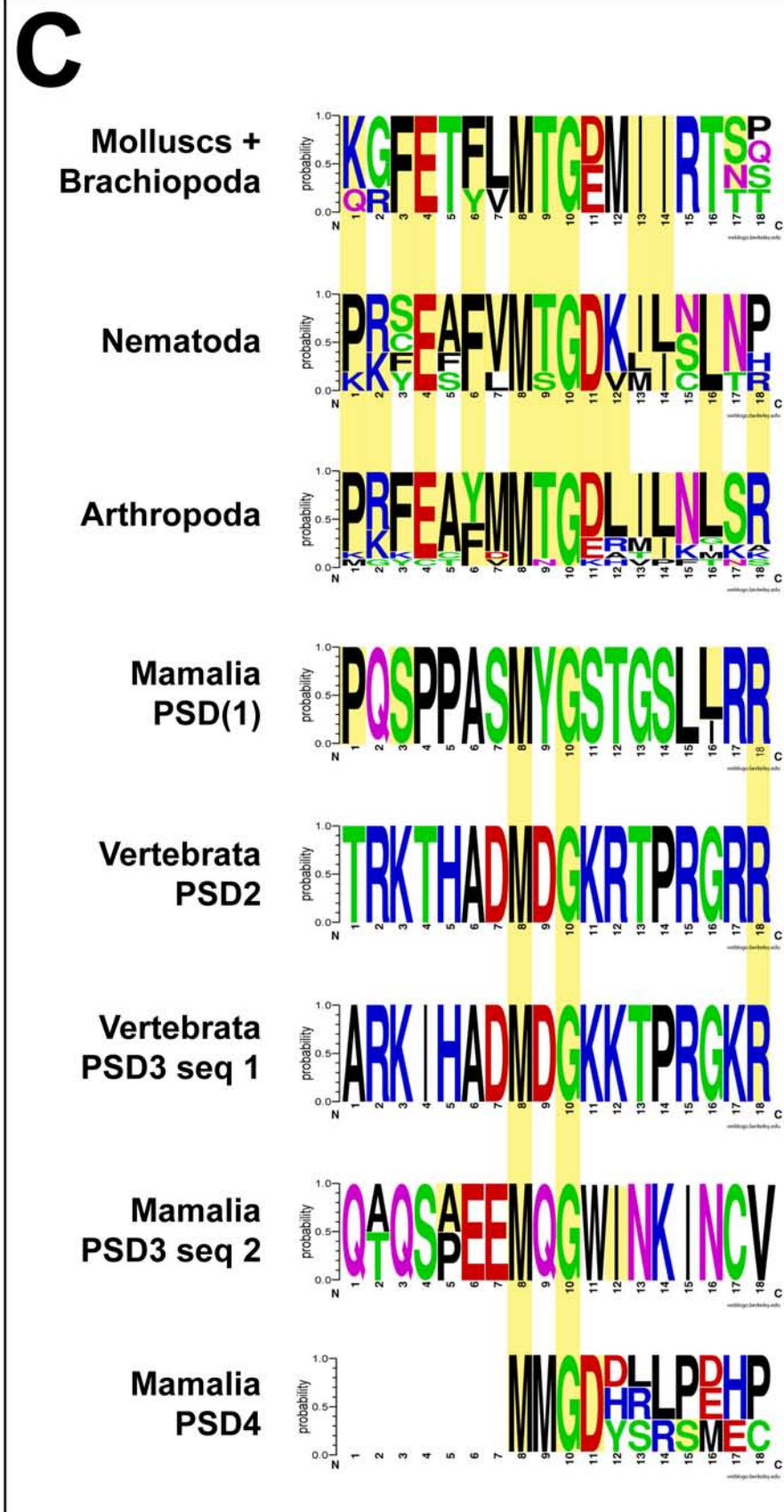
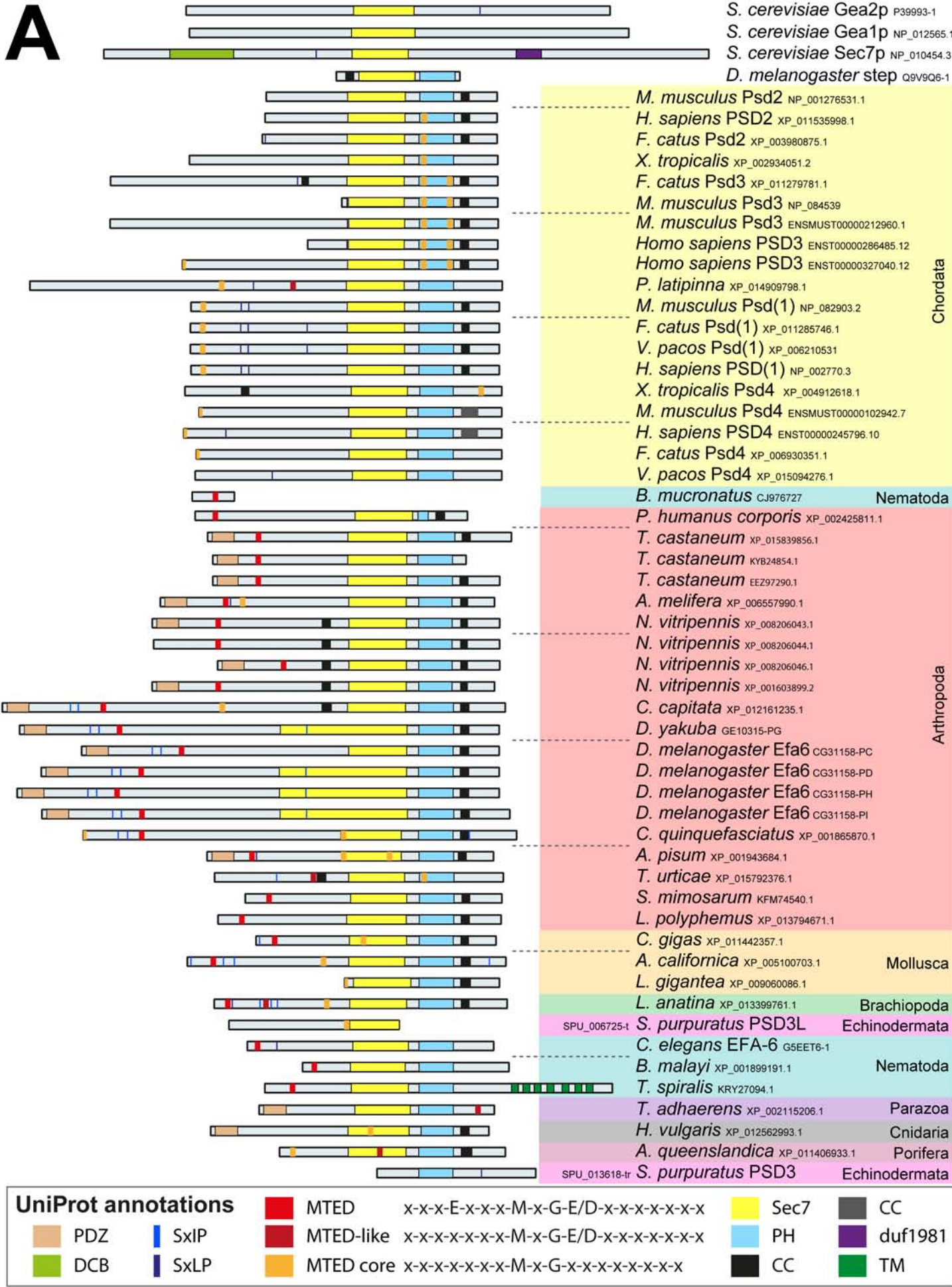


Fig. S2 Qu et al.

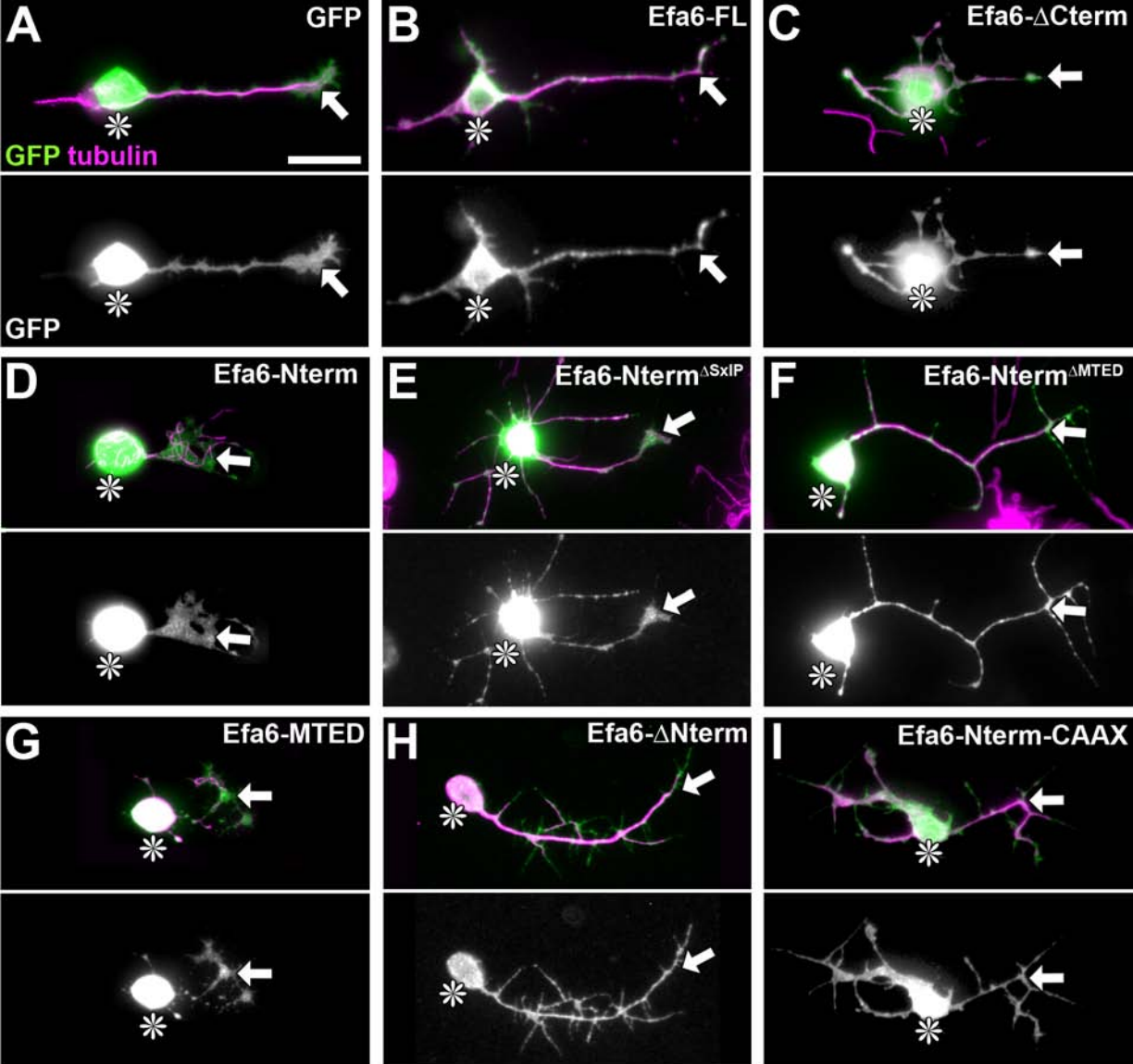
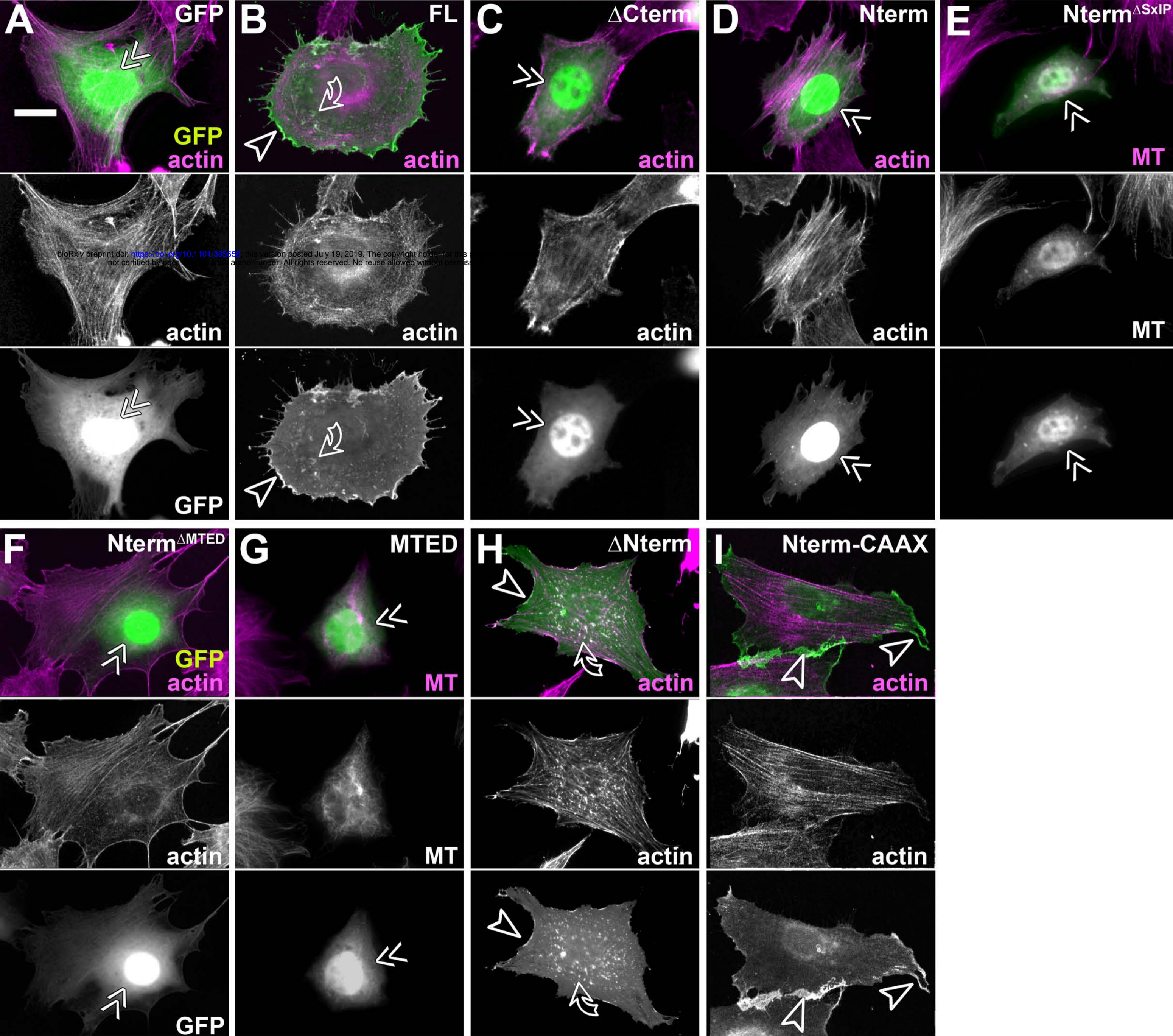
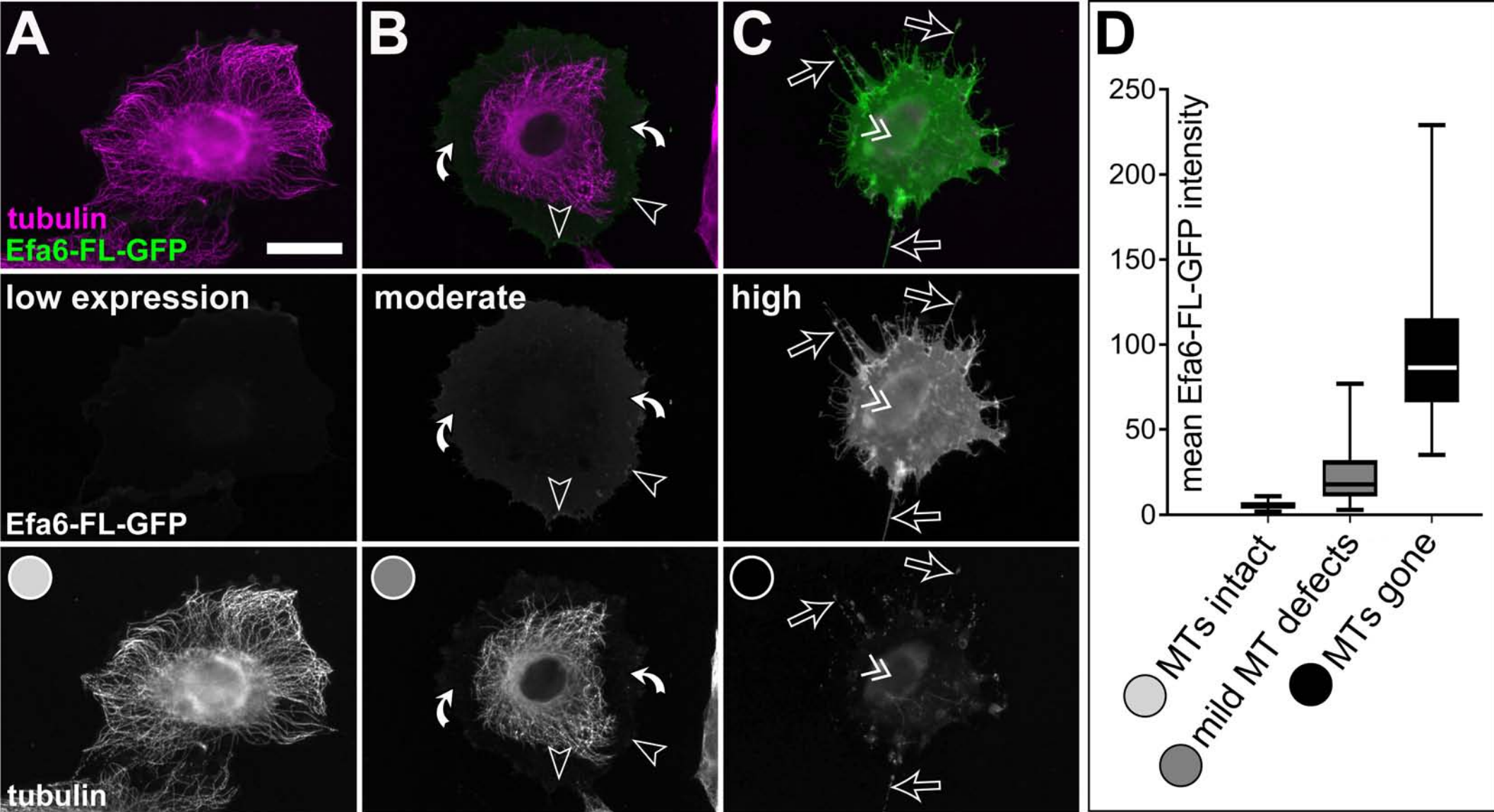


Fig. S3 Qu et al.

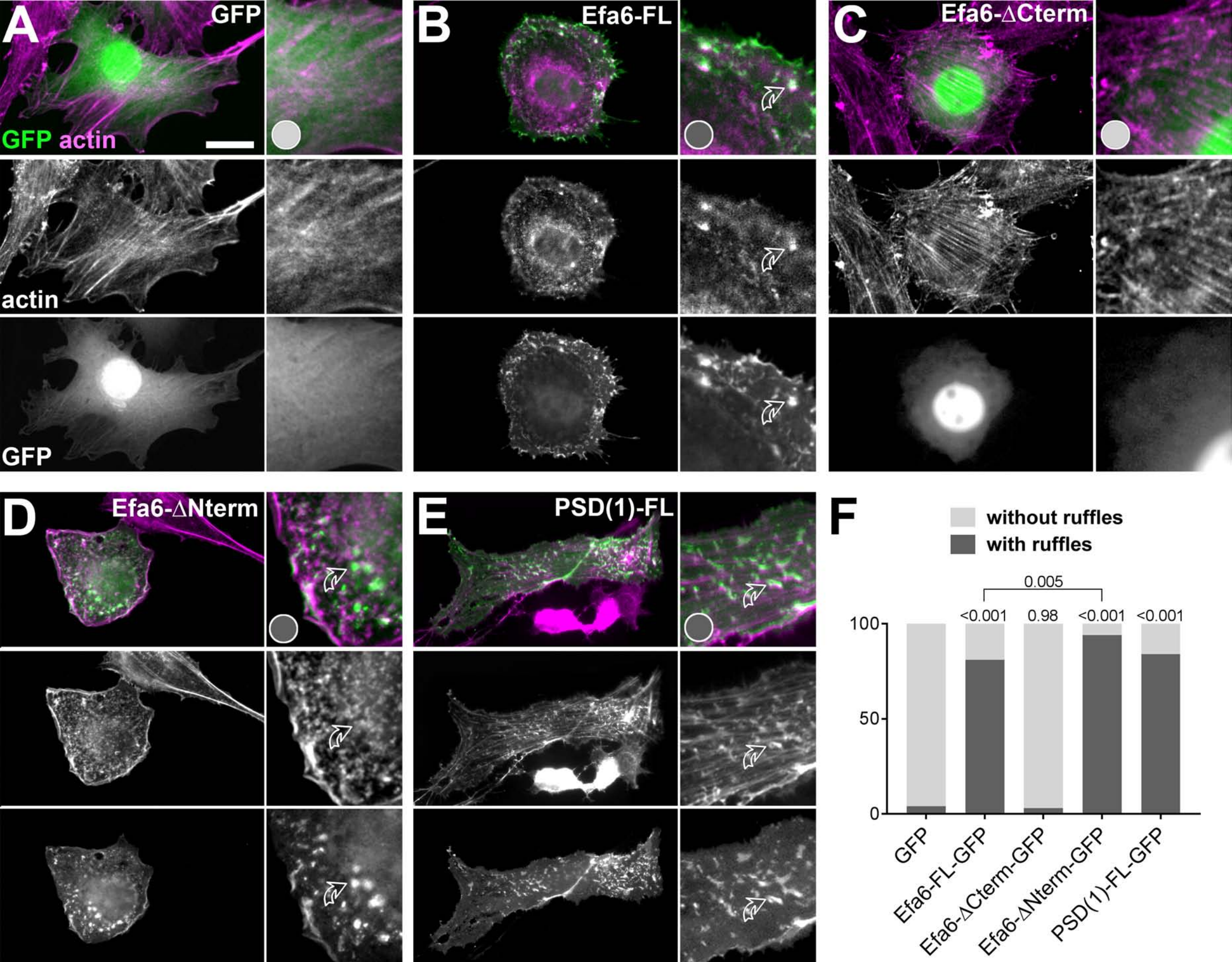


**Fig. S4** Qu et al.

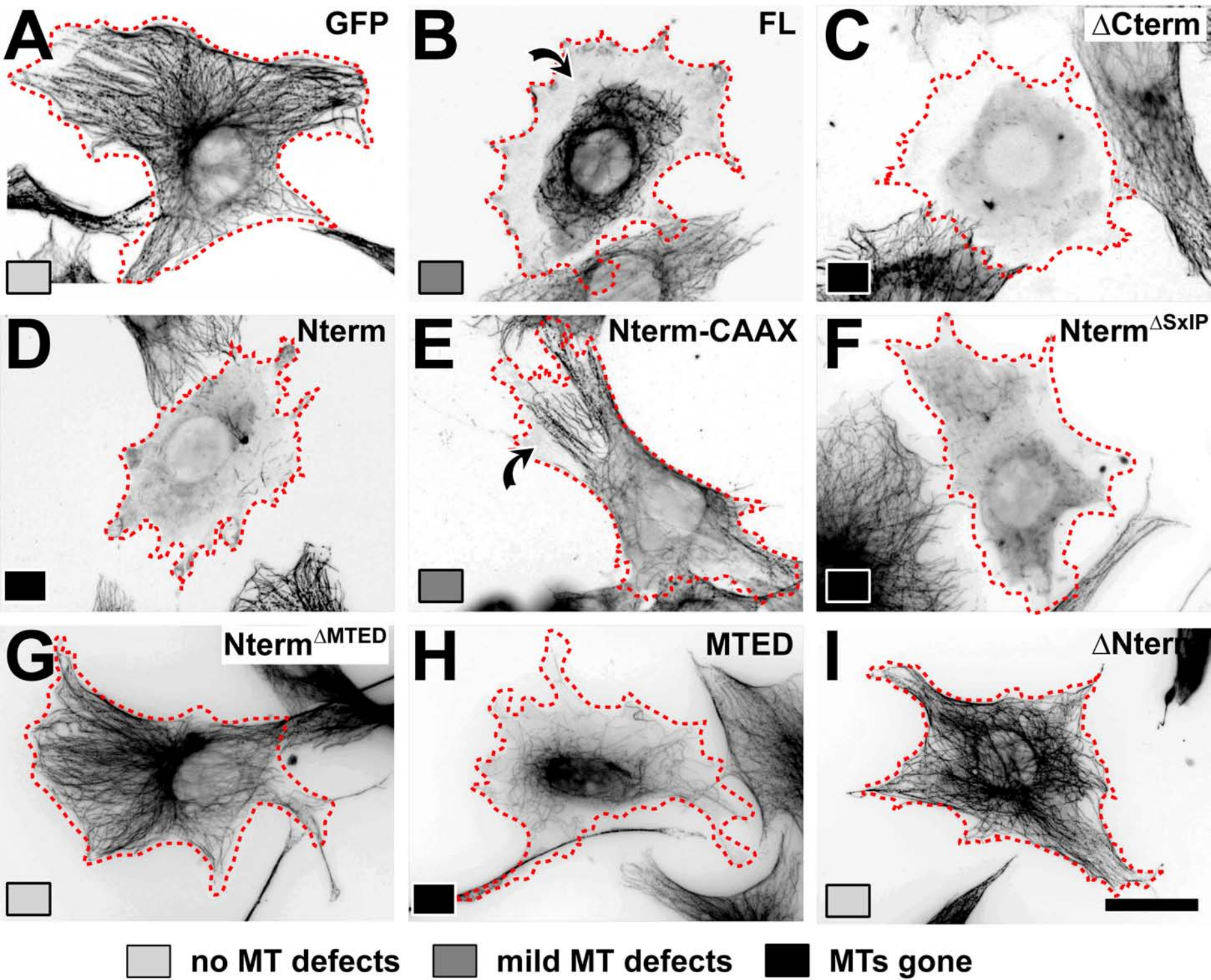




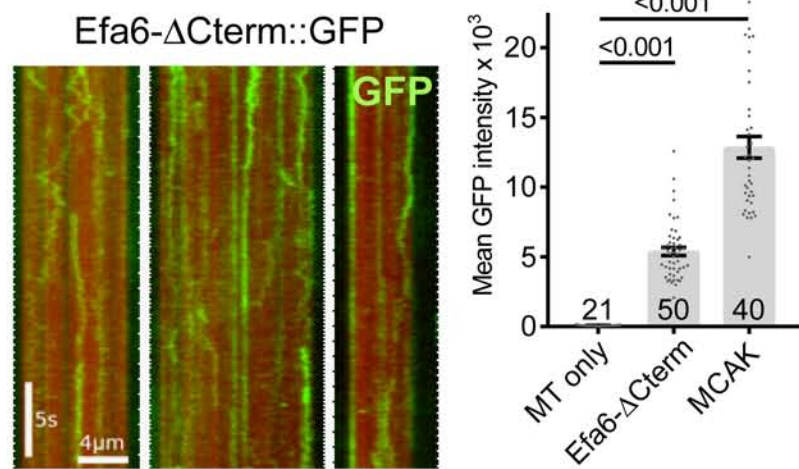
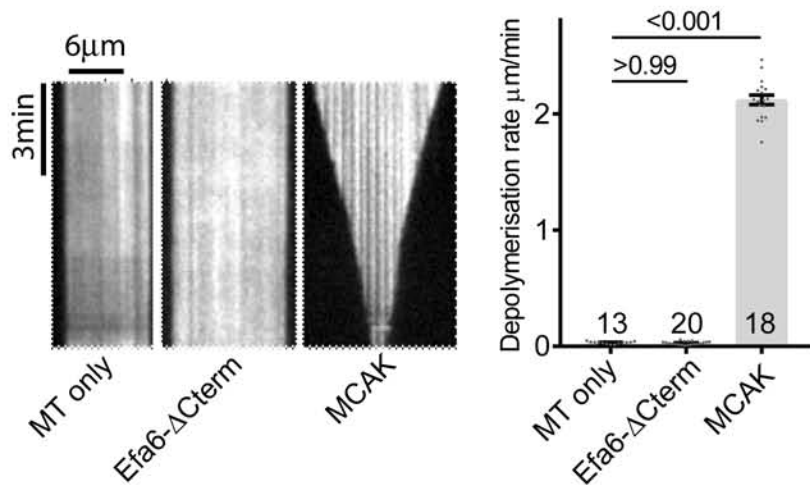
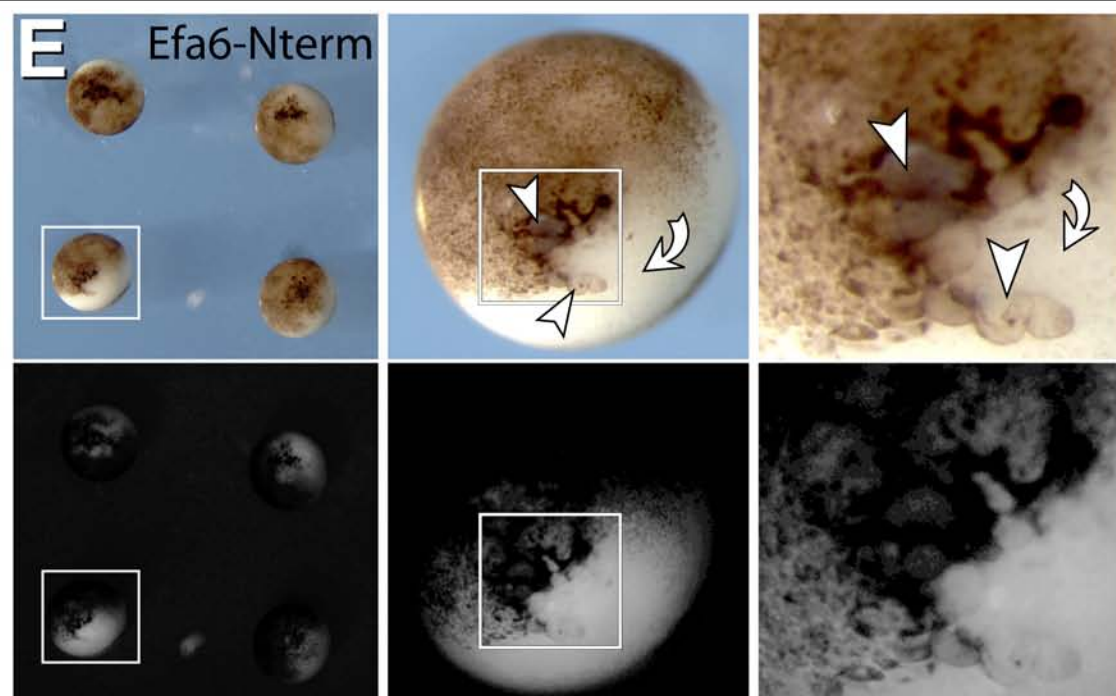
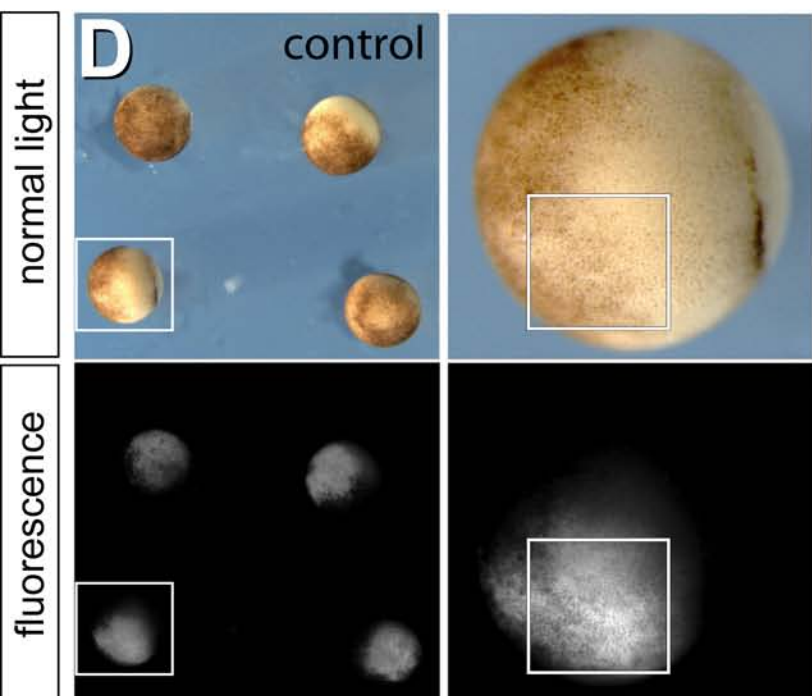
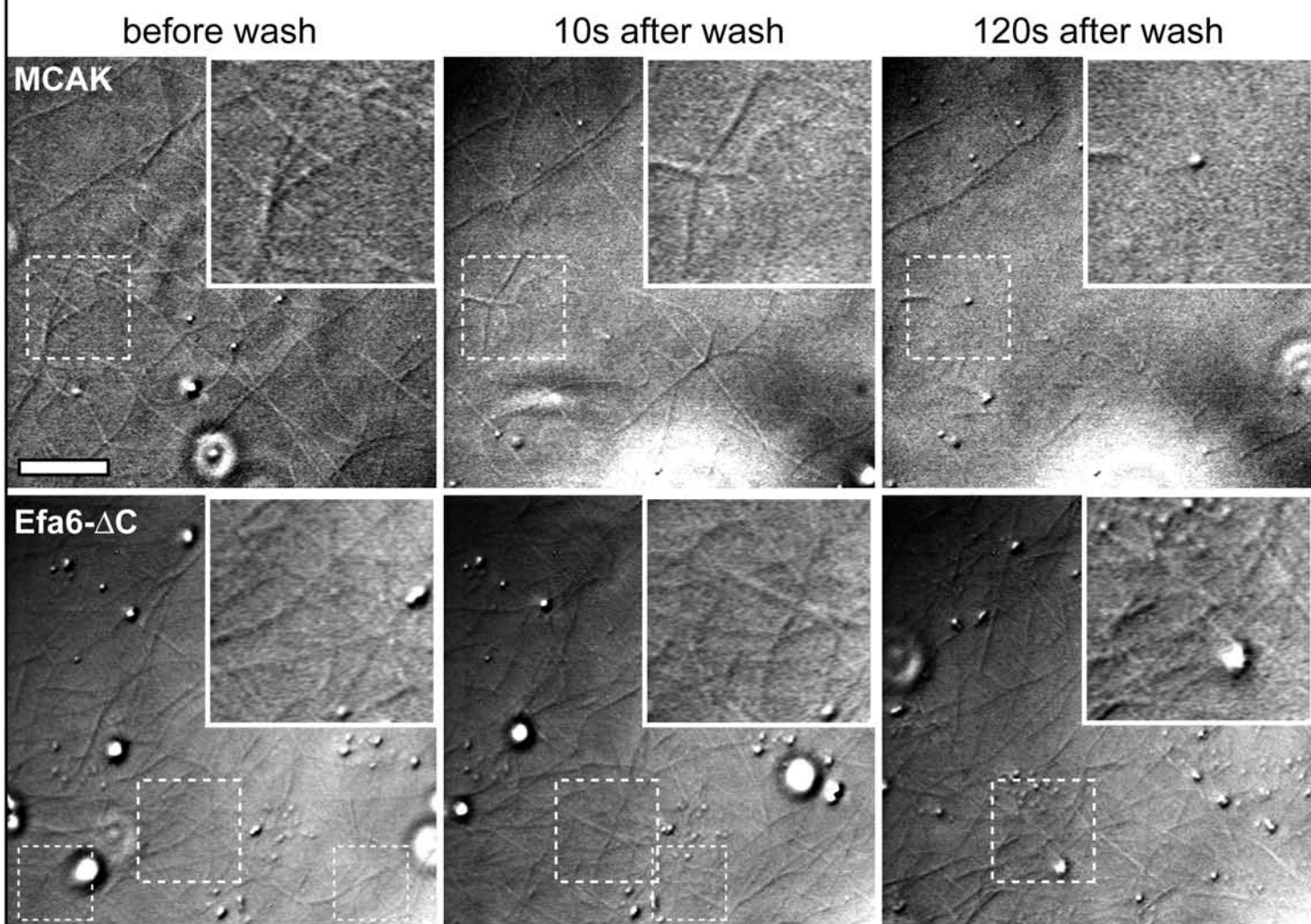
**Fig. S5** Qu et al.



**Fig. S6** Qu et al.



**Fig. S7** Qu et al.

**A** *In vitro* MT binding assay (TIRF)**B** *In vitro* MT depolymerisation assay**C** MT depolymerisation assay on *Xenopus* extract**Fig. S8** Qu et al.

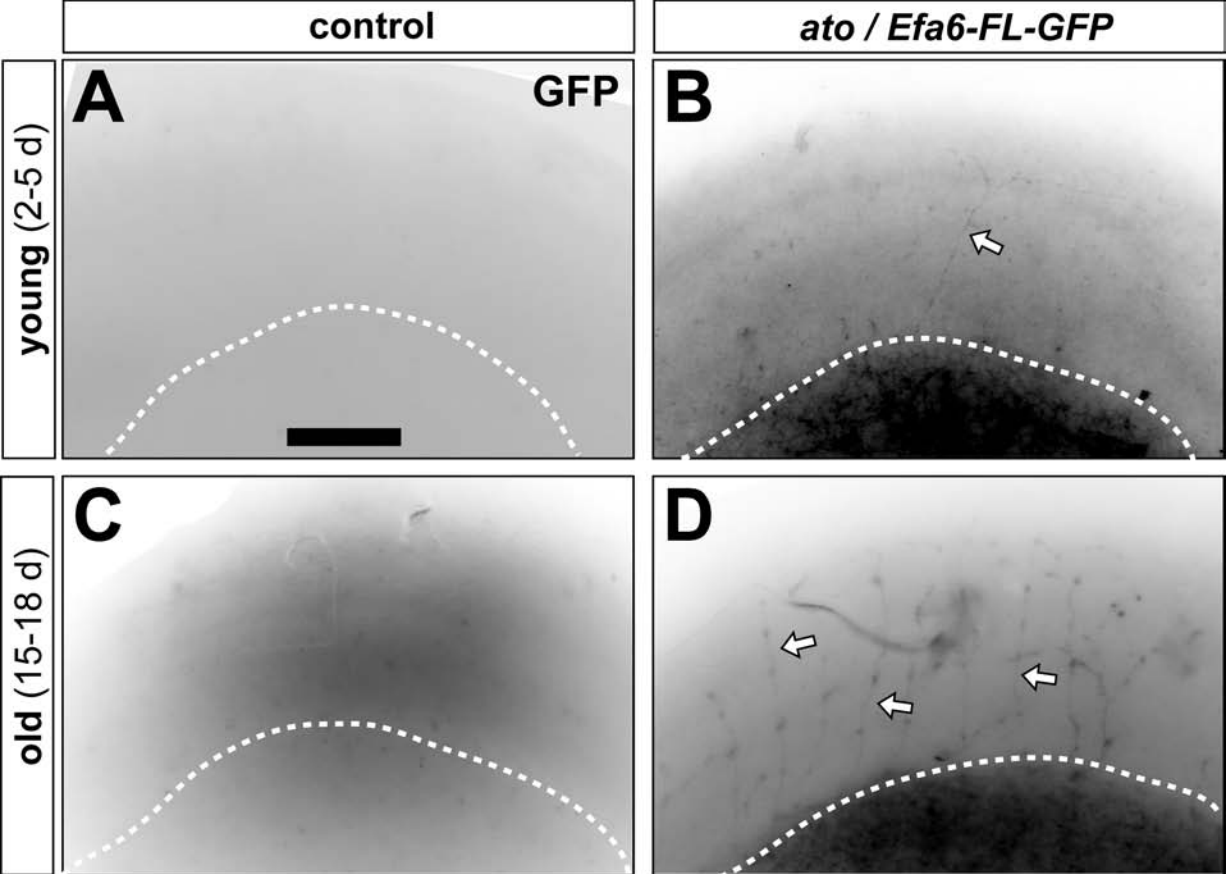


Fig. S9 Qu et al.

# MT disorganisation in *Efa6* mutants (binary data)

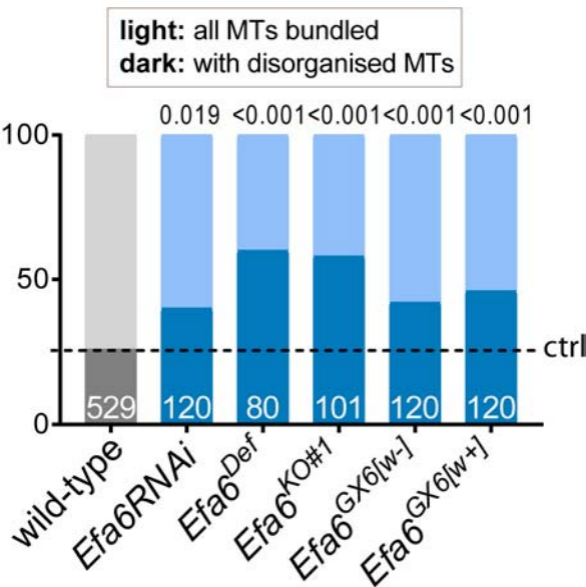


Fig. S10 Qu et al.